2011

Ion Transport, Viscoelastic, and Thermal Properties of Several Poly(Ethylene Glycol) and Poly(Propylene Glycol) Based Polymer Electrolytes

Benjamin Jacob Yancey

Ion Transport, Viscoelastic, and Thermal Properties of Several Poly(ethylene glycol) and Poly(propylene glycol) Based Polymer Electrolytes

Benjamin J Yancey

B.S. 2007 University of Mississippi

M.S. 2009 University of Mississippi

A Dissertation

Submitted to the Faculty of

The University of Mississippi

In Partial Fulfillment of the Requirements

For the degree of Doctor of Philosophy

in the Department of Chemistry and Biochemistry

The University of Mississippi

May 2011

ABSTRACT

This dissertation explores the relationship between ionic conductivity, viscosity, and thermal properties of several MePEG and MePPG based copolymer electrolytes. In particular two main copolymer modifications have been investigated namely copolymerization with "bulky groups" and cross polymerization of MePEG and MePPG monomers. The modifications were made to vary the fractional free volume of the MePEG polymers. All of the copolymers obeyed the Doolittle equation. For both the bulky copolymers and MePEG/MePPG copolymers, increases in the FFV corresponded to increases in the viscosity and decreases in FFV correspond to decreases in viscosity.

The FFV and H^+ conductivity for these copolymers were not correlated per the Forsythe equation. When the $V_{f,ether}$ was substituted for FFV in the forsythe equation, a strong correlation was observed indicating that the mechanism of proton conduction is dependent on the amount of ether units in the material.

The viscosity and ionic conductivity for each individual copolymer electrolyte were correlated following the Walden rule. The α values for all of the copolymer electrolytes were between 0.3 and 0.6 indicating that forces besides viscosity impede the ionic conductivity. These forces can include polymer rigidity, dissociation constant and the blocking of H^+ channels. Most of the copolymer electrolytes had similar α values which indicates that the same forces are affecting all of the copolymer electrolytes.

The C_p showed a correlation to the activation energy for viscosity only for the $MePPG_3$/$MePPG_2$ copolymers. There was no correlation observed for all of the other copolymer

electrolyte series. The correlation for the $MePPG_3$/$MePPG_2$ copolymers indicates that the molecular rearrangement in the material is dependent on the intermolecular forces present. There was no correlation observed between C_p and the activation energy for H^+ conductivity for neither the high or low acid concentration MePEG/MePPG copolymers nor the low acid concentration bulky copolymers. The high acid concentration bulky copolymer electrolytes showed correlations for the copolymer series. The correlation increased as the polarity of the bulky groups increased with the exception the MePEG/Ph_2Si copolymers had the highest correlation. The correlations seen indicate that the bulky groups actually impede the H^+ conductivity by altering the intermolecular forces in the materials.

Lastly, the acid dissociation constant for the $MePEG_7SO_3H$ acid was measured. The acid dissociation was implicated as a contributing force that impedes ionic conductivity by the Walden plots. It was found that the pK_a of the $MePEG_7SO_3H$ decreased as the fraction of $MePEG_7OH$ increased in the binary solvent system. This corresponded to the acid weakening due to the fact that the pK_a was actually further away from the pK_a of the protonated solvent than in aqueous media. The mean activity coefficient also increased as the fraction of $MePEG_7SO_3H$ increased. The results of the acid dissociation experiments further support the Grotthus mechanism as the prominent mechanism for H^+ conductivity for PEG based polymer electrolytes.

TABLE OF CONTENTS

PAGE

CHAPTERS

LIST OF TABLES

LIST OF FIGURES

LIST OF ABBREVIATIONS

ABBREVIATION	DEFINITION
MeOH	Methanol
PEM	Polymer electrolyte membrane
PEMFC	Polymer electrolyte membrane fuel cell
PEO	Poly(ethylene oxide)
PEG	Poly(ethylene glycol)
PPG	Poly(propylene glycol)
POSS	Polyhedral Oligomeric silsesquioxanes
MePEG	Poly(ethylene glycol) monomethyl ether
MePPG	Poly(propylene glycol) monomethyl ether
VTF	Vogel-Tamman-Fulcher
FFV	Fractional free volume
DSC	Differential Scanning Calorimetry
$MePEG_nOH$	Poly(ethylene glycol) monomethyl ether
$MePEG_nBr$	Methoxy poly(ethylene glycol) bromide
$MePEG_nSO_3H$	MePEG acid
THF	Tetrahydrofuran
Et_2O	Diethyl ether
GPC	Gel permeation chromatography

TMS-Cl	Chloro trimethylsilane

LIST OF SYMBOLS

SYMBOL	DEFINITION
S	Siemens
η	Viscosity
$1/\eta$	Fluidity
D	Density
σ	Conductivity
ρ	Resistivity
Z	Impedance
θ	Cell constant
Λ_m	Molar equivalent conductivity
v_f	Free volume
v_m	Molecular volume
v_w	van der Waals volume
V_f	Molar free volume
V_m	Molar volume
V_w	Molar van der Waals volume
T_g	Glass transition temperature
T_0	Ideal glass transition temperature

T_c	Crystallization temperature
T_m	Melting temperature
Cp	Specific heat capacity
q	Heat
M_n	Number average molecular weight
meq	milliequivalents

I. INTRODUCTION

The goal of this dissertation is to gain a primary understanding of the mechanism of proton conductivity and how proton conductivity is affected by the physical (viscosity, diffusion and free volume) and thermal properties (glass transition and specific heat capacity) of our sol-gel synthesized, anhydrous proton conducting electrolytes. Chapter 1 is focused on historic and background information of polymer electrolytes, fuel cells, free volume theory, acid dissociation and thermal properties.

1.1 – Fuel Cells

The demand for more efficient and greener energy sources has led to an increased interest in fuel cells. Of the different types of fuel cells, polymer electrolyte membrane fuel cells (PEMFC) are especially important for stationary and automotive applications. PEMFCs have a polymer electrolyte membrane that physically and electrically separates the anode from the cathode, and serves the critical role of conducting H^+ cations from the anode to the cathode. Polymer electrolytes need to have physical and chemical properties that support cation mobility and mechanical durability. [1-4]

Most hydrogen is produced by the steam reformation of coal or natural gas. This chemical process is shown in equations 1.1 and 1.2. Equation 1.1 is the generalized reaction for steam reformation. Equation 1.2 is the water gas shift reaction. Both of these reactions produce hydrogen but they also leave some carbon monoxide (CO) impurity in the synthesized hydrogen. The platinum catalytic anode in a PEM fuel cell has a low resistance to CO and can be easily

poisoned. The operation costs of fuel cells are increased by either having to have ultra-pure hydrogen or by more frequently replacing the anode of the fuel cell system. [5] There are several common replacements for the platinum anode based on alloying the platinum. Recently, Lee and McBreen developed several alloy replacements based on platinum-ruthenium-carbon, platinum-tin-carbon, and platinum-carbon alloys and found that the platinum-ruthenium-carbon anode had the highest performance. [6] Gotz and Wendt also developed anode replacements based on platinum, ruthenium, tungsten, tin, and molybdenum and found that platinum-ruthenium-tungsten was the superior anode material. [7] There have also been many other combinations used with the general focus on platinum and ruthenium alloyed with transition metals such as chromium, nickel, tin, iron, and gold. [8] CO poisoning of the platinum catalyst at low temperatures necessitates investigation of new polymer systems. The U.S. Department of Energy has set a primary goal for PEM fuel cell that can operate at conditions of 120 °C and 50 % relative humidity with a minimum conductivity of 0.1 S/cm (Siemens per centimeter).

$$C_nH_m + n\,H_2O \xrightarrow{\text{Catalyst}} n\,CO + (n + m/2)\,H_2 \qquad (1.1)$$

$$CO + H_2O \underset{}{\overset{\text{Catalyst}}{\rightleftharpoons}} CO_2 + H_2 \qquad (1.2)$$

Nafion, a sulfonated fluoropolymer, is a widely used polymer electrolyte in PEMFC, because of its chemical stability, mechanical properties, and high conductivity when wet. Nafion's major disadvantages, however, are the cost, poor hydrophobicity, and an ionic conductivity that is dependent on hydration of the membrane. These disadvantages typically limit the operation temperature of a Nafion based PEMFC to less than 80°C. [5]

Nafion membranes have been modified by the incorporation of inorganic moieties, such as silica and titanium oxide, into the polymer matrix to produce hybrid materials with increased

operating temperatures, but with decreased ionic conductivity at all temperatures and relative humidities. It is surmised that the incorporation of these moieties interrupts the hydrophilic channels present in Nafion. [9-11] One exception in these studies is that mesoporous silica with sulfonic acid functionalities shows increased conductivity at high temperature (95° C) over a wide range of relative humidities (50% to 100%). [12]

1.2 – PEG/POSS Hybrid Materials

Polyethylene glycol (PEG) and polyethylene oxide (PEO) based polymers have been shown to conduct small cations in the absence of water. Another similar compound, polypropylene glycol (PPG), also exhibits anhydrous small cation conductivity. Neither PEG nor PPG have the mechanical and chemical stability required for fuel cell operation. However, attachment of PEG or PPG to an inorganic crystalline matrix will result in a hybrid organic/inorganic material that combines the mechanical properties of the inorganic portion with the high anhydrous conductivity of PEG and PPG. [1, 13-19].

Siloxanes have been shown to be easy to functionalize, and are chemically and mechanically stable. [20-24] Siloxanes can be coupled with PEG and polyethylene glycol monomethyl ether (MePEG) by hydrosilylation of an allyl-modified PEG to form the organic/inorganic hybrid. [1, 20, 21, 25-27] The most widely used method for the formation of incompletely condensed siloxanes is the sol-gel condensation of chlorosilanes or alkoxysilanes.

Sol-gel chemistry has been used for the synthesis of ceramics, glasses, and thin films. Recently, sol-gel chemistry has been used to produce ion-conducting polymer electrolytes. [1, 27-29] This method is well-suited to the synthesis of polymer electrolytes due to the ease of polymerization by hydrolysis and condensation of an appropriate polymer precursor.

The chemical and physical properties (structure, thermal and mechanical stability) of the PEG/POSS system are fairly well understood. [1, 13, 14, 27] However, the properties of these materials related to ionic conductivity in polymers are less well understood (i.e. the relationship between free volume, viscosity, density, and ionic conductivity).

1.3 – Ion Transport and Viscoelastic Properties

Viscosity (η) is a physical property intrinsic to all liquid and semi-solid materials (i.e. gels) that describes a liquid's resistance to flow caused by either shear stress or external stress. Viscosity typically has a temperature dependent activation energy that is described by the Vogel-Tamman-Fulcher (VTF) equation (vide infra). Viscosity is a measure of the ratio of the force exerted in the lateral direction to the change in velocity of the fluid as a function of distance and is measured using a rheometer instrument.

There are four types of rheometers; capillary, rotational cylinder, cone and plate, and parallel plate. The capillary rheometer measures the laminar flow of a liquid through a capillary of known dimensions. The other three types of rheometers measure shear stress between two surfaces. Figure 1.1 shows a schematic for the rotational cylinder (A), cone and plate (B), and parallel plate (C) rheometers. [30]

For a rotational cylinder rheometer (Figure 1.1 A), a liquid is placed between two inset cylinders and measures the drag of a liquid on the external cylinder. For a cone and plate rheometer (Figure 1.1 B), the liquid is placed in a cup or on a plate and a shallow cone is rotated across the surface. The viscosity is determined from the resistance to the rotation, the rotation speed and the dimensions of the cone. The parallel plate rheometer (Figure 1.1 C) works in the

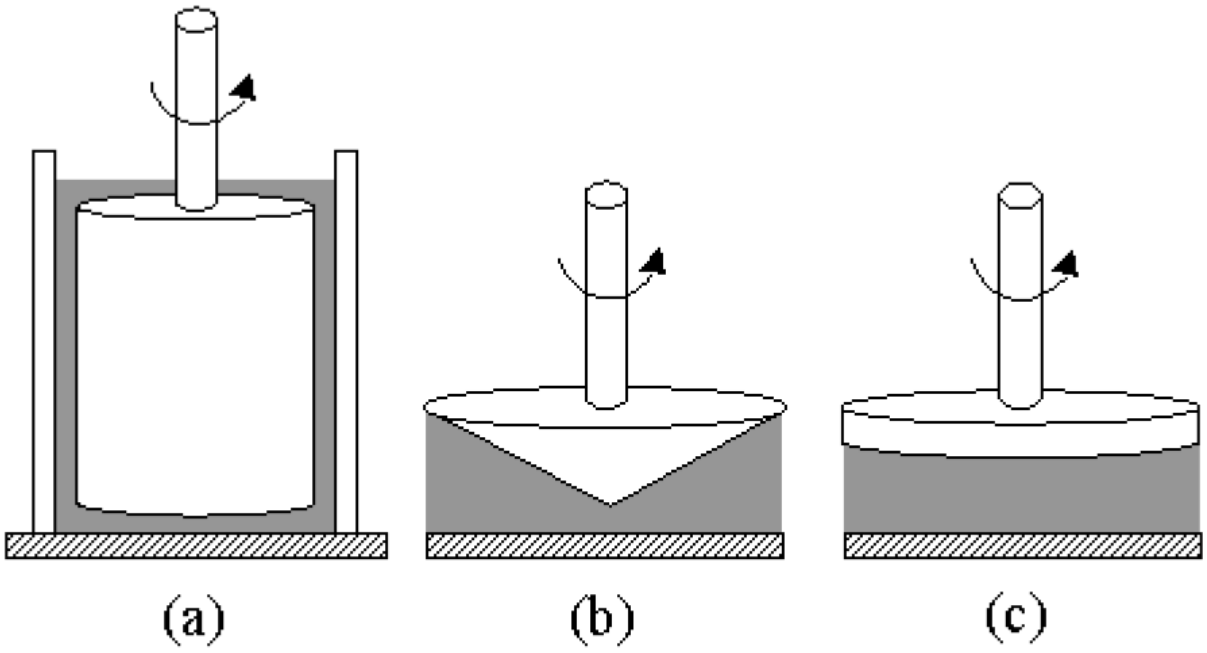

Figure 1.1: Rheometer Schematic. Schematic of rotational rheometers. A is a rotating cylinder rheometer, B is a cone and plate rheometer, and C is a parallel plate rheometer. Taken from reference 30.

same manner as the cone and plate rheometer but has a non-homogeneous velocity profile throughout the depth of the material.

Density (d) is also an intrinsic property of all materials including liquids and sol-gel polymers. The density is also a temperature dependent property (vide infra). The density of a material is its mass divided by volume. Density is experimentally measured by recording the mass of a known volume of sample. In our laboratory, we measure density using a microbalance with micropipettes.

Conductivity (σ) is the ability of a material to either allow small atoms or ions to passively diffuse through or to actively facilitate ionic transport through specific motions. Conductivity is the inverse of resistivity (ρ). Conductivity is a temperature dependent property that strongly depends on the mechanism of the conduction in the material. Ionic conduction in glassy liquid and sol-gel polymers are generally governed by the VTF equation (vide infra). The VTF equation reduces to the Arrhenius equation when the material does not have a temperature dependent activation energy. Obeying the VTF equation indicates that conductivity is likely governed by the reorganization of the segmental units of the polymer.

Conductivity of materials is most commonly measured using ac-impedance spectroscopy. This method applies an ac-potential and monitors the current response, to determine the in phase and out of phase impedances (Z) of the material. The response to the applied ac-potential is then plotted with the real impedance (Z') versus the negative of the imaginary impedance (-Z"), and is referred to as a Cole-Cole plot or a Nyquist plot. For a Nyquist plot, the applied ac-frequency increases from right to left. The impedance is then divided into components based on assumptions about the equivalent circuit elements. [31]

Figure 1.2 shows a typical Nyquist plot and the equivalent circuit for a conductivity

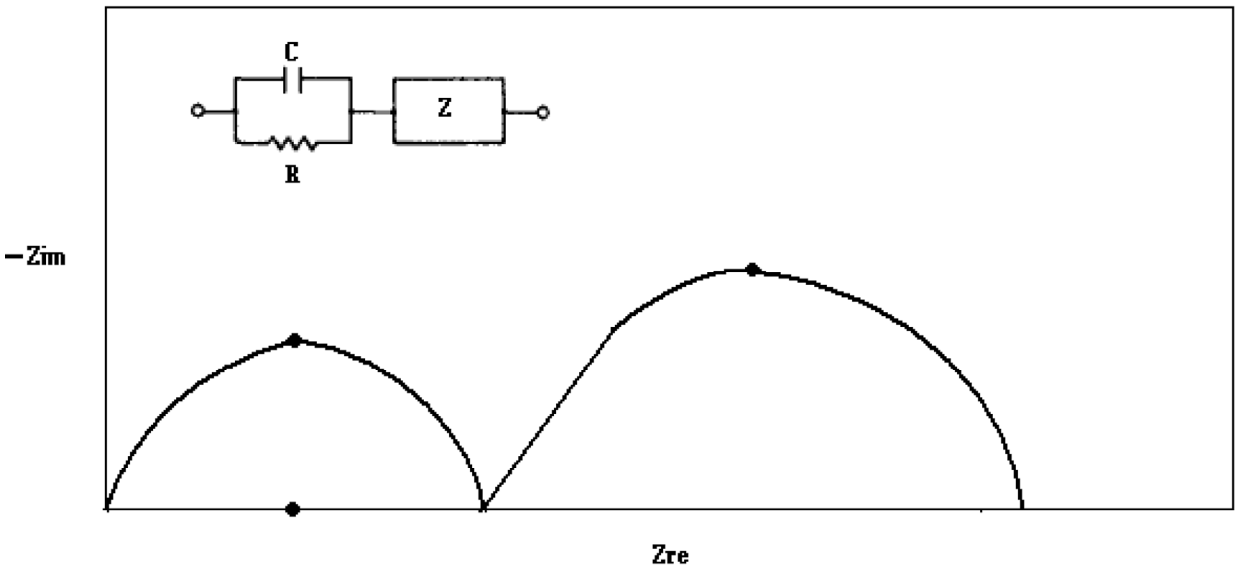

Figure 1.2: AC-Impedance Plot for Conductivity: Typical Nyquist plot for conductivity with its equivalent circuit shown

measurement. In the low frequency part of the plot (right side of plot), there is a skewed semicircle where the right leg is linear with a 45° angle to the real axis. This is referred to as the Warburg region and is represented in the equivalent circuit by the frequency dependent impedance element W (not in Figure 1.2). The Warburg region is where the impedance is controlled by the diffusion of the ionic species from the bulk solution to the electrode surface due to electrostatic attraction (i.e. electrode polarization). At high frequencies (left side of plot), a semicircle is formed that represents the resistance or the bulk conductivity of the material. At low frequencies, the current can draw ionic species from the bulk solution, but at high frequencies the current is alternated between the electrodes at a speed that does not allow electrostatically controlled diffusion from the bulk solution. Due to this, at the low frequencies a concentration gradient is formed that induces diffusion from the bulk solution. The circuit elements that are most important to this area of the Nyquist plot are a capacitor and a resistor in parallel. Because a resistor is a passive circuit element, it gives a completely in-phase response; while, a capacitor gives a 90° out-of-phase response. The bulk resistance is measured along the real impedance axis and bulk capacitance is measured along the imaginary axis. The capacitor represents a capacity that is intrinsic to polymer electrolytes. The high frequency semicircle is generally offset from the y-axis. This offset is due to the electrical resistance of the solution. [32, 33]

This equivalent circuit is similar to the Randle's cell (Figure 1.3), which is one of the most common ac-impedance circuit equivalence models. The difference between the Randle's cell, and the conductivity equivalent circuit, is that the Randle's cell accounts for Faradaic charge transfer to electroactive species; while, there is no charge transfer occurring during conductance of an ionic species. [31] This difference causes the Warburg region in the Nyquist plot in the

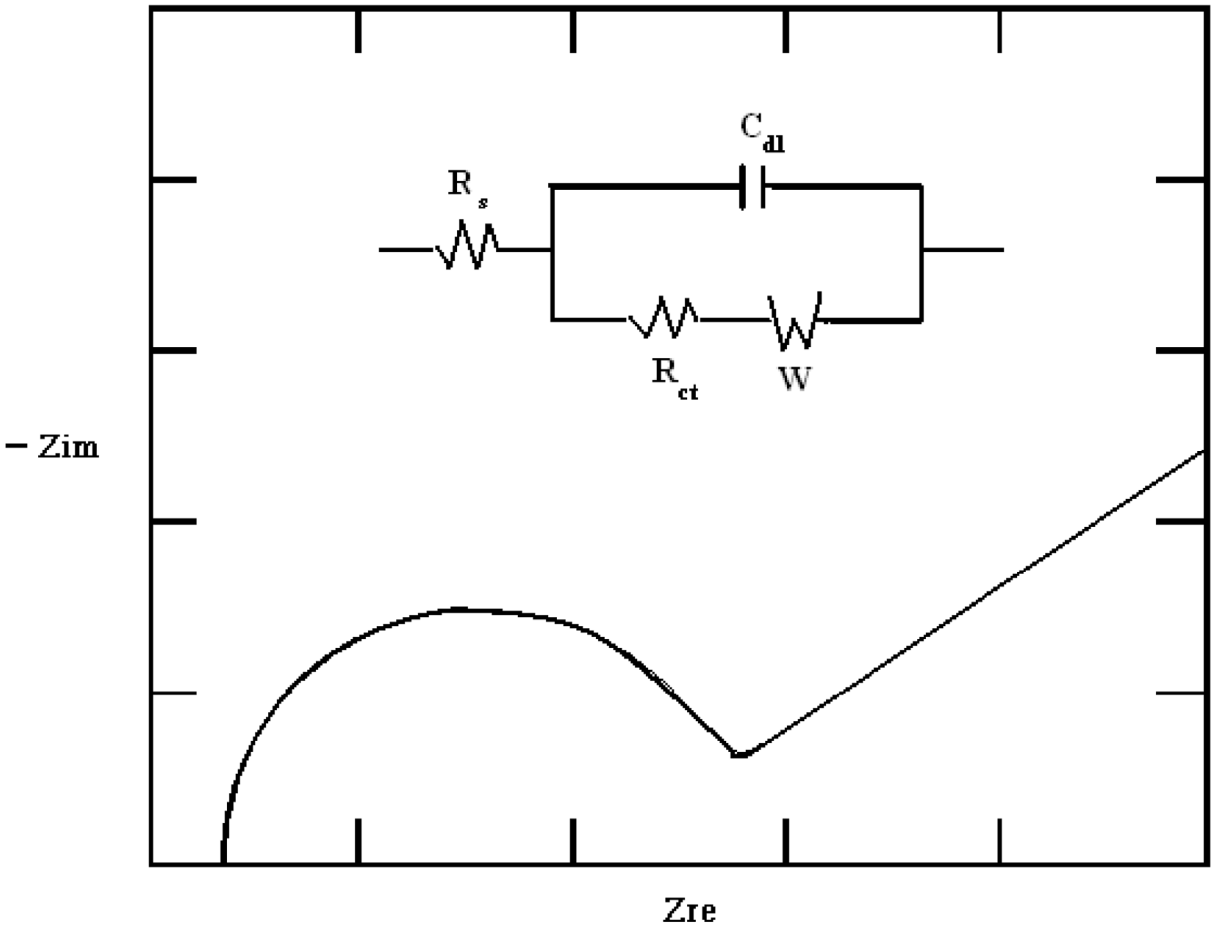

Figure 1.3: Randle's Cell: Typical Nyquist plot for a Randle's cell with its equivalent circuit shown.

Randle's cell not to intercept the semicircle at the real axis but at some value above the real axis.

Bulk ionic conductivity is determined from a Nyquist plot by the diameter of the high frequency semicircle. The diameter along the real axis is the resistance as represented by equation 1.3. In this equation, θ is the cell constant which is related to the geometry of the cell, and is determined by calibration with conductivity standards. The cell constant determined from the calibration is divided by the diameter in the Nyquist plot to calculate the conductivity. [34] Conductivity has the units of Siemens per centimeter (S/cm). Another commonly used unit of ionic mobility is molar equivalent conductivity (Λ), which is the conductivity of a sample divided by the concentration of diffusing species, and has the units of Siemens centimeter squared per mole (S cm^2/mol).

$$\sigma = \frac{1}{\rho} = \frac{\theta}{diam.} \qquad (1.3)$$

The mechanism of ionic conduction has been thoroughly studied and two mechanisms have been proposed and have been experimentally observed. For the vehicle mechanism, the H^+ is associated with a molecule or ion (the vehicle) through a strong hydrogen bond. The vehicle-H^+ complex then diffuses across the conducting material. In this mechanism, the conductivity is dependent on the rate of physical diffusion of the vehicle. For the Grotthus mechanism, the H^+ is handed from one hydrogen bonding site to another across the conducting material. [3]

For the Grotthus mechanism in water, an H^+ is exchanged between water molecules in its vicinity resulting in a net movement of H^+. Li^+ has been shown to follow the Grotthus mechanism in PEG through segmental motions of the ether units which are dependent on the T_g. [2] Similarly, in PEG, the Grotthus mechanism relies on passing the H^+ from one PEG ether oxygen to another along the same molecule or from one molecule to an adjacent molecule. This, also, results in the net movement of H^+ in the material. [3]

1.4 – Free Volume Theory

In free volume theory, all transport properties (η, σ, D, etc.) of a material are dependent on the free volume in the material. [35, 36] The diffusion of a particle through a material is described as a translation across a void in the particle's vicinity. [37] Molar free volume (V_f) is the difference between the total molar volume (V_m), that a mole of molecules is observed to occupy through their volume and molecular vibrations, and the molar van der Waals volume (V_w) that a mole of molecules directly occupy (equation 1.4). [37-39] The observed molar volume (V_m, equation 1.5) is determined using the measured density and molecular weight of the molecule. The van der Waals volume (V_w) is calculated by the group contribution method developed by Bondi where the average values of V_w of each atomic group in a molecule are summed together. [39] Fractional free volume (FFV, equation 1.6) is the ratio of molar free volume (V_f) to total molar volume (V_m). Fractional free volume is independent of size of the polymer and is a useful property for comparing materials. [39-41]

$$V_f = V_m - V_w \tag{1.4}$$

$$V_m = \frac{MW}{d} \tag{1.5}$$

$$FFV = \frac{V_f}{V_m} = \frac{(V_m - V_w)}{V_m} \tag{1.6}$$

The Vogel-Tammann-Fulcher (VTF) equation was developed to describe the temperature dependent activation energies of different transport properties. In the general form of the equation (eq. 1.7), y is the transport property, and A_y and D_y are constants specific to that property. A_y is a constant that is related to the pre-exponential constant in the Arrhenius equation, and D_y is the activation energy for the transport process. The temperature T_0, is the ideal, or infinitely slow cooling glass transition temperature, and is generally taken as

approximately 50 °C below the conventional glass transition temperature (T_g). [42-44] The constant B is similar to the activation energy, with units of temperature, observed in the Arrhenius equation and generally is used as the activation energy for systems that obey the VTF equation.

$$y = A_y T^{-1/2} \exp\left[\frac{-D_y T_0}{(T - T_0)}\right] \qquad \text{VTF} \qquad (1.7)$$

The VTF equation can be modified to model both viscosity (eq. 1.7a) and conductivity (eq. 1.7b). Both of these equations can be plotted similarly to an Arrhenius-style activation plot with log(y) vs. 1000/T.

$$1/\eta = -A \exp\left[\frac{B}{(T - T_0)}\right] \qquad (1.7a)$$

$$\sigma = A T^{-1\backslash 2} \exp\left[\frac{-B}{(T - T_0)}\right] \qquad (1.7b)$$

The Stokes-Einstein equation (eq. 1.8) and the Nernst-Einstein equation (eq. 1.9) predict that a higher polymer fluidity (i.e. smaller viscosity) will increase both the diffusion coefficient of a mobile ion, and the resulting ionic conductivity caused by this increase in ionic mobility. [45]

$$D_{phys} = \frac{kT}{6\pi\eta R_H} \qquad \text{Stokes-Einstein eq.} \qquad (1.8)$$

$$\sigma_{ION} = \frac{F^2}{RT}\left[z_+^2 D_+ C_+ + z_-^2 D_- C_-\right] \qquad \text{Nernst-Einstein eq.} \qquad (1.9)$$

Walden's rule (eq. 1.10a) further explores the relationship between fluidity and conductivity, and appears to be generally true for ideal solutions where no ion-ion interactions exist (Λ is molar equivalent conductivity, and η is viscosity). [45] However, for real electrolyte

solutions, Angell has suggested the fractional Walden rule (eq. 1.10b) as a better descriptor of ionic mobility in electrolytes with ion-ion interactions. [46, 47] In the fractional Walden Rule, α is a constant between zero and unity where $\alpha = 1$ represents ideal behavior (i.e. viscosity is the only force impeding the mobility of ions), and $0 < \alpha < 1$ represents the presence of other forces, such as ion-pairing, impeding ion mobility.

$$\Lambda\eta = \text{constant} \qquad \text{Walden's Rule} \qquad (1.10a)$$

$$\Lambda\eta^{\alpha} = \text{constant} \qquad \text{Fractional Walden's rule} \qquad (1.10b)$$

Doolittle developed an empirical formula to describe the viscosity/free volume relationship. [36, 48] In Doolittle's equation (equation 1.11), A and q are material specific constants and v_m and v_f are the molecular volume and free volume respectively. A is the fluidity extrapolated to zero free volume and q is a measure of the intermolecular forces within a liquid. [48] The ratio v_m/v_f is mathematically equivalent to the inverse of fractional free volume (1/FFV) so Doolittle's equation can be rewritten as equation 1.11a. This predicts that a smaller fractional free volume will result in a smaller fluidity (fluidity = viscosity^{-1}).

$$\frac{1}{\eta} = A\exp\left[-q\frac{v_m}{v_f}\right] \qquad \text{Doolittle's eq.} \qquad (1.11)$$

$$\frac{1}{\eta} = A\exp\left[\frac{-q}{FFV}\right] \qquad (1.11a)$$

Cohen and Turnbull combined the Stokes-Einstein equation (eq. 1.8) with the Doolittle equation (eq. 1.11), resulting in equation 1.12. [37] The Cohen-Turnbull equation shows that a larger free volume will increase the diffusion coefficient. Forsythe combined the Nernst-Einstein equation (eq. 1.9) with the Cohen-Turnbull equation (eq. 1.12) to obtain equation 1.13. [49]

Forsythe's equation also predicts that an increase in fractional free volume should increase the conductivity.

$$D = A\exp\left[-\frac{\gamma}{FFV}\right] \qquad \text{Cohen-Turnbull eq.} \quad (1.12)$$

$$\sigma = \left(\frac{ACF^2Z^2}{RT}\right)\exp\left[\frac{-\gamma}{FFV}\right] \qquad \text{Forsythe eq.} \quad (1.13)$$

1.5 – Thermal Properties

Differential scanning calorimetry (DSC) measurements can be used to determine several important thermal properties of polymers such as the glass transition temperature (T_g), specific heat capacity (C_p), crystallization temperature (T_c) and melting temperature (T_m). Figure 1.4 shows a representative plot of temperature versus heat flow taken by DSC. The thermal properties mentioned are denoted on the plot where applicable. Not all polymers will exhibit a T_g, T_c or a T_m.

The glass transition temperature of a polymer is one of the most important thermal properties of a glassy polymer. Below the glass transition temperature, the material is inflexible, free volume is at a constant minimum, and the material has reached its maximum stiffness and viscosity (>10^{13} P at T_g).[50] Below T_g, the reorganization of polymer units ceases and the polymer units are locked into configuration without any crystalline order (i.e. amorphous glass or vitreous state). Figure 1.5 depicts the behavior of the free volume of a polymer near the glass transition; below the glass transition, the polymer has a constant free volume and is at its minimum. As a material heats to the glass transition, the free volume rises rapidly until a temperature sufficiently above the glass transition (rubber phase). When the polymer reaches a

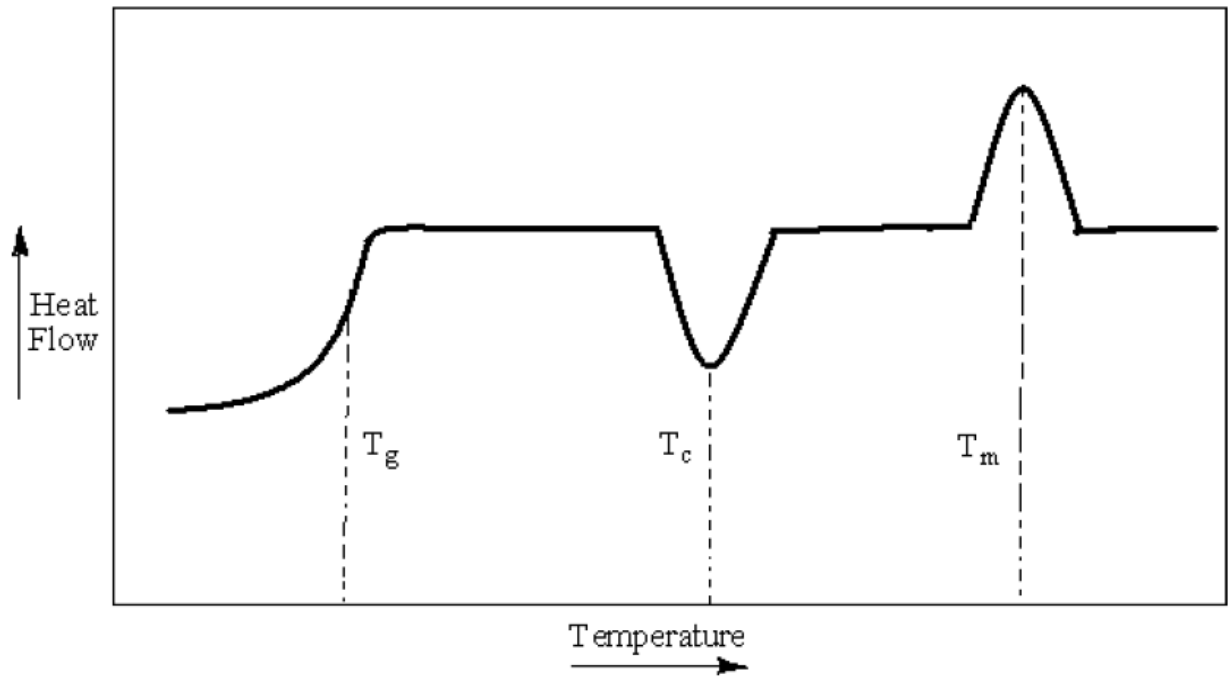

Figure 1.4: Representative DSC Plot: Representative plot of temperature versus heat flow data taken by DSC for a polymer.

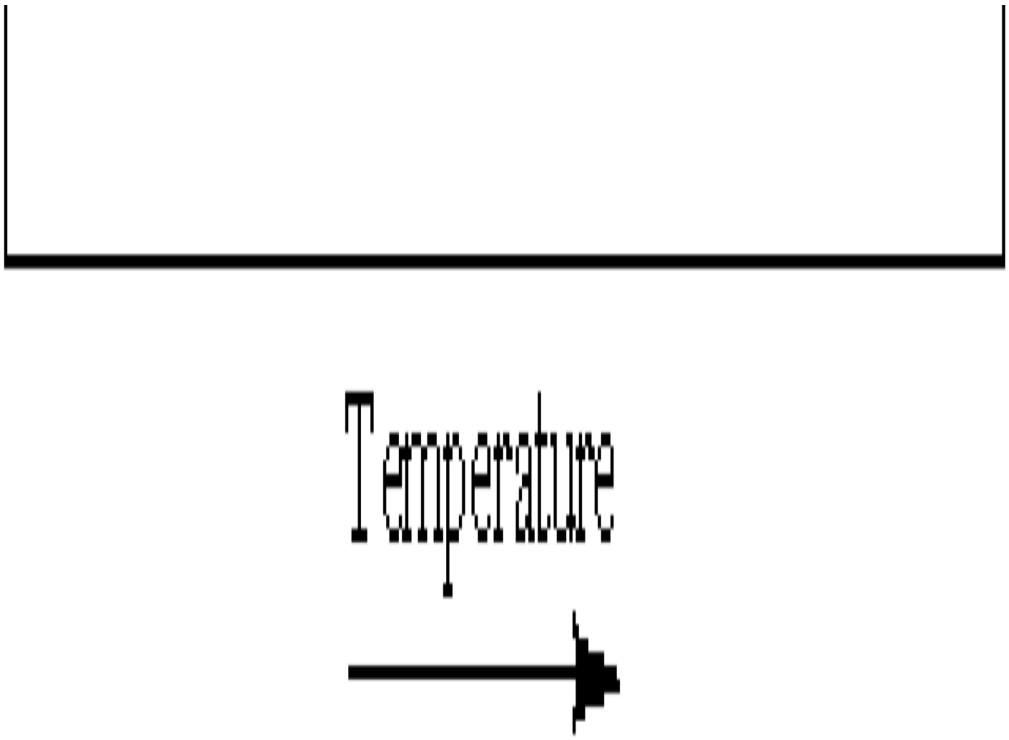

Figure 1.5: Free Volume/Temperature Relationship: Depiction of the effects of temperature on free volume near the glass transition temperature

sufficiently high temperature the free volume increases but not as rapidly as during the glass transition. In general the free volume of the polymer is directly related to T_g where a lower T_g reflects a lower free volume. These properties of materials in the vitreous state make them ineffectual for H^+ conductivity due to the low free volume, high viscosity and lack of molecular motion (the Grotthus mechanism depends on molecular motion).[51]

The specific heat capacity of a material is the amount of energy that it takes to increase the temperature of one gram of the material by one Kelvin. This property gives insight as to how a material will react when heat is applied over time. The heat capacity for a material in any state can be determined from DSC experiments. The heat capacity is given by equation 1.14 where (q/t) is the heat flow per second of the measurement and (ΔT/t) is the change in temperature per second (experimental constant). A higher heat capacity will allow a material to absorb heat with smaller increases in temperature, this would allow for materials to be manipulated for high temperature applications where thermal stability is required.

$$\frac{(q/t)}{\Delta T/t} = \frac{q}{\Delta T} = C_p \qquad (1.14)$$

The crystallization temperature (T_c) and melting temperature (T_m) are properties not held by every polymer. Some polymers have domains that when heated to a specific temperature range can rearrange from the amorphous phase into the crystalline phase, this temperature is the T_c. These crystalline domains will melt when further heated, this temperature is the T_m. For many polymers, in the amorphous phase there exist small domains that are crystalline; at T_c more domains change phase from amorphous to crystalline. A crystal has similar properties to the vitreous state in a polymer, in that, free volume is constant and the crystalline domains in the material have reached maximum stiffness and viscosity (>10^{13} P). The crystalline state is different from the vitreous state, because, the molecules are arranged in a repeatable, nonrandom

manner. The packing may be less efficient than expected when there are strong intermolecular forces such as hydrogen bonding, resulting in a larger than expected amount of free volume. Some amorphous polymers do not have crystalline domains and therefore do not exhibit these properties. As with the vitreous state, materials in the crystalline state are ineffectual for H^+ conductivity.[51]

1.6 – Acid Dissociation

The fractional Walden rule (eq. 1.10b) was developed because of the non-ideality of electrolyte solutions. The exponent α is included to account for effects such as ion-ion pairing. In PEMFC systems, generally an acid (proton donor) is present as an initial source of protons. This acid is either a small molecule added into the polymer solution or covalently attached to the polymer as a carboxylic or sulfonic acid group.[5] The acid must be a strong acid in order to reduce the ion-ion pairing that can impede proton conductivity.

The acid dissociation constant (K_a) in aqueous systems is generally determined by a pH titration with a strong base, represented by equation 1.15. In the equation, HA is a weak acid and B^- is a strong base; the base can be either negatively charged or neutral. A^- is the conjugate base of the weak acid and HB is the conjugate acid of the strong base. The hydrogen ion concentration is usually reported as the pH, which is related by equation 1.16. K_a is the acid dissociation constant and often is reported as pK_a which has the same relationship pH has to $[H^+]$. A pH meter measures the activity of an ion instead of directly measuring the ion concentration; the relationship between activity and hydrogen ion concentration is given in equation 1.17. In equation 1.17, γ is the activity coefficient and is related to the ionic strength of the solution and is defined by the Debye-Hückel equation (equation 1.18) where z is the charge of the chemical

species, A and B are solvent dependent constants, I is the ionic strength and a_i is the distance of closest approach . For dilute solutions, the value of the denominator approaches 1 resulting in the Debye-Hückel limiting equation (equation 1.19). For this situation, the activity coefficient is proportional to the ionic strength which is defined by equation 1.20 where C is the concentration and z is the charge of the *i*th ion. The thermodynamic acid dissociation constant (K_a^T) is related to the measured acid dissociation constant (K_a^M) by equation 1.21. K_a is related to the activities of species present by equation 1.22. In equation 1.22, the mean activity coefficient is included as a correction factor to account for non-ideality in the solution. For weak monoprotic acids, pH is related to pK_a and the ion concentrations by the well known Henderson-Hasselbalch equation (equation 1.23). When the activities are substituted into the Henderson-Hasselbalch equation it reduces to equation 1.23.

$$HA + B^- \underset{}{\overset{K_a}{\rightleftharpoons}} A^- + HB \qquad (1.15)$$

$$pH = -\log_{10}\left[H^+\right] \qquad (1.16)$$

$$a_{H^+} = \left[H^+\right]\gamma_{H^+} \qquad (1.17)$$

$$-\log\gamma_i = \frac{Az^2\sqrt{I}}{1+Ba_i\sqrt{I}} \qquad \text{Debye-Hückel equation} \qquad (1.18)$$

$$-\log\gamma_i = Az_i^2\sqrt{I} \qquad \text{Debye-Hückel limiting} \qquad (1.19)$$

$$I = \frac{1}{2}\sum C_i z_i^2 \qquad (1.20)$$

$$pK_a^T = pK_a^M + 0.507\sqrt{I} \qquad (1.21)$$

$$K_a^T = \frac{a_{H^+}a_{A^-}}{a_{HA}} \qquad (1.22)$$

$$pK_a^M = pH + \log\frac{[HA]}{[A^-]} \qquad \text{Henderson-Hasselbalch} \qquad (1.23)$$

Recently a pH titration has been employed to determine the pK_a of several acids in organic solvent/water binary systems. [52-54] The method involves measuring the pK_a in a series of binary organic/ water solvent systems of differing mole fractions. This data was then used to estimate the pK_a of the organic acids in water by plotting pK_a versus mole fraction of water. Extrapolation of the gathered data to a water mole fraction of 1 yields an estimated pK_a in water. Estimating the pK_a of an organic acid in an organic solvent would be possible using this method. The pKa can be used to determine the relative acidity of an organic acid in a particular solvent by comparing the solvent's pK_a to the organic acid's pK_a

II. EXPERIMENTAL METHODS

This chapter is focused on the synthesis of the MePEG and MePPG based copolymers and the $MePEG_7SO_3H$ acid. Included in this chapter are the experimental methods used to characterize the synthesized copolymers and the $MePEG_7SO_3H$ acid.

2.1 – Materials

Polyethylene glycol monomethyl ether ($CH_3(OCH_2CH_2)_nOH$ = $MePEG_nOH$, M_n = 164, 350, 550, 750, n = 3, 7.24, 12.0, 16.3; Aldrich) was dried at 60º C under vacuum for approximately 24 hours prior to use. This dissertation will refer to tri(ethylene glycol) monomethyl ether MW =164, as $MePEG_3OH$, the poly(ethylene glycol) monomethyl ether M_n = 350, as $MePEG_7OH$, M_n = 550 as $MePEG_{12}OH$, and M_n = 750 as $MePEG_{16}OH$. Triethoxysilane (Aldrich), diphenyl dimethoxysilane (Ph_2Si) (Aldrich), 3,3,3-trifluoropropyl trichlorosilane (TFPSi) (Aldrich), isopropyl trimethoxysilane (iBuSi) (Aldrich) were all used as received.

Polypropylene glycol monomethyl ether ($CH_3(OCH(CH_3)\text{-}CH_2)_nOH$ = $MePPG_nOH$, M_n = 148.2, 206.3, n = 2, 3; Aldrich) was dried at 60º C under vacuum for approximately 24 hours prior to use. For simplicity, this paper will refer to tri(propylene glycol) monomethyl ether M_n = 206.3 as $MePPG_3OH$, di(propylene glycol) monomethyl ether M_n = 148.2 as $MePPG_2OH$, poly(ethylene glycol) monomethyl ether M_n = 350 as $MePEG_7OH$, $MePEG_7$ and $MePPG_3$ copolymers as $MePEG_7/MePPG_3$, $MePEG_7$ and $MePPG_2$ copolymers as $MePEG_7/MePPG_2$, and $MePPG_3$ and $MePPG_2$ copolymers as $MePPG_3/MePPG_2$.Triethoxysilane (Aldrich), allyl bromide (Acros), and sodium sulfite (Fischer) were all used as received. Amberlite IRA-400(Cl) anion

exchange resin (Aldrich) and Amberlite IR-120H cation exchange resin (Aldrich) were used as received. Phosphorus tribromide was prepared as a 1.98 M solution in dry diethyl ether using 55.91 g phosphorus tribromide dissolved into 85 mL of ether. Sodium hydride (Aldrich) was rinsed thoroughly with hexanes and filtered prior to use to remove any mineral oil. Dry tetrahydrofuran (THF) and diethyl ether (Et_2O) were obtained from a Distillation Dispensary System, under argon, immediately prior to use, and kept under an inert atmosphere.

2.2 – Methods

2.2.1 – Density

The density of the polymer samples was measured gravimetrically by drawing the neat liquid into a tared 2 μL micropipette which was weighed using an ATI Cahn C-33 microbalance. [27] The sample mass was then divided by the 2 μL volume to yield the density. Concentrations of $MePEG_7SO_3H$ acid were calculated by dividing the density (g/mL) of the neat acid by the molecular weight (g/mol) yielding mol/mL with values being reported as mol/L. The concentrations of the $MePEG_7SO_3H$ acid / $MePEG_n$ Copolymer mixtures were calculated by converting the mass of both the acid and the polymer to volume using their respective densities. Then the mass of acid was converted to moles by using the acid's molecular weight and was divided by the total volume of the acid plus polymer. This method specifically assumes that the volumes are additive.

$$concen_{sample} = \frac{density(g/cm^3)}{MW(g/mol)} = \frac{mol}{cm^3} \qquad (2.1)$$

2.2.2 – Viscosity

The viscosity of the polymer samples was measured using a Brookfield DV-III Ultra Programmable Rheometer. A CPE-40 spindle was used and the viscosities measured under a

flow of dry nitrogen at 3 different rotational speeds which were averaged. The rotational speeds were selected to keep the torque in a range of 10-100%. The samples were dried at 50 °C under vacuum prior to measurement.

2.2.3 – Gel Permeation Chromatography

Gel permeation chromatography (GPC) measurements were performed using a Polymer Laboratories ELS-2100 evaporative light scattering detector with two 30 cm PL Mixed-D analytical columns. Polystyrene molecular weight standards (PL-EasiCal PS-2, MW range 580-480,000) were used to calibrate the MW range prior to running unknown samples. THF was then allowed to elute through the column for 30 minutes to remove any remaining samples and to equilibrate the system. Unknown samples were made by dissolving 2-3 mg of sample in 1 g THF.

2.2.4 – Conductivity

AC-impedance measurements were performed using a PAR 283 potentiostat equipped with a Perkin-Elmer 5210 lock-in amplifier. [27] Dried electrolyte solutions of the $MePEG_7SO_3H$ and $MePEG_n$ siloxane polymers were cast onto locally constructed electrodes, sealed upright in a jacketed vacuum cell connected to a vacuum pump and temperature controlled water circulator. Prior to measurement, the samples were dried under vacuum at 55°C until the measured conductivity values did not change (12-24 hrs). Conductivity is determined from a Nyquist plot by the diameter of the high frequency semicircle. The diameter is equivalent to the bulk resistance by equation 2.2, where θ is the cell constant, which is related to the geometry of the cell and is determined by calibration with NIST low conductivity standards. [34]

$$\sigma = \frac{1}{\rho} = \frac{\theta}{diam.} \qquad (2.2)$$

2.2.5 – DSC

Differential scanning calorimetry was performed using a Perkin-Elmer DSC 4000. The DSC spectra were collected from -70 °C to 200 °C. The samples were held at -70°C for 2 minutes and then heated at 10 °C/min to 200 °C and held there for 2 minutes. The spectra were normalized by dividing the heat flow by the sample mass. The heat capacity was calculated using equation 1.14. The glass transition temperature (T_g) was determined as the inflection point of the sigmoidal region of the DSC heat flow curve.

2.2.6 – NMR

Nuclear magnetic resonance (NMR) measurements were made with either a Bruker AC-300 or a Bruker DRX-500 instrument.

2.2.7 – Ion Exchange

Strong acid, ion exchange columns were prepared by placing 50 mL (95 meq) of Amberlite IR-120H ion exchange resin (1.9 meq/mL) in a chromatography column with a porous frit. Hydrochloric acid (1 M, 300 mL, 300 meq) was allowed to flow through the column to exchange all of the cation sites to H^+. Deionized water was then allowed to flow through the column until the pH of the column was near neutral pH (~6.0-8.0). A strong base exchange column was similarly prepared with 50 mL (70 meq) of Amberlite IRA-400(Cl) ion exchange resin (1.4 meq/mL), followed by charging with sodium hydroxide (1 M, 225 mL, 225 meq), and rinsing with deionized water to a near neutral pH.

2.2.8 – pH Titration

pH was measured using a Fisher Scientific Accumet AB15 pH meter equipped with an Accumet combination pH electrode. The pH titrations were performed using 0.01 M $MePEG_7SO_3H$ acid concentration and 0.1 M triethylamine as the strong base. pH was recorded at

intervals until the end point which was taken to be the point where addition of base only slightly increased the pH. Titrations were performed in a series binary solution consisting of $MePEG_7OH$ and deionized water varying the mole fraction (X) of $MePEG_7OH$ from 0.0 to 0.8.

2.3 – Bulky Copolymer Synthesis

2.3.1 – Synthesis of Poly(ethylene glycol) Allyl Methyl Ether ($MePEG_3OCH_2CHCH_2$) (2a)

These compounds were prepared according to previous reports. [1, 27, 55] For this method, NaH (4.12 g, 172 mmol, 1.1 equivalents) and THF (40 mL) were added to an air free round bottom flask and were slurried. Dried tri(ethylene glycol) methyl ether ($MePEG_3OH$, 25.30 g, 154.3 mmol) was dissolved in dry THF (20 mL) and was added dropwise to the slurry. The mixture was stirred under argon for a half hour at room temperature to allow for complete deprotonation. Allyl bromide (18.77 g, 155.1 mmol, 1 equivalent) was dissolved in THF (20mL) and was added dropwise to the slurried mixture. A white precipitate of NaBr was formed upon reaction. The reaction was stirred over night at room temperature to complete the reaction. Approximately 10 mL of isopropyl alcohol was added to the reaction mixture to quench any unreacted NaH. The precipitate was removed by gravity filtration and the filtrate was extracted with 50 mL 0.5 M NaCl solution and three washings of chloroform. The organic layers were combined and dried over Na_2SO_4. The Na_2SO_4 was removed by gravity filtration and the product was concentrated by rotary evaporation. A clear colorless viscous liquid (**2a**) was recovered (23.65 g, 115.9 mmol, 75.15% yield). NMR (^1H, in $CDCl_3$), δ (ppm) 3.32 (s, 3H), 3.51-3.70 (m, 12H), 3.96 (m, 2H), 5.18 (dd, 2H), 5.84 (m, 1H). NMR (^{13}C, in $CDCl_3$), δ (ppm) 58.43, 68.94, 70.01-70.12, 71.44, 71.44, 116.32, 134.37.

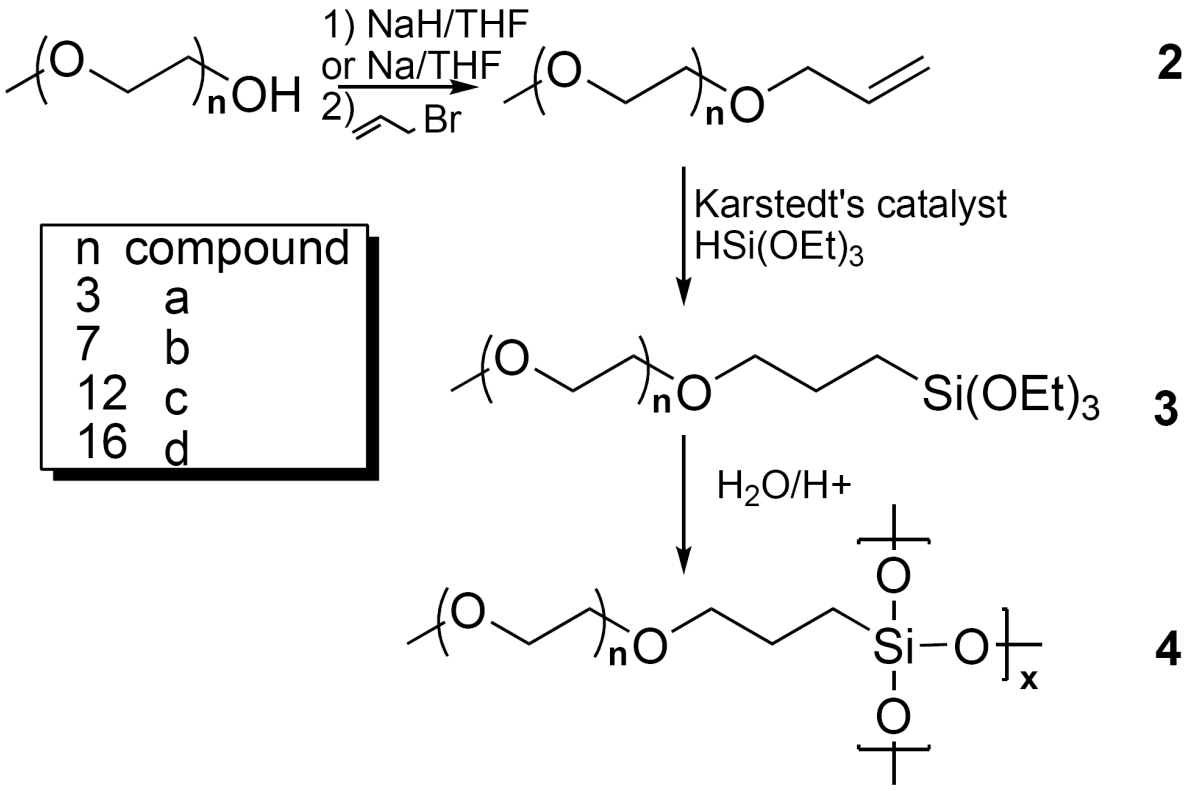

Figure 2.1: Polymer Synthesis: Synthesis of MePEG polymers

2.3.2 – Synthesis of Poly(ethylene glycol) Allyl Methyl Ether ($MePEG_7OCH_2CHCH_2$) (2b)

$MePEG_7OCH_2CHCH_2$ (**2b**) was prepared in the same manner as $MePEG_3$-OCH_2CHCH_2 (**2a**) using the following: Na (2.03 g, 88.26 mmol), $MePEG_7OH$ (20.27 g, 57.91 mmol), and allyl bromide (7.01 g, 57.98 mmol). A clear colorless liquid (**2b**) was recovered (23.88 g, 61.23 mmol, 105.7% yield). We conclude that the excess yield was due to absorption of water and polar solvents by the highly hydroscopic product. NMR (^1H, in $CDCl_3$), δ (ppm) 3.35 (s, 3H), 3.48-3.80 (m, 28H), 3.99 (m, 2H), 5.18 (dd, 2H), 5.88 (m, 1H). NMR (^{13}C, in $CDCl_3$), δ (ppm) 58.52, 68.91, 70.00-70.11 (several peaks), 71.41, 71.68, 116.55, 134.28.

2.3.3 – Synthesis of Poly(ethylene glycol) Allyl Methyl Ether ($MePEG_{12}OCH_2CHCH_2$) (2c)

$MePEG_{12}OCH_2CHCH_2$ (**2c**) was prepared in the same manner as $MePEG_3$-OCH_2CHCH_2 (**2a**) using the following: NaH (1.46 g, 60.8 mmol), $MePEG_{12}OH$ (26.66 g, 48.5 mmol), and allyl bromide (5.97 g, 49.3 mmol). A clear colorless liquid (**2c**) was recovered (22.78 g, 38.6 mmol, 79.7 % yield). NMR (^1H, in $CDCl_3$), δ (ppm) 3.38 (s, 3H), 3.5-3.76 (m, 48H), 4.02 (m, 2H), 5.26 (dd, 2H), 5.91 (m, 1H). NMR (^{13}C, in $CDCl_3$), δ (ppm) 58.51, 68.89, 69.99-70.09, 71.39, 71.67, 116.55, 134.26.

2.3.4 – Synthesis of Poly(ethylene glycol) Allyl Methyl Ether ($MePEG_{16}OCH_2CHCH_2$) (2d)

Compound $MePEG_{16}OCH_2CHCH_2$ (**2d**) was prepared in the same manner as $MePEG_3OCH_2CHCH_2$ (**2a**) using the following: NaH (0.98 g, 40.8 mmol), $MePEG_{16}OH$ (21.24 g, 28.3 mmol), and ally bromide (3.63 g, 30.0 mmol). A colorless waxy solid (**2d**) was recovered (21.16g, 26.8 mmol, 94.7% yield) NMR (^1H, in $CDCl_3$), δ (ppm) 3.32 (s, 3H), 3.5-3.68 (m, 64H), 3.96 (m, 2H), 5.17 (dd, 2H), 5.85 (m, 1H). NMR (^{13}C, in $CDCl_3$), δ (ppm) 58.51, 68.89, 69.99-70.09, 71.39, 71.67, 116.55, 134.26.

2.3.5 – Synthesis of Polymer Precursor ($MePEG_3OCH_2CH_2CH_2Si(OEt)_3$) (3a)

$MePEG_3$ monomer was prepared by the following procedure: [1, 27, 55] Triethoxysilane (12.09 g, 73.6 mmol) and **2a** (15.00 g, 73.5 mmol) were added to an air-free Schlenk tube. Karstedt's catalyst (~ 30 μL) was added to the Schlenk tube, which was then heated to 60 °C under argon. NMR were taken periodically until it showed a complete disappearance of the allyl protons. The reaction mixture was heated to 50 °C under vacuum for 15 minutes to remove excess triethoxysilane. The Karstedt's catalyst was removed with activated charcoal in THF under inert atmosphere, followed by gravity filtration. The THF was removed by rotary evaporation. A clear colorless liquid (**3a**) was recovered (22.41 g, 60.9 mmol, 82.85 % yield). NMR (^1H, in $CDCl_3$), δ (ppm) 0.64 (m, 2H), 1.21 (m, 9H), 1.55 (m, 2H), 3.34 (s, 3H), 3.39 (m, 2H), 3.52-3.68 (m, 12H), 3.77 (m, 6H).

2.3.6 – Synthesis of Polymer Precursor ($MePEG_7OCH_2CH_2CH_2Si(OEt)_3$) (3b)

$MePEG_7$ monomer (**3b**) was prepared in the same manner as $MePEG_3$ monomer (**2a**) using the following: triethoxysilane (9.52 g, 58.0 mmol), **2b** (22.45 g, 57.6 mmol), Karstedt's catalyst (~30 μL). A clear colorless liquid (**3b**) was recovered (20.49 g, 36.9 mmol, 64.1% yield). NMR (^1H, in $CDCl_3$), δ (ppm) 0.59 (m, 2H), 1.20 (m, 9H), 1.65 (m, 2H), 3.35 (s, 3H), 3.39 (m, 2H), 3.50-3.63 (m. 28H), 3.80 (m, 6H).

2.3.7 – Synthesis of Polymer Precursor ($MePEG_{12}OCH_2CH_2CH_2Si(OEt)_3$) (3c)

$MePEG_{12}$ monomer (**3c**) was prepared in the same manner as $MePEG_3$ monomer (**3a**) using the following: triethoxysilane (6.36 g, 38.7 mmol), **2c** (22.78 g, 38.6 mmol), Karstedt's catalyst (~30 μL). A clear colorless liquid (**3c**) was recovered (20.06 g, 26.6 mmol, 68.91 %). NMR (^1H, in $CDCl_3$), δ (ppm) 0.62 (m, 2H), 1.22 (m, 9H), 1.59 (m, 2H), 3.38 (s, 3H), 3.40 (m, 2H), 3.54-3.64 (m, 48H), 3.84 (m, 6H).

2.3.8 – Synthesis of Polymer Precursor ($MePEG_{16}OCH_2CH_2CH_2Si(OEt)_3$) (3d)

$MePEG_{16}$ monomer (**3d**) was prepared in the same manner as $MePEG_3$ monomer (**3a**) the following: triethoxysilane (4.50 g, 27.4 mmol), **2d** (21.16 g, 26.8 mmol), Karstedt's catalyst (~30 μL). A clear colorless liquid (**3d**) was recovered (14.67 g, 15.4 mmol, 57.5% yield). NMR (^1H, in $CDCl_3$), δ (ppm) 0.62 (m, 2H), 1.23 (m, 9H), 1.61 (m, 2H), 3.39 (s, 3H), 3.41 (m, 2H), 3.54-3.67 (m, 64H), 3.86 (m, 6H).

2.3.9 – Preparation of Sol-Gel Polymer ($MePEG_3OCH_2CH_2CH_2SiO_{1.5}$) (4a)

$MePEG_3$ polymer was polymerized according to the following procedure: [27, 55] an excess (6 equivalents) of acidic water (pH ~ 3, one drop conc. HCl in 100 mL water) was added to **3a** (6.490 g, 17.64 mmol) in a sample vial. The solution was mixed well and was allowed to hydrolyze at room temperature for 12h to 24h. The excess water and ethanol were then removed by rotary evaporation and the resulting gel placed in a vacuum oven at 60 ºC for 24 hr. The resulting gel (**4a**) was a clear colorless viscous liquid. GPC analysis showed one peak with an M_w value of 2929 Da (M_n = 2023, PDI= 1.4478). NMR (^1H, in $CDCl_3$), δ (ppm) 0.63 (broad, 2H), 1.69 (broad, 2H), 3.39 (s, 3H), 3.42 (broad, 2H), 3.51-3.80 (m, 12H).

2.3.10 – Preparation of Sol-Gel Polymer ($MePEG_7OCH_2CH_2CH_2SiO_{3/2}$) (4b)

$MePEG_7$ polymer (**4b**) was polymerized in the same manner as $MePEG_3$ polymer (**4a**) using the following: **3b** (7.96 g, 14.4 mmol). The resulting gel (**4b**) was a clear colorless viscous liquid. GPC analysis showed two peaks with M_w values of 3620 Da (M_n = 2932, PDI = 1.2347) and 483 Da (M_n = 343, PDI = 1.4082). NMR (^1H, in $CDCl_3$), δ (ppm) 0.62 (broad, 2H), 1.61 (broad, 2H), 3.37 (s, 3H), 3.42 (broad, 2H), 3.43-3.73 (m, 28H).

Polymer		Mass (g) MePEG	mmol MePEG	Mass (g) copolymer	mmol copolymer	X copolymer
$MePEG_3$	**4a**	6.490	17.64	———	———	———
$MePEG_3/Ph_2Si$	**5a**	5.003	19.47	0.509	2.57	0.117
$MePEG_3$/TFPSi	**6a**	5.005	19.47	0.517	3.47	0.151
$MePEG_3$/iBuSi	**7a**	5.272	20.51	0.541	5.06	0.198
$MePEG_7$	**4b**	7.960	14.37	———	———	———
$MePEG_7/Ph_2Si$	**5b**	4.223	9.53	0.456	2.30	0.195
$MePEG_7$/TFPSi	**6b**	4.178	9.43	0.423	2.84	0.231
$MePEG_7$/iBuSi	**7b**	3.998	9.02	0.402	3.76	0.294
$MePEG_{12}$	**4c**	3.260	4.32	———	———	———
$MePEG_{12}/Ph_2Si$	**5c**	2.525	3.93	0.266	1.34	0.255
$MePEG_{12}$/TFPSi	**6c**	2.584	4.02	0.266	1.79	0.308
$MePEG_{12}$/iBuSi	**7c**	3.247	5.05	0.320	2.99	0.372
$MePEG_{16}$	**4d**	1.600	1.68	———	———	———
$MePEG_{16}/Ph_2Si$	**5d**	4.020	4.77	0.400	2.02	0.298
$MePEG_{16}$/TFPSi	**6d**	5.030	5.97	0.501	3.36	0.360
$MePEG_{16}$/iBuSi	**7d**	4.054	4.81	0.406	3.79	0.441

Table 2.1: Bulky Copolymer Composition: Comonomer amounts and percentage for copolymers synthesized

2.3.11 – Preparation of Sol-Gel Polymer ($MePEG_{12}OCH_2CH_2CH_2SiO_{3/2}$) (4c)

$MePEG_{12}$ polymer (**4c**) was polymerized in the same manner as $MePEG_3$ polymer (**4a**) using the following: **3c** (2.51 g, 3.33 mmol). The resulting gel (**4c**) was a clear colorless viscous liquid. GPC analysis showed two peaks with M_w values of 4617 Da (M_n = 3828, PDI = 1.2061) and 833 Da (M_n = 704, PDI = 1.1832). NMR (^1H, in $CDCl_3$), δ (ppm) 0.64 (broad, 2H), 1.61 (broad, 2H), 3.39 (s, 3H), 3.43 (broad, 2H), 3.55-3.73 (m, 48H).

2.3.12 – Preparation of Sol-Gel Polymer ($MePEG_{16}OCH_2CH_2CH_2SiO_{3/2}$) (4d)

$MePEG_{16}$ polymer (**4d**) was polymerized in the same manner as $MePEG_3$ polymer (**4a**) using the following: **3d** (1.60 g, 1.68 mmol). The resulting gel (**4d**) was a colorless waxy solid. GPC analysis showed two peaks with M_w values of 4864 Da (M_n = 4230, PDI = 1.1499) and 830 Da (M_n = 585, PDI = 1.4188). NMR (^1H, in $CDCl_3$), δ (ppm) 0.63 (broad, 2H), 1.62 (broad, 2H), 3.38 (s, 3H), 3.41 (broad, 2H), 3.55-3.71 (m, 64H).

2.3.13 – Preparation of $MePEG_3$ / Ph_2Si Copolymer (5a)

The $MePEG_3$ / Ph_2Si Copolymer (**5a**) was polymerized in a similar manner to the $MePEG_3$ Polymer (**4a**), using the following procedure: $MePEG_3$ Monomer (**3a**), (5.003 g, 19.47 mmol) and diphenyl dimethoxysilane (0.509g, 2.57mmol, 0.116 mole fraction) were mixed together in a vial. An excess (6 equivalents) of acidic water (pH ~ 3, one drop conc. HCl in 100 mL water) was then added. The water, HCl and liberated alcohols were removed at 50 °C under vacuum. The resulting gel was a clear colorless liquid with no visible phase separation. GPC analysis showed one peak with an M_w value of 2348 Da (M_n = 1564, PDI = 1.5013). NMR (^1H, in $CDCl_3$), δ (ppm), MePEG: 0.62 (broad, 2H), 1.67 (broad, 2H), 3.37 (s, 3H), 3.40 (broad, 2H), 3.50-3.82 (m, 12H); diphenyl: 7.36 (broad, 6H), 7.66 (broad, 4h).

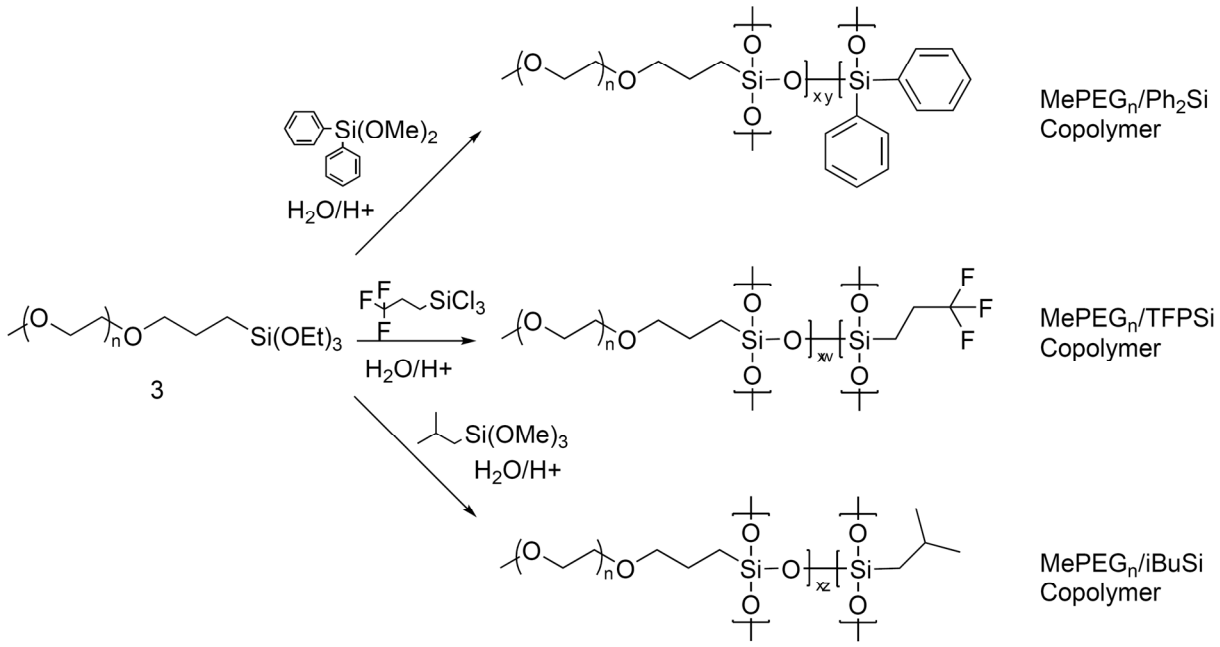

Figure 2.2: Bulky Copolymer Synthesis: Synthesis of MePEG copolymers

2.3.14 – Preparation of $MePEG_7$ / Ph_2Si Copolymer (5b)

The $MePEG_7$ / Ph_2Si Copolymer (**5b**) was prepared similarly to the $MePEG_3$ / Ph_2Si Copolymer above, using the following: $MePEG_7$ Monomer (**3b**) (4.22 g, 7.62 mmol) and diphenyl dimethoxysilane (0.46 g, 1.88 mmol, 0.1956 mole fraction). The resulting gel was a clear colorless liquid with no visible phase separation. GPC analysis showed two peaks with M_w values of 3696 Da (M_n = 2826, PDI = 1.3079) and 490 Da (M_n = 343, PDI = 1.4286). NMR (^1H, in $CDCl_3$), δ (ppm), MePEG: 0.65 (broad, 2H), 1.61 (broad, 2H), 3.39 (s, 3H), 3.42 (broad, 2H), 3.54-3.72 (m, 28H); diphenyl: 7.34 (broad, 6H), 7.68 (broad, 4H).

2.3.15 – Preparation of $MePEG_{12}$ / Ph_2Si Copolymer (5c)

The $MePEG_{12}$ / Ph_2Si Copolymer (**5c**) was prepared similarly to the $MePEG_3$ / Ph_2Si Copolymer above, using the following: $MePEG_{12}$ Monomer (**3c**) (2.51 g, 3.33 mmol) and diphenyl dimethoxysilane (0.256 g, 1.05 mmol, 0.240 mole fraction). The resulting gel was a clear colorless liquid with no visible phase separation. GPC analysis showed two peaks with M_w values of 4889 Da (M_n = 4126, PDI = 1.1849) and 780 Da (M_n = 591, PDI = 1.3198). NMR (^1H, in $CDCl_3$), δ (ppm), MePEG: 0.66 (broad, 2H), 1.62 (broad, 2H), 3.31 (s, 3H), 3.40 (broad, 2H), 3.56-3.73 (m, 48H); diphenyl: 7.34 (broad, 6H), 7.64 (broad, 4H).

2.3.16 – Preparation of $MePEG_{16}$ / Ph_2Si Copolymer (5d)

The $MePEG_{16}$ / Ph_2Si Copolymer (**5d**) was prepared similarly to the $MePEG_3$ / Ph_2Si Copolymer above, using the following: $MePEG_{16}$ Monomer (**3d**) (4.02 g, 4.21 mmol) and diphenyl dimethoxysilane (0.40 g, 1.64 mmol, 0.2976 mole fraction). The resulting gel was a colorless waxy solid with no visible phase separation. GPC analysis showed two peaks with M_w values of 5005 Da (M_n = 4226, PDI = 1.1843) and 774 Da (M_n = 501, PDI = 1.5449). NMR (^1H,

in $CDCl_3$), δ (ppm), MePEG: 0.62 (broad, 2H), 1.60 (broad, 2H), 3.37 (s, 3H), 3.41 (broad, 2H), 3.53-3.72 (m, 64H); diphenyl: 7.30 (broad, 4H), 7.66 (broad, 6H).

2.3.17 – Preparation of $MePEG_3$ / TFPSi Copolymer (6a)

The $MePEG_3$ / TFPSi Copolymer (**6a**) was prepared similarly to the $MePEG_3$ / Ph_2Si Copolymer above, using the following: $MePEG_3$ Monomer (**3a**) (5.005 g, 19.47 mmol) and 3,3,3-trifluoropropyl trichlorosilane (0.517 g, 2.57 mmol, 0.151 mole fraction). The resulting material was a rubbery solid that would not melt below 210 °C and would not dissolve in any common organic solvent. GPC analysis showed one peak with an M_w value of 10661 Da (M_n = 3688, PDI= 2.8907). NMR (^1H, in $CDCl_3$), δ (ppm), MePEG: 0.64 (broad, 2H), 1.65 (broad, 2H), 3.40 (s, 3H), 3.46 (broad, 2H), 3.51-3.80 (m, 12H); 3,3,3-trifluoropropyl: 2.11 (broad, 2H), 2.41 (broad, 2H).

2.3.18 – Preparation of $MePEG_7$ / TFPSi Copolymer (6b)

The $MePEG_7$ / TFPSi Copolymer (**6b**) was prepared similarly to the $MePEG_3$ / Ph_2Si Copolymer above, using the following: $MePEG_7$ Monomer (**3b**) (4.18 g, 7.55 mmol) and 3,3,3-trifluoropropyl trichlorosilane (0.42 g, 1.81 mmol, 0.2314 mole fraction). The resulting gel was a clear colorless liquid with no visible phase separation. GPC analysis showed two peaks with M_w values of 5144 Da (M_n = 3618, PDI = 1.4218) and 476 Da (M_n = 347, PDI = 1.3718). NMR (^1H, in $CDCl_3$), δ (ppm), MePEG: 0.65 (broad, 2H), 1.61 (broad, 2H), 3.38 (s, 3H), 3.42 (broad, 2H), 3.55-3.74 (m, 28H); 3,3,3-trifluoropropyl: 2.16 (broad, 2H), 2.38 (broad, 2H).

2.3.19 – Preparation of $MePEG_{12}$ / TFPSi Copolymer (6c)

The $MePEG_{12}$ / TFPSi Copolymer (**6c**) was prepared similarly to the $MePEG_3$ / Ph_2Si Copolymer above, using the following: $MePEG_{12}$ Monomer (**3c**) (2.50 g, 3.32 mmol) and 3,3,3-trifluoropropyl trichlorosilane (0.256 g, 1.11 mmol, 0.251 mole fraction). The resulting gel was a

clear colorless liquid with no visible phase separation. GPC analysis showed two peaks with M_w values of 8107 Da (M_n = 5904, PDI = 1.3731) and 803 Da (M_n = 627, PDI = 1.2807). NMR (^{1}H, in $CDCl_3$), δ (ppm), MePEG: 0.68 (broad, 2H), 1.63 (broad, 2H), 3.39 (s, 3H), 3.43 (broad, 2H), 3.56-3.73 (m, 48H); 3,3,3-trifluoropropyl: 2.14 (broad, 2H), 2.50 (broad, 2H).

2.3.20 – Preparation of $MePEG_{16}$ / TFPSi Copolymer (6d)

The $MePEG_{16}$ / TFPSi Copolymer (**6d**) was prepared similarly to the $MePEG_3$ / Ph_2Si Copolymer above, using the following: $MePEG_{16}$ Monomer (**3d**) (5.03 g, 5.27 mmol) and 3,3,3-trifluoropropyl trichlorosilane (0.50 g, 2.16 mmol, 0.3604 mole fraction). The resulting gel was a colorless waxy solid with no visible phase separation. GPC analysis showed two peaks with M_w values of 6237 Da (M_n = 4983, PDI = 1.2517) and 755 Da (M_n = 529, PDI = 1.4272). NMR (^{1}H, in $CDCl_3$), δ (ppm), MePEG: 0.63 (broad, 2H), 1.60 (broad, 2H), 3.36 (s, 3H), 3.40 (broad, 2H), 3.52-3.69 (m, 64H); 3,3,3-trifluoropropyl: 2.11 (broad, 2H) 2.66 (broad, 2H).

2.3.21 – Preparation of $MePEG_3$ / iBuSi Copolymer (7a)

The $MePEG_3$ / iBuSi Copolymer (**7a**) was prepared similarly to the $MePEG_3$ / Ph_2Si Copolymer above, using the following: $MePEG_3$ Monomer (**3a**) (5.272 g, 20.51 mmol) and isobutyl trimethoxysilane (0.541 g, 5.06 mmol, 0.198 mole fraction). The resulting gel was a clear colorless liquid with no visible phase separation. GPC analysis showed one peak with an M_w value of 2265 Da (Mn = 1149, PDI= 1.9713). NMR (^{1}H, in CDCl3), δ (ppm), MePEG; 0.63 (broad, 2H), 1.69 (broad, 2H), 3.39 (s, 3H), 3.42 (broad, 2H), 3.51-3.80 (m, 12H); isobutyl: 0.62 (broad, 2H), 0.96 (broad, 6H), 1.86 (broad, 1H).

2.3.22 – Preparation of $MePEG_7$ / iBuSi Copolymer (7b)

The $MePEG_7$ / iBuSi Copolymer (**7b**) was prepared similarly to the $MePEG_3$ / Ph_2Si Copolymer above, using the following: $MePEG_7$ Monomer (**3b**) (4.00 g, 7.22 mmol) and

isobutyl trimethoxysilane (0.40 g, 2.24 mmol, 0.2939 mole fraction). The resulting gel was a clear colorless liquid with no visible phase separation. GPC analysis showed two peaks with M_w values of 3462 Da (M_n = 2660, PDI = 1.3015) and 490 Da (M_n = 339, PDI = 1.4454). NMR (^{1}H, in $CDCl_3$), δ (ppm), MePEG: 0.63 (broad, 2H), 1.62 (broad, 2H), 3.38 (s, 3H), 3.43 (broad, 2H), 3.53-3.73 (m, 28H); isobutyl: 0.63 (broad, 2H), 0.96 (broad, 6H), 1.87 (broad, 1H).

2.3.23 – Preparation of $MePEG_{12}$ / iBuSi Copolymer (7c)

The $MePEG_{12}$ / iBuSi Copolymer (**7c**) was prepared similarly to the $MePEG_3$ / Ph_2Si Copolymer above, using the following: $MePEG_{12}$ Monomer (**3a**) (2.51 g, 3.33 mmol) and isobutyl trimethoxysilane (0.255 g, 1.43 mmol, 0.300 mole fraction). The resulting gel was a clear colorless liquid with no visible phase separation. GPC analysis showed two peaks with M_w values of 4797 Da (M_n = 3889, PDI = 1.2335) and 868 Da (M_n = 719, PDI = 1.2072). NMR (^{1}H, in $CDCl_3$), δ (ppm), MePEG: 0.66 (broad, 2H), 1.61 (broad, 2H), 3.39 (s, 3H), 3.44 (broad, 2H), 3.56-3.73 (m, 48H); isobutyl: 0.66 (broad, 2H), 0.98 (broad, 6H), 1.90 (broad, 1H).

2.3.24 – Preparation of $MePEG_{16}$ / iBuSi Copolymer (7d)

The $MePEG_{16}$ / iBuSi Copolymer (**7d**) was prepared similarly to the $MePEG_3$ / Ph_2Si Copolymer above, using the following: $MePEG_{16}$ Monomer (**3d**) (4.02 g, 4.21 mmol) and isobutyl trimethoxysilane (0.41 g, 2.30 mmol, 0.441 mole fraction). The resulting gel was a colorless waxy solid with no visible phase separation. GPC analysis showed two peaks with M_w values of 9764 Da (M_n = 3337, PDI = 2.9260) and 820 Da (M_n = 389, PDI = 2.1080). NMR (^{1}H, in $CDCl_3$), δ (ppm), MePEG: 0.65 (broad, 2H), 1.61 (broad, 2H), 3.38 (s, 3H), 3.42 (broad, 2H), 3.55-3.71 (m, 64H); isobutyl: 0.64 (broad, 2H), 0.96 (broad, 6H), 1.87 (broad, 1H).

2.4 – MePEG/MePPG Copolymer Synthesis

2.4.1 – Synthesis of Poly(ethylene glycol) Allyl Methyl Ether ($MePEG_7OCH_2CHCH_2$) (2b)

$MePEG_7$ Allyl (**2b**) was synthesized according to a method in the literature. [1, 27, 55] For this method, NaH (2.57 g, 107 mmol) and THF (40 mL) were added to an air free round bottom flask and were slurried. Dried poly(ethylene glycol) methyl ether ($MePEG_7OH$, 25.00 g, 71.43 mmol) was dissolved in dry THF (20 mL) and was added dropwise to the slurry. The mixture was stirred under argon for a half hour at room temperature to allow for complete deprotonation. Allyl bromide (12.96g, 107 mmol) was dissolved in THF (20mL) and was added dropwise to the slurried mixture. A white precipitate of NaBr was formed upon reaction. The reaction was stirred over night at room temperature to complete the reaction. Approximately 10 mL of isopropyl alcohol was added to the reaction mixture to quench any unreacted NaH. The precipitate was removed by gravity filtration and the filtrate was extracted with 50 mL 0.5 M NaCl solution and three washings of chloroform. The organic layers were combined and dried over Na_2SO_4. The Na_2SO_4 was removed by gravity filtration and the product was concentrated by rotary evaporation. A clear viscous liquid (**2b**) was obtained (23.25 g, 59.6 mmol, 83.5 % yield). NMR (^1H, in $CDCl_3$), δ (ppm) 3.35 (s, 3H), 3.48-3.80 (m, 28H), 3.99 (m, 2H), 5.18 (dd, 2H), 5.88 (m, 1H). NMR (^{13}C, in $CDCl_3$), δ (ppm) 58.52, 68.91, 70.00-70.11 (several peaks), 71.41, 71.68, 116.55, 134.28.

2.4.2 – Synthesis of Tri(propylene glycol) Allyl Methyl Ether ($MePPG_3OCH_2CHCH_2$) (2e)

$MePPG_3$ Allyl (**2e**) was synthesized according to the method used to prepare **2b** using the following: NaH (4.87 g, 202.9 mmol), $MePPG_3OH$ (20.91g, 101.5 mmol), and allyl bromide (19.63g, 162.2 mmol). A clear viscous liquid (**2e**) was recovered (18.11 g, 73.6 mmol, 72.5 %

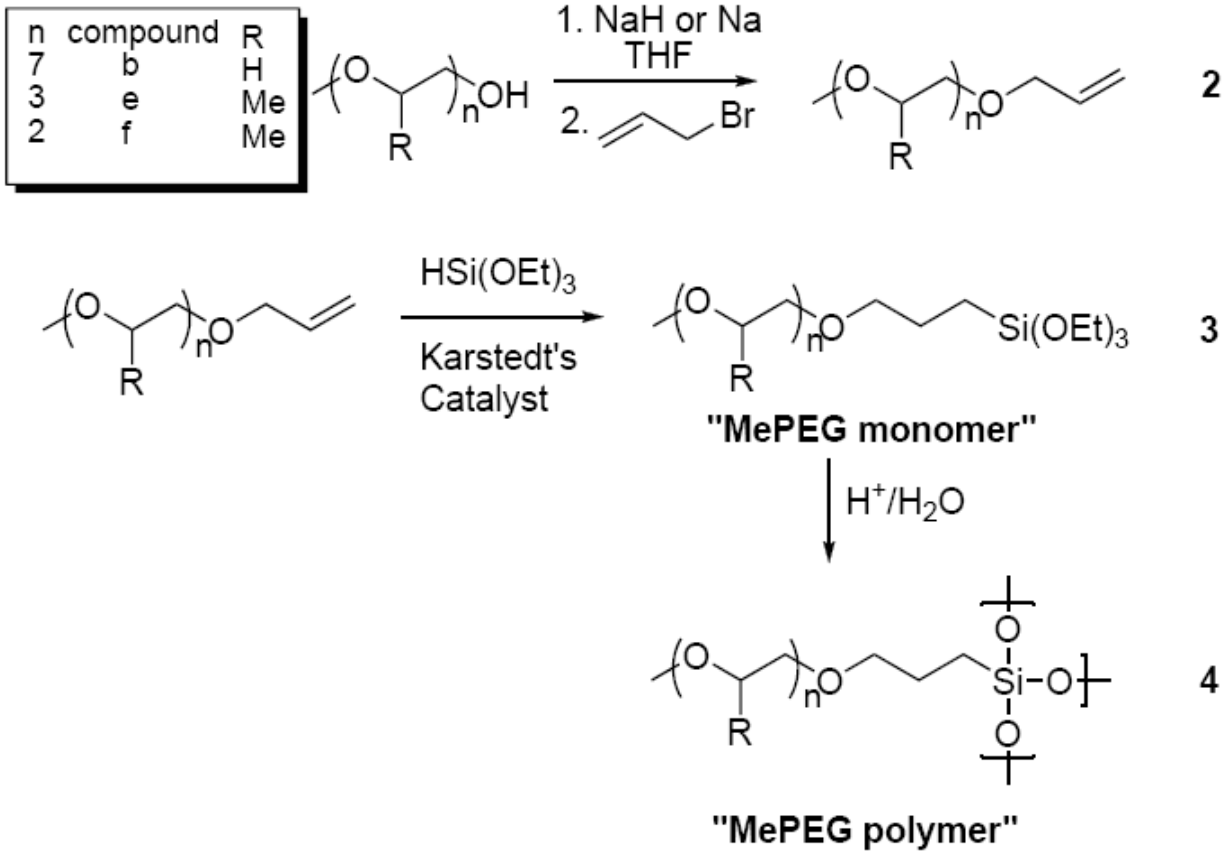

Figure 2.3: Polymer Synthesis: Synthesis of MePEG and MePPG polymers.

yield). NMR (^{1}H, in $CDCl_3$), δ (ppm) 1.1(s, 9H) 3.27-3.41(m, 9H) 3.99 (d, 2H) 5.12 (dd, 2H) 5.83 (m, 1H). NMR (^{13}C, in $CDCl_3$), δ (ppm) 17.02, 56.60, 58.98, 70.02, 72.89-75.85, 116.10, 135.45.

2.4.3 – Synthesis of Di(propylene glycol) Allyl Methyl Ether ($MePPG_2OCH_2CHCH_2$) (2f)

$MePPG_2$ Allyl (**2f**) was synthesized according to the method used to prepare **2b** using the following: NaH (6.10g, 254.1 mmol), $MePPG_2OH$ (25.13 g, 169.6 mmol), and allyl bromide (40.00 g, 330.6 mmol). A clear viscous liquid (**2f**) was recovered (22.34 g, 118.7 mmol, 70.0 % yield). NMR (^{1}H, in $CDCl_3$), δ (ppm) 1.16 (s, 6H) 3.34-3.62 (m, 6H) 4.07 (d, 2H) 5.21 (dd, 2H) 5.91 (m, 1H). NMR (^{13}C, in $CDCl_3$), δ (ppm) 17.35, 56.88, 59.25, 70.26, 73.19-76.05, 116.50, 135.48.

2.4.4 – Synthesis of Polymer Precursor ($MePEG_7OCH_2CH_2CH_2Si(OEt)_3$) (3b)

$MePEG_7$ monomer (**3b**) was synthesized according to method previously reported. [1, 27, 55] Triethoxysilane (12.88 g, 78.5 mmol) and **2b** (23.25g, 59.6 mmol) were added to an air-free Schlenk tube. Karstedt's catalyst (~ 80 μL) was added to the Schlenk tube, which was then heated to 60 °C under argon. NMR were taken periodically until it showed a complete disappearance of the allyl protons. The reaction mixture was heated to 50 °C under vacuum for 15 minutes to remove excess triethoxysilane. The Karstedt's catalyst was removed with activated charcoal in THF under inert atmosphere, followed by gravity filtration. The THF was removed by rotary evaporation. A clear colorless liquid (**3b**) was recovered (26.63 g, 48.1 mmol, 80.7 % yield). NMR (^{1}H, in $CDCl_3$), δ (ppm) 0.49 (m, 2H), 1.10 (m, 9H), 1.55 (m, 2H), 3.24 (s, 3H), 3.30 (m, 2H), 3.41-3.51 (m, 28H), 3.71 (m, 6H).

2.4.5 – Synthesis of Polymer Precursor ($MePPG_3OCH_2CH_2CH_2Si(OEt)_3$) (3e)

$MePPG_3$ monomer (**3e**) was prepared in the same manner as **3b** using the following: triethoxysilane (14.50 g, 88.4 mmol), **2b** (18.11 g, 73.6 mmol), and Karstedt's catalyst (~80 µL). A clear viscous liquid (**3b**) was recovered (28.30 g, 69.0 mmol, 93.8 % yield). NMR (^1H, in $CDCl_3$), δ (ppm) 0.57 (m, 2H), 1.07 (m, 9H), 1.17 (m, 9H), 1.58 (m, 2H), 3.29-3.54 (m. 9H), 3.80 (m, 6H).

2.4.6 – Synthesis of Polymer Precursor ($MePPG_2OCH_2CH_2CH_2Si(OEt)_3$) (3c)

$MePPG_2$ monomer (**3c**) was prepared in the same manner as **3a** using the following: triethoxysilane (30.60 g, 186.6 mmol), **2c** (22.34 g, 169.6 mmol), and Karstedt's catalyst (~80 µL). A clear viscous liquid (**3c**) was recovered (31.16 g, 88.5 mmol, 52.2 % yield). NMR (^1H, in $CDCl_3$), δ (ppm) 0.56 (m, 2H), 1.07 (m, 6H), 1.16 (m, 9H), 1.60 (m, 2H), 3.25-3.54 (m. 6H), 3.76 (m, 6H).

2.4.7 – Synthesis of Sol-Gel Polymer ($MePEG_7OCH_2CH_2CH_2SiO_{3/2}$) (4b)

$MePEG_7$ polymer was prepared by the following procedure: [1, 27, 55] an excess (6 equivalents) of slightly acidic water (pH ~ 3, one drop conc. HCl in 100 mL distilled water) was added to a **3b** (3.75 g, 6.77 mmol) in a sample vial. The solution was mixed well and allowed to hydrolyze at room temperature for 12h - 24h. The excess water and ethanol were removed by rotary evaporation and the resulting gel was placed in a vacuum oven at 60 ºC for 24h. The resulting gel **4b** was clear viscous liquid.

2.4.8 – Synthesis of Sol-Gel Polymer ($MePPG_3OCH_2CH_2CH_2SiO_{3/2}$) (4e)

$MePPG_3$ polymer (**4b**) was prepared in the same manner as the $MePEG_7$ polymer (**4b**) using the following: **3e** (4.11 g, 10.0 mmol). The resulting gel **4e** was a clear viscous liquid.

Polymer / Copolymer	$MePEG_7$		$MePPG_3$		$MePPG_2$		GPC M_w (Da)	
	mmol	X[a]	mmol	X	mmol	X	High M_w	Low M_w
$MePEG_7$ polymer	6.77	1.00	-	-	-	-	3813	546
$MePPG_3$ polymer	-	-	10.0	1.00	-	-	2652	-
$MePPG_2$ polymer	-	-	-	-	12.43	1.00	3163	-
$MePEG_7$ / $MePPG_3$ copolymer	5.52	0.75	1.85	0.25	-	-	5017	550
	4.04	0.49	4.14	0.51	-	-	4140	577
	2.24	0.25	6.73	0.75	-	-	2794	-
$MePEG_7$ / $MePPG_2$ copolymer	5.74	0.75	-	-	1.90	0.25	4165	527
	4.39	0.50	-	-	4.40	0.50	4166	539
	2.58	0.25	-	-	7.73	0.75	3332	450
$MePPG_3$ / $MePPG_2$ copolymer	-	-	7.90	0.75	2.64	0.25	2191	-
	-	-	5.56	0.50	5.57	0.50	2485	-
	-	-	2.93	0.25	8.81	0.75	3813	-

[a] Mole Fraction of $MePEG_7$ component

Table 2.2: MePEG/MePPGCopolymer composition: Comonomer mass, mmol and mole fraction and molecular weight (determined by GPC) for MePEG/MePPG copolymers

2.4.9 – Synthesis of Sol-Gel Polymer ($MePPG_2OCH_2CH_2CH_2SiO_{3/2}$) (4f)

$MePPG_2$ polymer (**4f**) was prepared in the same manner as the $MePEG_7$ polymer (**4b**) using the following: **3f** (4.38 g, 12.43 mmol). The resulting gel **4f** was a clear viscous liquid.

2.4.10 – Synthesis of Sol-Gel Mixed copolymers (8a-c, 9a-c, 10a-c)

The sol-gel mixed copolymers were synthesized in the same was as the $MePEG_7$ polymer (**4b**). The millimoles and mole fractions of the comonomers are summarized in table 2.2. Also included in table 2.2 is the GPC data for the copolymers. The two comonomers were mixed together and an excess (6 equivalents) of slightly acidic water (pH ~ 3, one drop conc. HCl in 100 mL distilled water) was added. The solution was mixed well and allowed to hydrolyze at room temperature for 12h - 24h. The excess water and ethanol were removed by rotary evaporation and the resulting gel was placed in a vacuum oven at 60 ºC for 24h.

2.5 – $MePEG_7SO_3H$ Acid Synthesis

2.5.1 – Synthesis of Methoxy Poly(ethylene glycol) Bromide ($MePEG_7Br$) (11)

This material was prepared according to the following procedure: [1, 13, 17, 25-27, 55] $MePEG_7OH$ (40.20 g, 114.9 mmol) was added to diethyl ether (50 mL) in a round bottom Schlenk flask under argon. PBr_3 (35 mL of 1.98 M solution, 69.3 mmol) was added to the Schlenk flask slowly while the flask was in an ice bath. After addition, the ice bath was removed and the reaction mixture was stirred under argon for 18h. The reaction mixture was then poured over 100 grams of cracked ice and was extracted one time with 100 mL Et_2O and two times with 100ml dichloromethane. The organic layers were combined and were dried over Na_2SO_4. The Na_2SO_4 was removed by gravity filtration and the solvents were removed by rotary evaporation. A clear colorless viscous liquid $MePEG_7Br$ (**11**) was recovered (36.43 g, 88.2 mmol, 76.8 %).

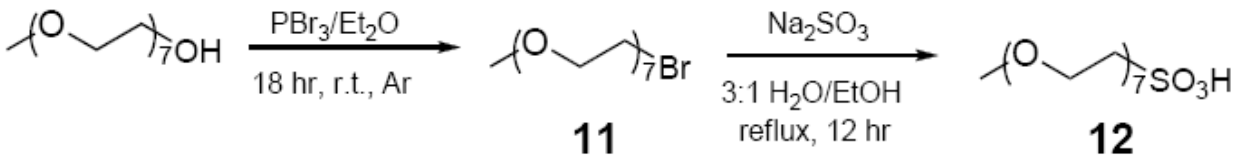

Figure 2.4: Acid Synthesis: Synthesis of $MePEG_7SO_3H$ acid

NMR (^{1}H, in $CDCl_3$), δ (ppm) 3.27 (s, 3H), 3.45 (m, 2H), 3.55 (m, 28H), 3.72 (t, 2H). NMR (^{13}C, in $CDCl_3$), δ (ppm) 30.36, 59.00, 70.07-70.59 (several peaks), 71.12, 71.86.

2.5.2 – Synthesis of Methoxy Poly(ethylene glycol) Sulfonic Acid ($MePEG_7SO_3H$) (12)

This material was prepared using the following procedure: [1, 13, 17, 25-27, 55] Na_2SO_3 (4.19 g, 33.25 mmol) and **8** (10.00 g, 24.2 mmol) were added to a 3:1 water/ethanol solution (60 mL). The reaction solution was heated to boiling and allowed to reflux for 18h. The remaining solid was filtered. The solvents were removed by rotary evaporation. The product was then successively dissolved in less polar organic solvents (EtOH, Acetone, dichloromethane). The undissolved solid was filtered each time and the product concentrated by rotary evaporation leaving $MePEG_7SO_3Na$. The $MePEG_7SO_3Na$ salt was ran through a strong base ion exchange column twice and then was ran through a strong acid exchange column twice. The product was concentrated by rotary evaporation. A clear color and colorless viscous liquid (**12**) was recovered (2.92 g, 7.1 mmol, 29.1 %). The acidity of the acid was assayed by titrating to pH 7 with tetrabutylammonium hydroxide to yield a measurement of 104.6 % acidity. Neat $MePEG_7SO_3H$ has a density of 1.21 g/mL which gives a neat concentration of 2.93 M. NMR (^{1}H, in $CDCl_3$), δ (ppm) 3.23 (t, 2H), 3.35 (s,3H), 3.50-3.70 (m, 65H), 3.87 (t, 2H).

2.6 – End Group Analysis

End group analysis was performed on all of the prepared copolymers to test for uncondensed Si–OH from the sol-gel condensation to form the polymers. The uncondensed –OH groups were reacted with chlorotrimethylsilane, $(CH_3)_3Si$-Cl (Scheme 3) to label each residual OH group with a trimethylsilyl group that can be integrated in the NMR spectra. In one experiment, $MePEG_7$ polymer (0.035 g, 0.079 mmol) was dissolved in 20 mL toluene in an

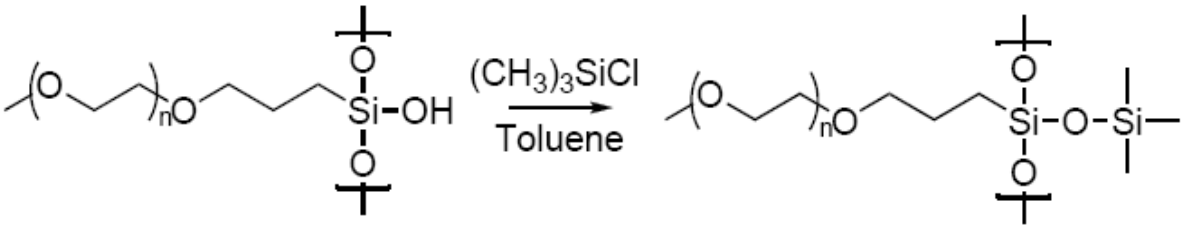

Scheme 2.5: End Group Analysis Scheme: End group analysis labeling reaction.

argon purged flask. Then, a large excess of chlorotrimethylsilane (0.5 mL, 4 mmol) was added. The reaction mixture was stirred for 6 hours. After which, 2.0 g K_2CO_3 was added to remove HCl and stirred for 1 hour. The solution was filtered, and the toluene was removed by rotary evaporation. The flask was then evacuated to $\sim$ 100 mtorr for 30 minutes to ensure the removal of excess TMS-Cl (B.P. = 57° C). The resulting product was a clear and colorless viscous liquid. ^{1}H-NMR was taken of the product, and the integration of the trimethylsilyl peak at δ = 0.10 ppm was ratioed to the $-OCH_3$ peak of the MePEG group, showing the presence of 5.7% uncondensed OH groups in this polymer.

III. RESULTS AND DISCUSSION OF BULKY COPOLYMERS

In this chapter, I report the analysis of a series of sol-gel polymers ($MePEG_nO(CH_2)_3Si(OCH_2CH_3)_3$, n=3, 7.24, 12.0, 16.3) and co-polymers (isobutyl trimethoxysilane, diphenyl dimethoxysilane, and 3,3,3-trifluoropropyl trichlorosilane). These sol-gel polymers and copolymers were combined with $MePEG_7SO_3H$ acid to create proton-conducting electrolytes. These electrolytes are viscous liquids or waxy solids at room temperature. These copolymer electrolytes were investigated to determine the relationship between fractional free volume and transport properties as outlined in free volume theory.

3.1 – Fractional Free Volume (FFV)

Free volume in the copolymers was calculated from the density of the copolymers using equations 3.1 through 3.3.[55, 56]

$$V_m = \frac{MW}{d} \tag{3.1}$$

$$V_f = V_m - V_w \tag{3.2}$$

$$FFV = \frac{V_f}{V_m} = \frac{(V_m - V_w)}{V_m} \tag{3.3}$$

In equations 3.1-3.3, the molar volume (V_m) is the actual volume occupied by one mole of copolymer, and was calculated from the molecular weight and the density of the sample (eq 3.1). The van der Waals volume (V_w), is the volume directly occupied by one mole of copolymer, and was calculated using the Bondi group contribution method, which sums the contributions to

volume from each functional group. [39-41] The molar free volume (V_f) and the fractional free volume (FFV) were calculated from V_w and V_m (eq 3.2 and 3.3). The FFV is calculated by dividing the molar free volume (V_f) by the molar volume (V_m) of the polymer, and is summarized in Table 3.1. In general, the copolymers display a small difference between the FFV of the pure polymer and the copolymers, with most samples having a FFV within 3% of the pure polymer.

The FFV and $V_{f\,PEG}$ of an electrolyte mixture of the $MePEG_7SO_3H$ acid and a $MePEG_n$ copolymer are calculated by weighing the relative contributions by the mole fractions of the components.[55, 56] The volume fraction of PEG ($V_{f\,PEG}$) represents the volume of the copolymer that is occupied by PEG ether units. The volume fraction of PEG in an electrolyte mixture (Table 3.2) of $MePEG_nSO_3H$ acid and $MePEG_n$ copolymer is calculated with Equation 3.4.

In equation 3.4, n_{acid} and n_{poly} are the moles of $MePEG_7SO_3H$ acid and $MePEG_n$ polymer, $V_{w,PEG,acid}$ and $V_{w,PEG,poly}$ are the van der Waals volumes of the PEG components in the $MePEG_7SO_3H$ acid and $MePEG_n$ polymer, and $V_{w,acid}$ and $V_{w,poly}$ are the van der Waals volumes of the whole $MePEG_7SO_3H$ acid and $MePEG_n$ polymer molecules.

$$V_{f,PEG,mix} = \frac{n_{acid}V_{w,PEG,acid} + n_{poly}V_{w,PEG,poly}}{n_{acid}V_{w,acid} + n_{poly}V_{w,poly}} \qquad (3.4)$$

The FFV of an electrolyte mixture of the $MePEG_n$ copolymer with the $MePEG_7SO_3H$ acid is similarly derived from equation 3.3, yielding equation 3.5.[55, 56] Equation 3.5 relates the molar volumes (V_m), van der Waals volumes (V_w), and mole fractions of the acid (X_{acid}) and copolymer (X_{copoly}). The calculated values of the FFV and the volume fractions of PEG in the copolymer/acid mixtures are summarized in table 3.2

Polymer		MW (g/mol)[a]	Density (g/mL)	Molar volume (V_m)[b]	van der Waals volume (V_w)[c]	$V_{f, PEG}$	FFV
$MePEG_3$ polymer	**4a**	257.0	1.192	215.6	150.9	0.724	0.300
$MePEG_3/Ph_2Si$	**5a**	249.0	1.197	208.0	145.9	0.648	0.299
$MePEG_3$/TFPSi	**6a**	239.9	1.216	197.3	137.5	0.636	0.303
$MePEG_3$/iBuSi	**7a**	228.5	1.178	194.0	136.0	0.681	0.299
$MePEG_7$ polymer	**4b**	443.0	1.166	379.9	259.7	0.845	0.316
$MePEG_7/Ph_2Si$	**5b**	395.3	1.060	376.4	233.6	0.700	0.380
$MePEG_7$/TFPSi	**6b**	375.0	1.121	344.0	221.9	0.711	0.358
$MePEG_7$/iBuSi	**7b**	344.2	1.141	318.1	215.1	0.812	0.322
$MePEG_{12}$ polymer	**4c**	643.0	1.143	562.6	376.0	0.895	0.332
$MePEG_{12}/Ph_2Si$	**5c**	545.7	1.156	472.1	318.6	0.819	0.325
$MePEG_{12}$/TFPSi	**6c**	519.6	1.173	442.9	298.5	0.789	0.326
$MePEG_{12}$/iBuSi	**7c**	481.7	1.149	419.2	284.6	0.889	0.321
$MePEG_{16}$ polymer	**4d**	843.0	1.143	737.5	492.7	0.930	0.332
$MePEG_{16}/Ph_2Si$	**5d**	651.1	1.155	586.6	395.4	0.869	0.326
$MePEG_{16}$/TFPSi	**6d**	592.9	1.164	550.7	368.5	0.811	0.335
$MePEG_{16}$/iBuSi	**7d**	518.4	1.149	510.0	345.9	0.954	0.320
$MePEG_7SO_3H$ acid		414.1	1.212	341.7	267.4	0.973	0.330

[a] MW for polymers and copolymers is the weighted MW of the monomeric units.
[b] V_m for polymers and copolymers is the weighted V_m calculated using the weighted MW of the monomeric units
[c] V_w for polymers and copolymers is the weighted Vw calculated by the Bondi group contribution method

Table 3.1: FFV and $V_{f,PEG}$ of Copolymers: Fractional free volumes for $[MePEG_nSiO_{1.5}]_x$ copolymers and $MePEG_7SO_3H$ acid.

Polymer		[$MePEG_7SO_3H$] (mol/L)	$V_{f,PEG,mixture}$ [a]	$FFV_{mixture}$ [b]
$MePEG_3$ polymer	**4a**	0.26	0.7427	0.3017
		1.32	0.8201	0.3101
$MePEG_3/Ph_2Si$	**5a**	0.26	0.7473	0.3004
		1.32	0.8307	0.3089
$MePEG_3$/TFPSi	**6a**	0.26	0.7577	0.3044
		1.32	0.8345	0.3109
$MePEG_3$/iBuSi	**7a**	0.26	0.7371	0.3003
		1.32	0.8198	0.3073
$MePEG_7$ polymer	**4b**	0.26	0.8548	0.3179
		1.32	0.8874	0.3229
$MePEG_7/Ph_2Si$	**5b**	0.26	0.7850	0.3749
		1.32	0.8495	0.3563
$MePEG_7$/TFPSi	**6b**	0.26	0.8260	0.3525
		1.32	0.8729	0.3438
$MePEG_7$/iBuSi	**7b**	0.26	0.8382	0.3244
		1.32	0.8806	0.3265
$MePEG_{12}$ polymer	**4c**	0.26	0.9019	0.3314
		1.32	0.9343	0.3307
$MePEG_{12}/Ph_2Si$	**5c**	0.26	0.9112	0.3258
		1.32	0.9397	0.3277
$MePEG_{12}$ / TFPSi	**6c**	0.26	0.9232	0.3266
		1.32	0.9436	0.3280
$MePEG_{12}$/iBuSi	**7c**	0.26	0.9055	0.3221
		1.32	0.9372	0.3255
$MePEG_{16}$ polymer	**4d**	0.26	0.9311	0.3315
		1.32	0.9343	0.3307
$MePEG_{16}/Ph_2Si$	**5d**	0.26	0.9398	0.3266
		1.32	0.9397	0.3282
$MePEG_{16}$/TFPSi	**6d**	0.26	0.9464	0.3308
		1.32	0.9436	0.3304
$MePEG_{16}$/iBuSi	**7d**	0.26	0.9355	0.3230
		1.32	0.9372	0.3261

[a] $V_{f\,PEGmixture}$ for copolymer electrolytes is the weighted $V_{f\,PEGmixture}$ of the monomeric units and the $MePEGSO_3H$ acid. Eq. 2.6

[b] $FFV_{mixture}$ for copolymer electrolytes is the weighted $FFV_{mixture}$ of the monomeric units and the $MePEGSO_3H$ acid. Eq. 2.7

Table 3.2: FFV and $V_{f,PEG}$ of Acid Mixtures: Volume Fractions of PEG ($V_{f,PEG}$) for 0.26 M and 1.32 M $MePEG_7SO_3H$ acid copolymer electrolyte mixtures.

$$FFV_{mixture} = \frac{(V_{m,acid}X_{acid} + V_{m,copoly}X_{copolu}) - (V_{w,acid}X_{acid} + V_{w,copoly}X_{copoly})}{(V_{m,acid}X_{acid} + V_{m,copoly}X_{copoly})} \quad (3.5)$$

The $V_{f,PEG}$ decreases in both concentrations of electrolyte samples and the copolymer samples versus the pure polymers because the addition of the bulky groups dilutes the volume of PEG. In addition, the $V_{f,\,PEG}$ is lower in low acid concentration electrolyte mixtures of the copolymers, than in the high acid concentration electrolyte mixtures. Our acid, $MePEG_7SO_3H$, contains PEG, and thus, makes a substantial contribution to the $V_{f,\,PEG}$ in the higher acid concentration electrolyte mixtures. We see for the longer PEG copolymers that the addition of the acid changes the $V_{f,\,PEG}$ very little compared to the effect that is observed on the lower molecular weight copolymers. This is because the high molecular weight copolymers have a $V_{f,PEG}$ closer to the $MePEG_7SO_3H$ acid than the small molecular weight copolymers. Because of this close match in $V_{f,PEG}$, the addition of $MePEG_7SO_3H$ acid does not change $V_{f,PEG}$.

The trend in the $FFV_{mixture}$ is the same as for the pure copolymers with there being a less than 3 % difference from the copolymers to their respective pure polymers. The addition of the $MePEG_7SO_3H$ acid results in very little change in the mixture over the pure polymers because the FFV_{acid} value is very close to the FFV_{copoly} value. There is likely a relationship between the FFV and $V_{f,\,PEG}$. This would be expected to be due to random motions of the PEG chains, the longer the PEG chains (high $V_{f,\,PEG}$) the larger the effect of random motions of the PEG chains (higher FFV).

3.2 – Gel Permeation Chromatography (GPC)

We performed a GPC analysis of the polymer molecular weights, in order to determine the effect of the bulky groups on the nature of the polymerization reaction in the MePEG polymer system. We expected that the addition of the bulky groups would not change the observed molecular weight. GPC can detect cross-linking, and measure the degree of polymerization (by observing the change in M_W and M_N). Our group has recently examined polymer cross-linking, and its effects on free volume as well as transport properties, in our sol-gel polymers. [55] We found that conductivity is dependent on both viscosity and free volume.

Table 3.3 summarizes the M_W and M_N data obtained by GPC for our $MePEG_n$ copolymers. Two GPC peaks were observed for all of the copolymers except for the $MePEG_3$ copolymers, with the low MW peak likely corresponding to one monomer or dimer unit of the polymer. We used polystyrene molecular weight standards to calibrate the GPC. Our group has found that when polystyrene MW standards are used, the GPC underestimates the actual number average (M_n) molecular weights of short chain MePEG polymers with an average underestimation of 39%. [27] The lack of the low MW peak in the $MePEG_3$ polymer is likely due to the difficulty of detecting small M_w polymers with an Evaporative Light Scattering detector where sensitivity $\propto MW^2$.

In the $MePEG_3$, $MePEG_7$ and $MePEG_{12}$ polymers, the high M_W GPC peak of the polymer has M_w and M_n values that are very similar to the corresponding values in its copolymers (except the TFPSi copolymers). This result indicates that these polymers have a low polydispersity index (PDI). However, the $MePEG_n$ / TFPSi copolymers have much higher M_w values than the other copolymers, suggesting that these copolymers have a higher degree of polymerization.

The higher PDI would also indicate that there is a larger amount of molecular weight dispersity for these copolymers, and may be indicative of an increase inrandomness in the

Polymer	"High" MW peak[c]				"Low" MW peak[d]			
	M_w (Da)	M_n (Da)	PDI[a]	# monomer[b]	M_w (Da)	M_n (Da)	PDI[a]	# monomer[b]
$MePEG_3$ **4a**	2929	2023	1.448	11.4	N/A			
$MePEG_3/Ph_2Si$ **5a**	2348	1564	1.501	9.4	N/A			
$MePEG_3$/TFPSi **6a**	10661	3688	2.891	44.4	N/A			
$MePEG_3$/iBuSi **7a**	2265	1149	1.971	9.9	N/A			
$MePEG_7$ **4b**	3620	2932	1.235	8.2	483	343	1.408	1.1
$MePEG_7/Ph_2Si$ **5b**	3696	2826	1.308	9.3	490	343	1.429	1.2
$MePEG_7$/TFPSi **6b**	5144	3618	1.422	13.3	476	347	1.372	1.2
$MePEG_7$/iBuSi **7b**	3462	2660	1.302	9.5	490	339	1.445	1.4
$MePEG_{12}$ **4c**	4617	3828	1.206	7.2	833	704	1.183	1.3
$MePEG_{12}/Ph_2Si$ **5c**	4889	4126	1.185	9.0	780	591	1.320	1.4
$MePEG_{12}$/TFPSi **6c**	8107	5904	1.373	15.6	803	627	1.281	1.5
$MePEG_{12}$/iBuSi **7c**	4797	3889	1.234	10.0	868	719	1.207	1.8
$MePEG_{16}$ **4d**	4864	4230	1.150	5.8	830	585	1.419	1.0
$MePEG_{16}/Ph_2Si$ **5d**	5005	4226	1.184	7.4	774	501	1.545	1.1
$MePEG_{16}$/TFPSi **6d**	6237	4983	1.252	9.7	755	529	1.427	1.2
$MePEG_{16}$/iBuSi **7d**	9764	3337	2.926	16.7	820	389	2.108	1.4

[a] PDI = M_W/M_N

[b] # of monomers is calculated by dividing M_w by the weighted monomer molecular weight

[c] "High" MW peak is the peak observed with the highest M_w when more than one peak is present

[d] "low" MW peak is the peak observed with the lowest M_w when more than one peak is present

Table 3.3: GPC Data: GPC data for copolymers with weight average molecular weight (M_w), number average molecular weight (M_n) and polydispersity index (PDI)

polymerization. This result likely indicates that there is a variety of different copolymer structural units. There is little variation for the low molecular weight, "monomer" peaks, as the molecular weights of the monomers in each $MePEG_n$ copolymer series are very similar. There is an increasing trend in measured M_W for the $MePEG_{16}$ copolymers, with $MePEG_{16}$ polymer > $MePEG_{16}$ / Ph_2Si copolymer > $MePEG_{16}$ / TFPSi copolymer > $MePEG_{16}$ / iBuSi copolymer. This same increasing trend is also observed with the PDIs. The last trend is that the smaller the measured M_W, the larger the PDI. This indicates an increased randomness in the polymerization which is accounted for by considering that the smaller molecular weight monomers are in higher concentration, and therefore, have a corresponding faster rate of polymerization, resulting in increased randomness.

Our group has previously observed that our $MePEG_n$ polymers have M_W values consistent with an eight oligomer unit POSS-type cube structure.[55] Most of the copolymers seem to also have M_W values indicating around eight oligomers, except for the TFPSi copolymers, which are consistently higher (Table 3.3). Our group has used polystyrene M_W standards to calibrate our GPC, which we have previously shown to lead to an overestimation of the molecular weight of PEG polymers.[55] The larger M_W values, when viewed in terms of the number of oligomers, and considering the overestimation of M_W from the polystyrene standards, indicates that these copolymers must have a larger, more random structure compared to the compact and cubic POSS structure. We infer this to mean, that, these copolymers have a higher degree of cross-linking. Interestingly, the PDIs of the copolymers with more than eight oligomers, are significantly greater, which is also consistent with a greater degree of cross-linking (i.e. there is a larger possibility of different contributing structures).

3.3 – End Group Analysis

We performed an end group analysis to determine if the copolymers had different condensation percentages relative to the pure polymers, that might be due to the introduction of the bulky copolymers. In these experiments, any uncondensed Si-OH bonds will be labeled with a trimethylsilyl group, and recorded in the NMR spectra. Table 3.4 summarizes the number of Si-OH groups per monomer unit, and the percentage of uncondensed Si-OH groups. For the large $MePEG_{16}$ copolymers, all of the copolymers had less uncondensed Si-OH groups compared to the pure polymer. The $MePEG_{16}$ / TFPSi copolymer have the lowest percent of uncondensed Si-OH groups of all the polymer and copolymer samples. For the $MePEG_3$, $MePEG_7$ and $MePEG_{12}$ copolymers, all the copolymers, with the exception of the isobutyl copolymers, had a lower concentration of uncondensed Si-OH than their corresponding pure polymers.

3.4 – Viscosity

The viscosity of the copolymers was measured to determine how the addition of bulky copolymers affects the viscosity relative to the pure polymers, and how viscosity is affected by free volume. Figures 3.1-3.4 show the activation plots for viscosity for all copolymer sets (the line shown is the best fit VTF line eq.1.7a). For the $MePEG_3$ and $MePEG_{16}$ copolymer sets, the pure polymers had the lowest viscosity. For the $MePEG_{12}$ copolymer set, the pure polymer had the second lowest viscosity and for the $MePEG_7$ the pure polymer had the highest viscosity. We expect that the addition of bulky comonomers would decrease the viscosity, which, in some cases it did but there are other factors that will affect the viscosity. One of these factors is cross linking, which we previously saw evidence for. According to the Doolittle equation (eq 1.11a), a decrease in free volume will result in a higher viscosity.

Figure 3.5 shows the Doolittle plot (eq. 1.11a) for all of the $MePEG_n$ polymers and copolymers at 25 °C. The Doolittle plot shows the relationship between the viscosity and the fractional free volume. For the linear best fit line shown, the R^2 value was 0.53 and the P-value

Polymer		Average Number Si-OH per monomer[a]	Area of ^{1}H NMR -OTMS[b]	Percent uncondensed Si-OH[c]	Number of uncondensed Si-OH per monomer unit[d]
$MePEG_3$	**4a**	3.00	5.77	21.4	0.642
$MePEG_3/Ph_2Si$	**5a**	2.86	3.93	14.6	0.418
$MePEG_3$/TFPSi	**6a**	3.00	2.48	9.2	0.276
$MePEG_3$/iBuSi	**7a**	3.00	6.84	25.3	0.759
$MePEG_7$	**4b**	3.00	1.53	5.7	0.171
$MePEG_7/Ph_2Si$	**5b**	2.82	0.78	2.9	0.082
$MePEG_7$/TFPSi	**6b**	3.00	0.44	1.6	0.048
$MePEG_7$/iBuSi	**7b**	3.00	1.85	6.9	0.207
$MePEG_{12}$	**4c**	3.00	2.72	10.1	0.303
$MePEG_{12}/Ph_2Si$	**5c**	2.78	3.70	13.7	0.381
$MePEG_{12}$/TFPSi	**6c**	3.00	0.49	1.8	0.054
$MePEG_{12}$/iBuSi	**7c**	3.00	6.99	25.9	0.777
$MePEG_{16}$	**4d**	3.00	2.06	7.6	0.228
$MePEG_{16}/Ph_2Si$	**5d**	2.74	0.64	2.4	0.066
$MePEG_{16}$/TFPSi	**6d**	3.00	0.38	1.4	0.042
$MePEG_{16}$/iBuSi	**7d**	3.00	0.55	2.0	0.060

[a] Number Si-OH per monomer is the weighted number of Si-OH based on 3 Si-OH for MePEG siloxane, 3,3,3-trifluoropropyl siloxane, and isobutyl siloxane and 2 Si-OH for diphenyl siloxane
[b] ^{1}H NMR –OTMS is the integration under the peak of the –OTMS peak at δ 0.10 ppm
[c] % uncondensed Si-OH is equal to ^{1}H NMR –OTMS divided by # Si-OH per monomer times 9 protons per TMS
[d] #Si-OH/monomer x % uncondensed Si-OH

Table 3.4: End Group Analysis: End group analysis with ^{1}H-NMR integrations and % uncondensed –OH

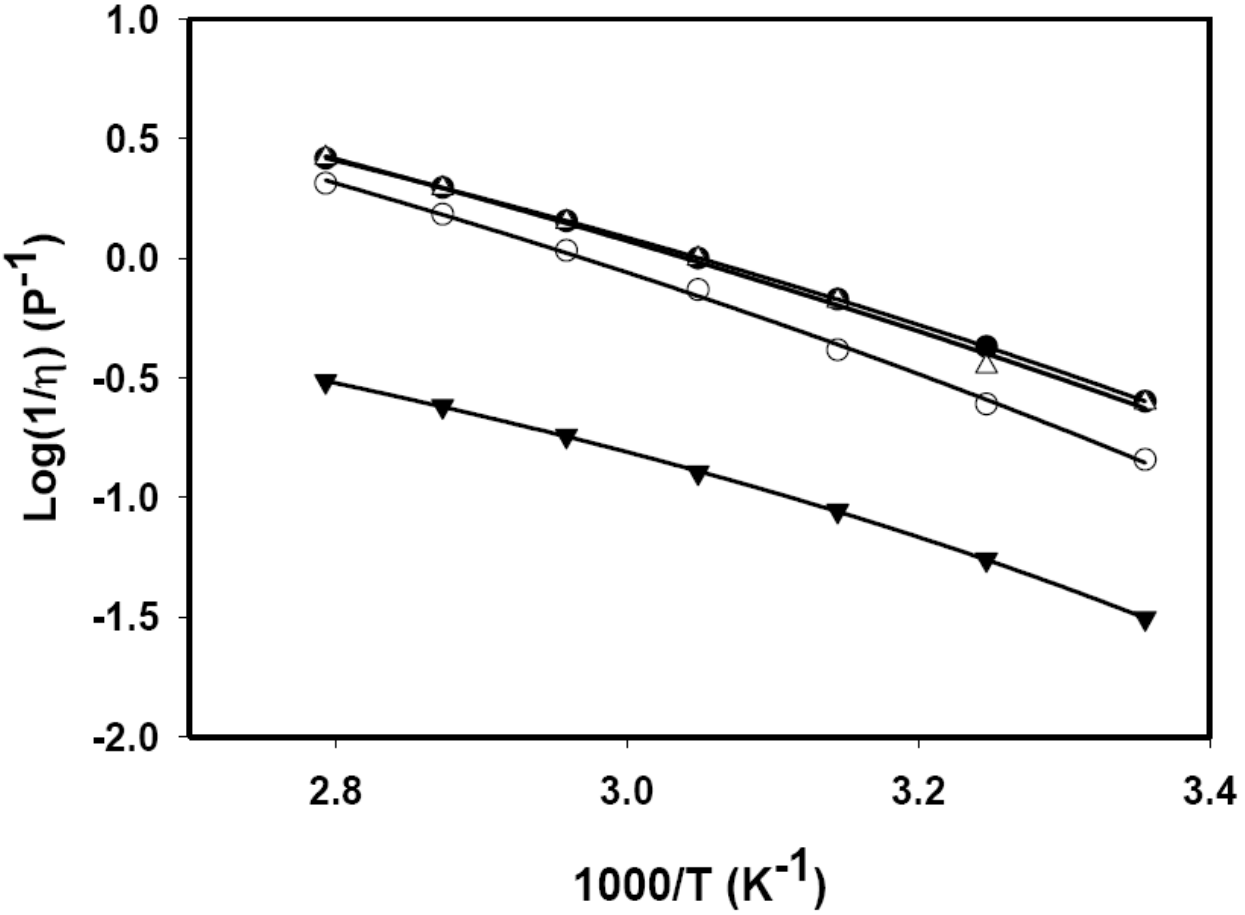

Figure 3.1: Fluidity Activation Plot: Activation Plot for fluidity for $MePEG_3$ copolymers with VTF best fit line shown: ● $MePEG_3$ polymer (**4a**); ○ $MePEG_3/Ph_2Si$ (**5a**); ▼ $MePEG_3$ /TFPSi (**6a**); Δ $MePEG_3$/iBuSi (**7a**).

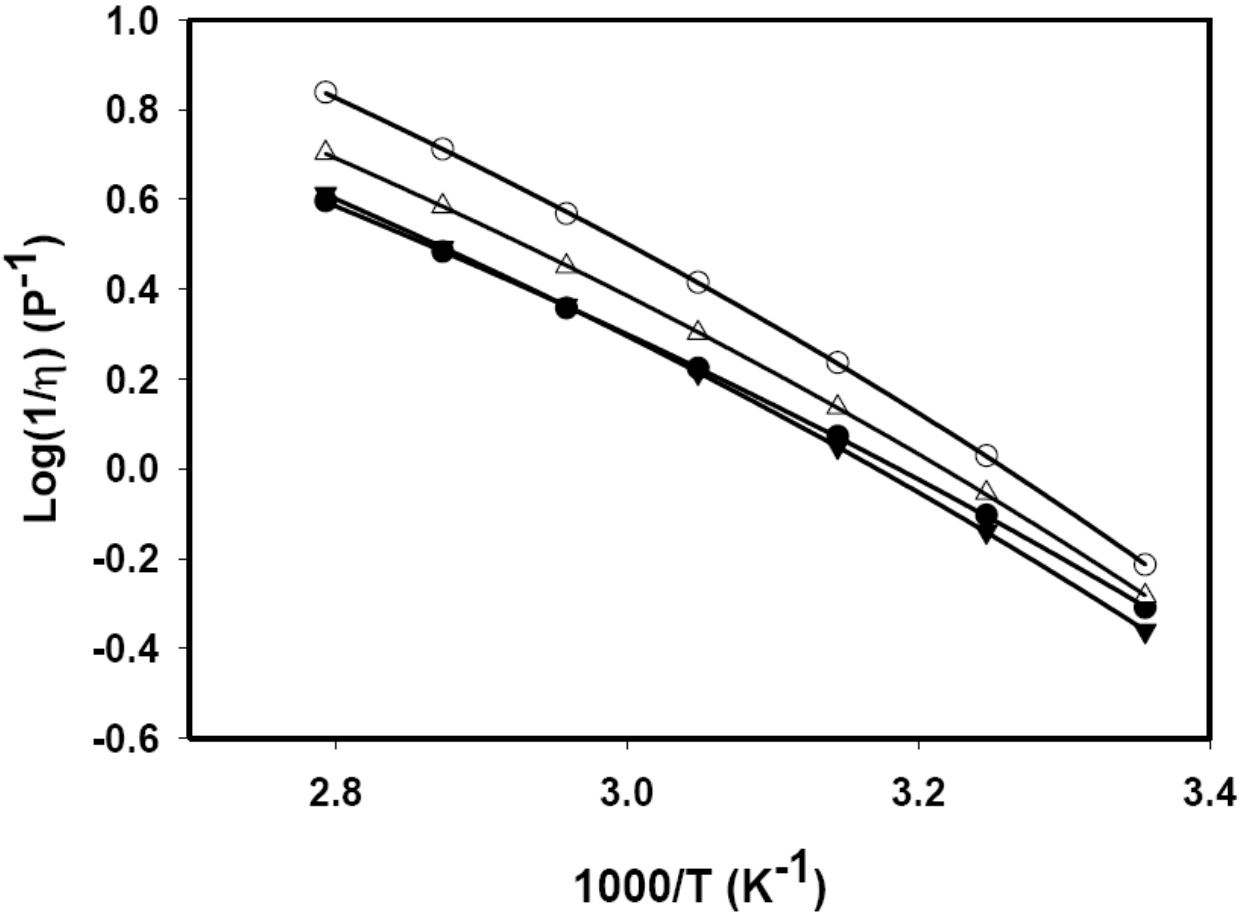

Figure 3.2: Fluidity Activation Plot: Activation Plot for fluidity for $MePEG_7$ copolymers with VTF best fit line shown: ● $MePEG_7$ polymer (**4b**); ○ $MePEG_7/Ph_2Si$ (**5b**); ▼ $MePEG_7$/TFPSi (**6b**); Δ $MePEG_7$/iBuSi (**7b**).

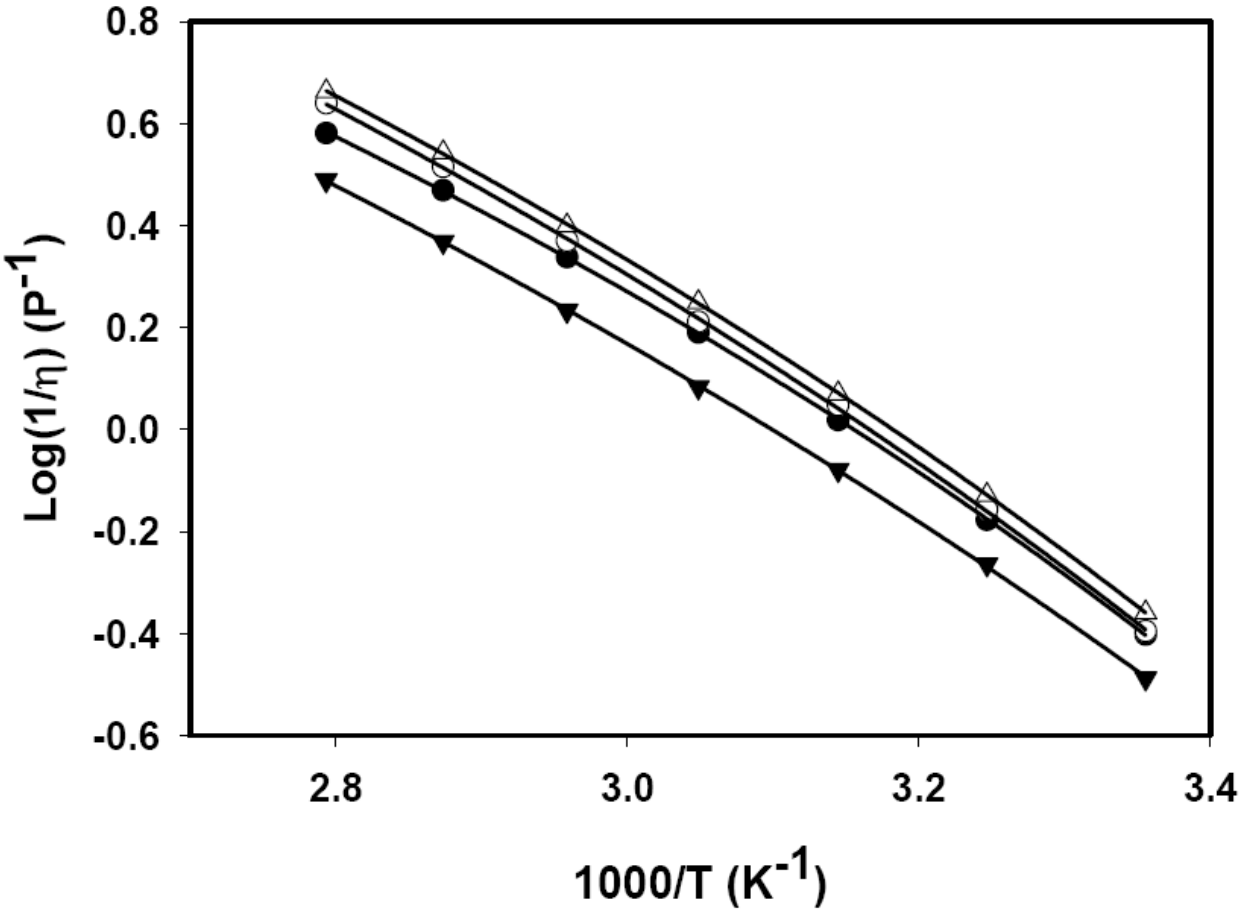

Figure 3.3: Fluidity Activation Plot: Activation Plot for fluidity for $MePEG_{12}$ copolymers with VTF best fit line shown: ● $MePEG_{12}$ polymer (**4c**); ○ $MePEG_{12}/Ph_2Si$ (**5c**); ▼ $MePEG_{12}$ /TFPSi (**6c**); Δ $MePEG_{12}$/iBuSi (**7c**).

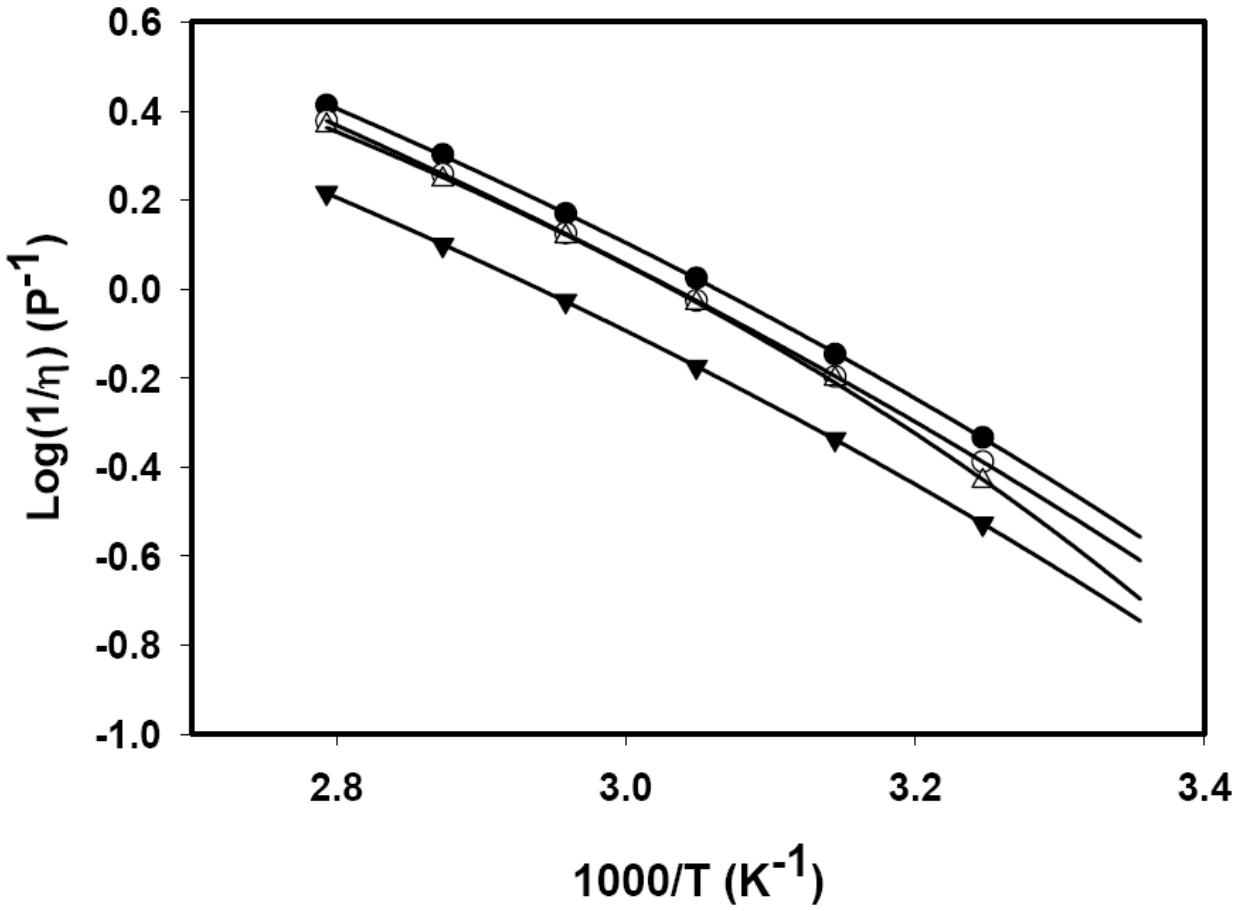

Figure 3.4: Fluidity Activation Plot: Activation Plot for fluidity for $MePEG_{16}$ copolymers with VTF best fit line shown: ● $MePEG_{16}$ polymer (**4d**); ○ $MePEG_{16}/Ph_2Si$ (**5d**); ▼ $MePEG_{16}$ /TFPSi (**6d**); Δ $MePEG_{16}$/iBuSi (**7d**). No fluidity measurements were taken at 25 °C because the $MePEG_{16}$ polymers are waxy solids below 30 °C.

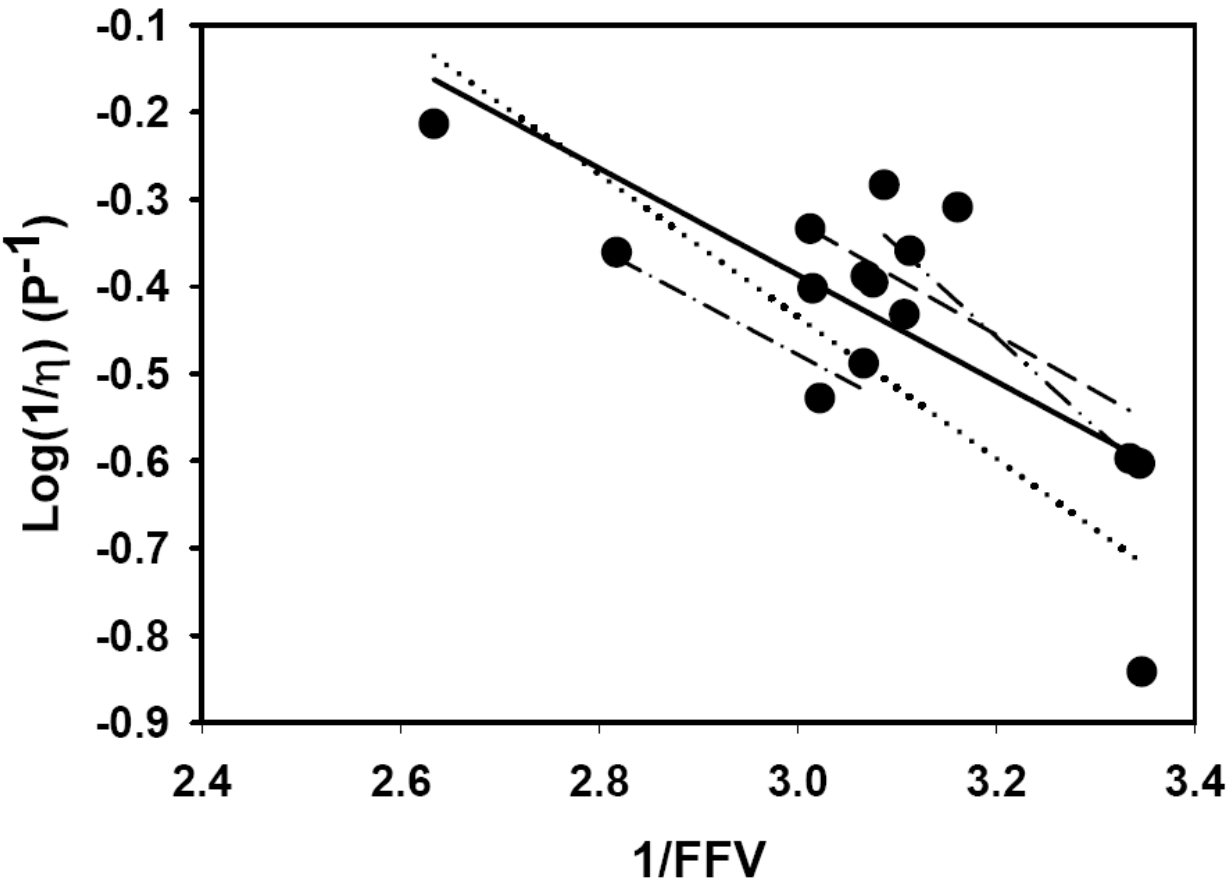

Figure 3.5: Doolittle Plot: Doolittle plot for all $MePEG_n$ copolymers with best fit linear line shown. Eq 1.11a $y = -0.611x + 1.446$, $R^2 = 0.534$, p-value =0.0020,
——— All copolymers, – – – – – $MePEG_n$ polymers, · · · · · · · $MePEG_n/Ph_2Si$,
– · – · – $MePEG_n$/TFPSi, – · · – · · $MePEG_n$/iBuSi

was 0.002. The low P-value indicates that the result is significant, and that the relationship between fractional free volume and viscosity is not random, and likely correlated. The moderate R^2 value suggests that FFV is not the only factor in control of viscosity.

Each individual copolymer series (i.e. the pure $MePEG_n$ polymer, and the copolymers with the Ph_2Si, TFPSi, and iBuSi bulky groups) showed a high correlation coefficient ($R^2 > 0.80$), but the slope of each linear fit was different. The slope in a Doolittle plot is proportional to the material specific constant q in the Doolittle equation (eq. 1.11a). The Doolittle parameters are summarized in table 3.5. The factor q in the Doolittle equation represents the magnitude of the intermolecular forces that resist molecular motion (i.e. the molecular basis of viscosity). [48] These differences in the value of q, calculated from the slope of the Doolittle plot, indicate that the inclusion of the bulky comonomers alters the intermolecular forces in the copolymers by dilution with hydrophobic groups. This result suggests we can produce copolymers with a large range of viscosities by varying the amounts, and polarities, of different bulky groups.

Figure 3.6 shows how the number of PEG repeating units affects the viscosity of the pure $MePEG_n$ polymers (the line is added as a visual reference). Based on the work of Markovic, we expect that viscosity will initially have a sharp decrease with increasing n, and then after reaching a minima, will slowly increase as n increases. [21] Our polymers followed this trend. As Figure 3.6 shows, there is a large decrease in viscosity from the $MePEG_3$ polymer to the $MePEG_7$ polymer but there is an increase for both the $MePEG_{12}$ and $MePEG_{16}$ polymers. This result compares very favorably to Markovic's work with completely condensed PEG/POSS hybrid polymers. Markovic suggested that this trend for hybrid inorganic/organic polymers is due to a competition between the mechanical stability of the inorganic portion and the flexibility of the organic portion.

Copolymer Series	q	A
MePEG polymer	0.536	3.01×10^5
MePEG/Ph_2Si	0.453	4.73×10^4
MePEG/TFPSi	0.165	5.18×10^2
MePEG/iBuSi	1.03	1.09×10^9

Table 3.5: Doolittle Constants: Doolittle constants determined from the individual copolymer series.

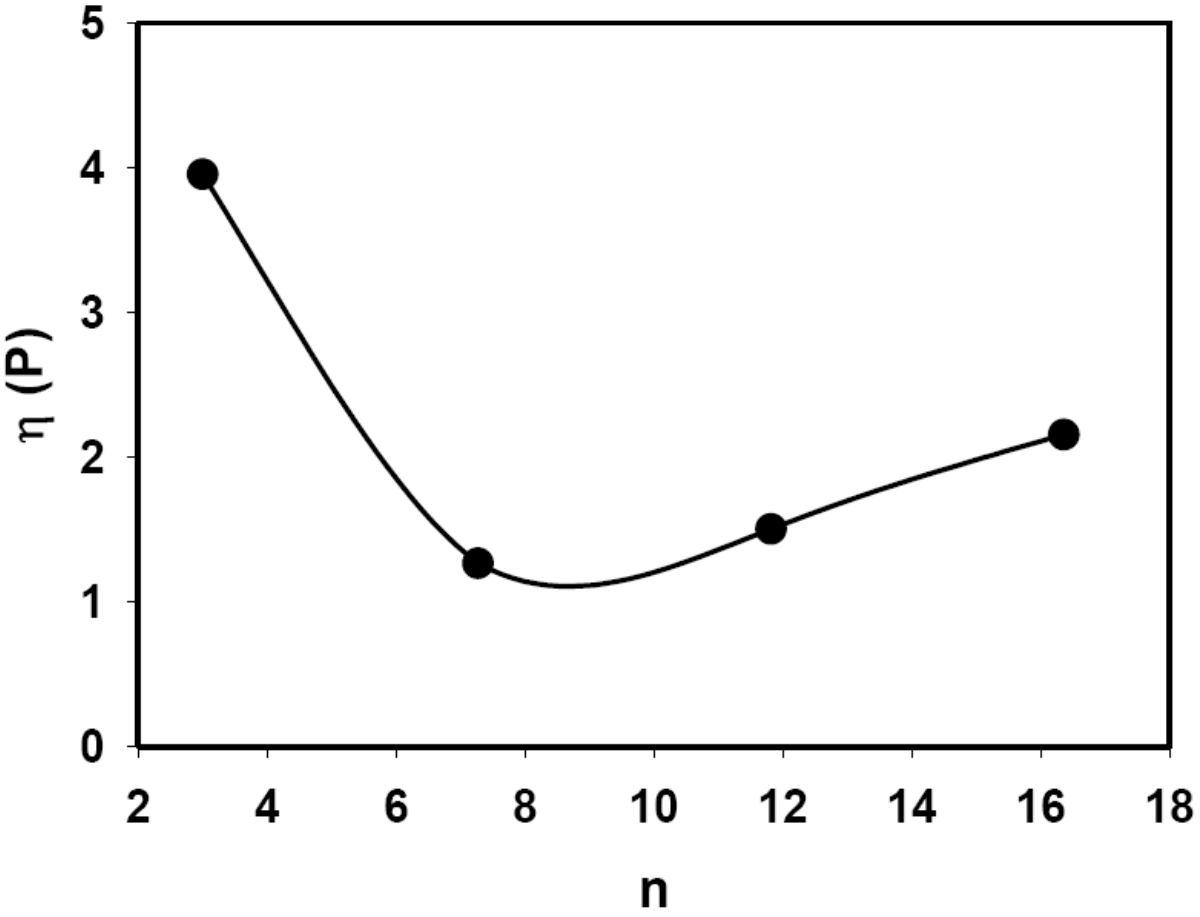

Figure 3.6: Viscosity vs. PEG_n Plot: Plot of viscosity versus the number of PEG_n units. The line drawn is to guide the eye.

3.5 – Ionic conductivity

Figures 3.7-3.13 show Arrhenius activation plots for ionic conductivity for all copolymer electrolytes, made with both low (0.26 M) and high (1.32 M) $MePEG_7SO_3H$ acid concentrations. Comparing Figures 3.7-3.9 with 3.10-3.13, the low acid concentration electrolytes have a much lower conductivity than the high $MePEG_7SO_3H$ acid concentration electrolytes. This result was expected, because, the Forsythe equation (eq. 1.13) predicts that the conductivity increases with an increase in the concentration of charge carriers. The electrolytes made from the pure $MePEG_n$ polymers (**4b-d**) had the highest conductivity at the low $MePEG_7SO_3H$ acid concentration. This includes $MePEG_7$ and $MePEG_{12}$ which have approximately the same proton conductivity as the $MePEG_7$/iBuSi and $MePEG_{12}$/TFPSi copolymers respectively. The electrolytes made from the pure $MePEG_n$ polymers (**4a-d**) also had the highest conductivity at high $MePEG_7SO_3H$ acid concentrations, with the exception of the $MePEG_{16}$ copolymer electrolyte set (Figure 3.13) which has the lowest conductivity.

These results correspond well with the viscosity data in Figures 3.1-3.4 and Figure 3.5, in that the copolymers with highest fluidity also had the highest conductivity. These results also are in agreement with the Stokes-Einstein (eq 1.7) and Nernst-Einstein equations (1.8) which together predict that an increase of fluidity will result in an increase of ionic conductivity.

Figure 3.14 shows a Forsythe plot correlating molar equivalent conductivity (Λ) with FFV for all of the $MePEG_n$ copolymers at 25 °C. The best fit linear fit shown, has a very low R^2 value (0.0025) and a p-value (0.80) both indicating a non-significant result. It is highly likely (> 80 %) that, in this system, there is no correlation between equivalent molar conductivity and FFV. It has been previously observed that for the MePEG polymer system there is a correlation between conductivity and $V_{f\,PEG}$.[27, 55] We have suggested that the conductivities dependence

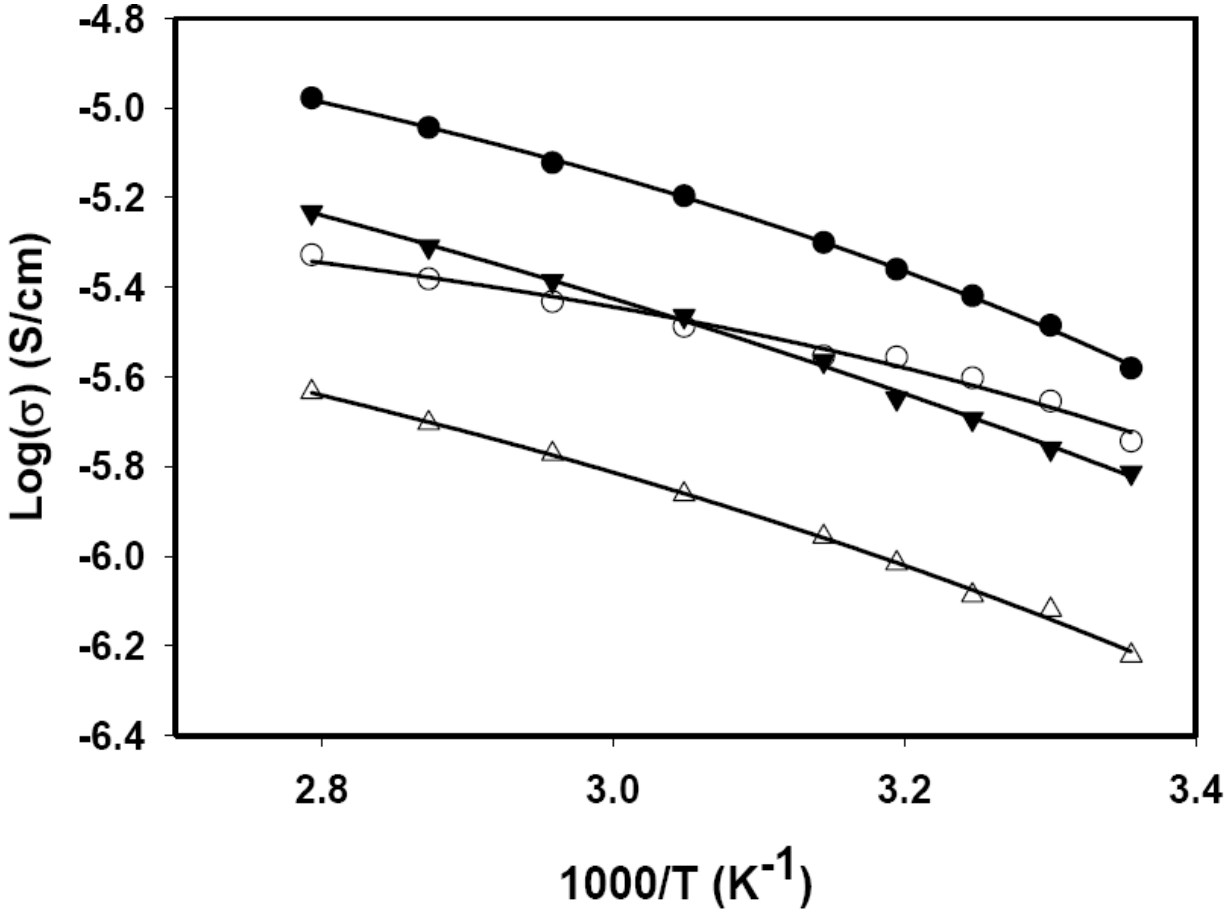

Figure 3.7: Activation Plot for Proton Conductivity: Activation Plot for proton conductivity for $MePEG_7$ copolymers and 0.26 M $MePEG_7SO_3H$ concentration with VTF best fit line shown: ● $MePEG_7$ polymer (**4b**); ○ $MePEG_7/Ph_2Si$ (**5b**); ▼ $MePEG_7$/TFPSi (**6b**); Δ $MePEG_7$/iBuSi (**7b**).

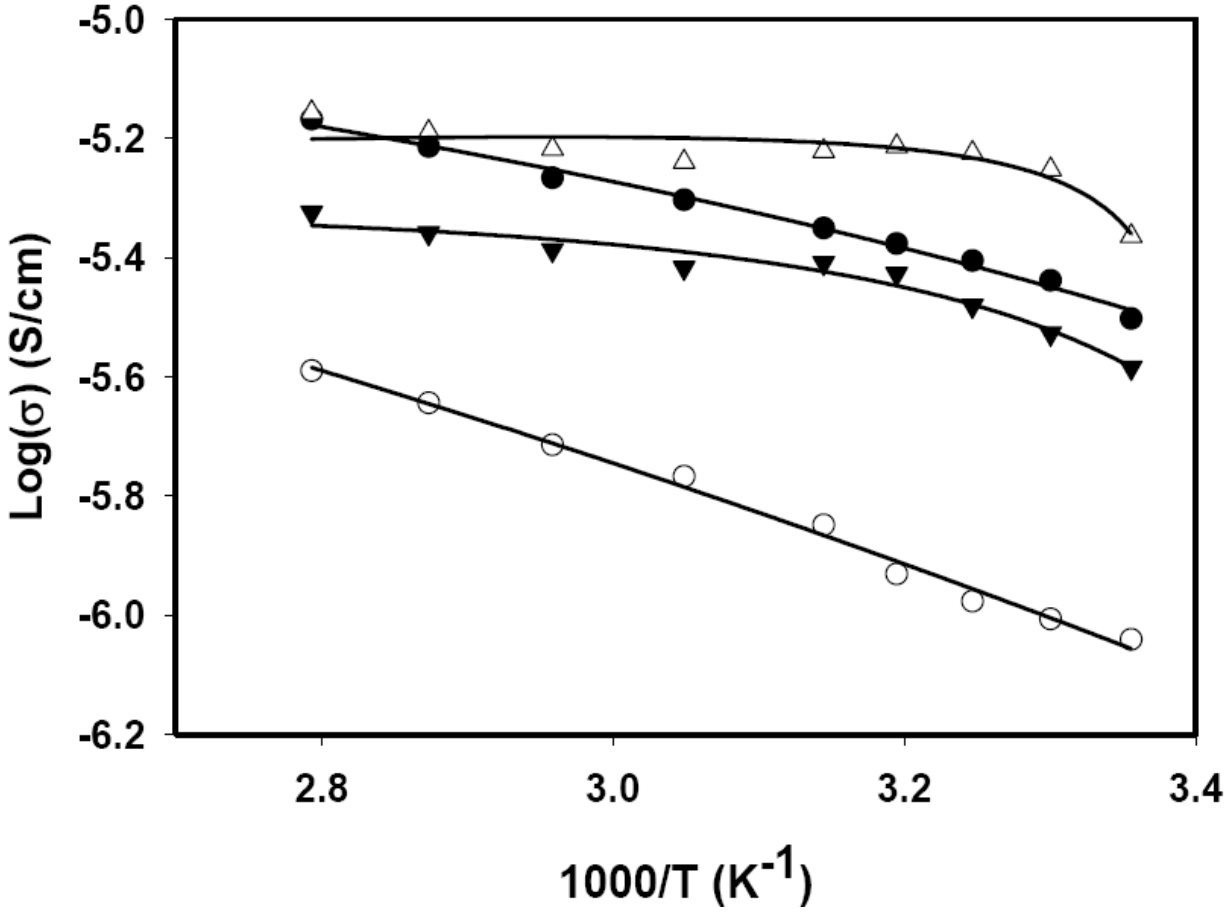

Figure 3.8: Activation Plot for Proton Conductivity: Activation Plot for proton conductivity for $MePEG_{12}$ copolymers and 0.26 M $MePEG_7SO_3H$ concentration with VTF best fit line shown: ● $MePEG_{12}$ polymer (**4c**); ○ $MePEG_{12}/Ph_2Si$ (**5c**); ▼ $MePEG_{12}$/TFPSi (**6c**); Δ $MePEG_{12}$/iBuSi (**7c**).

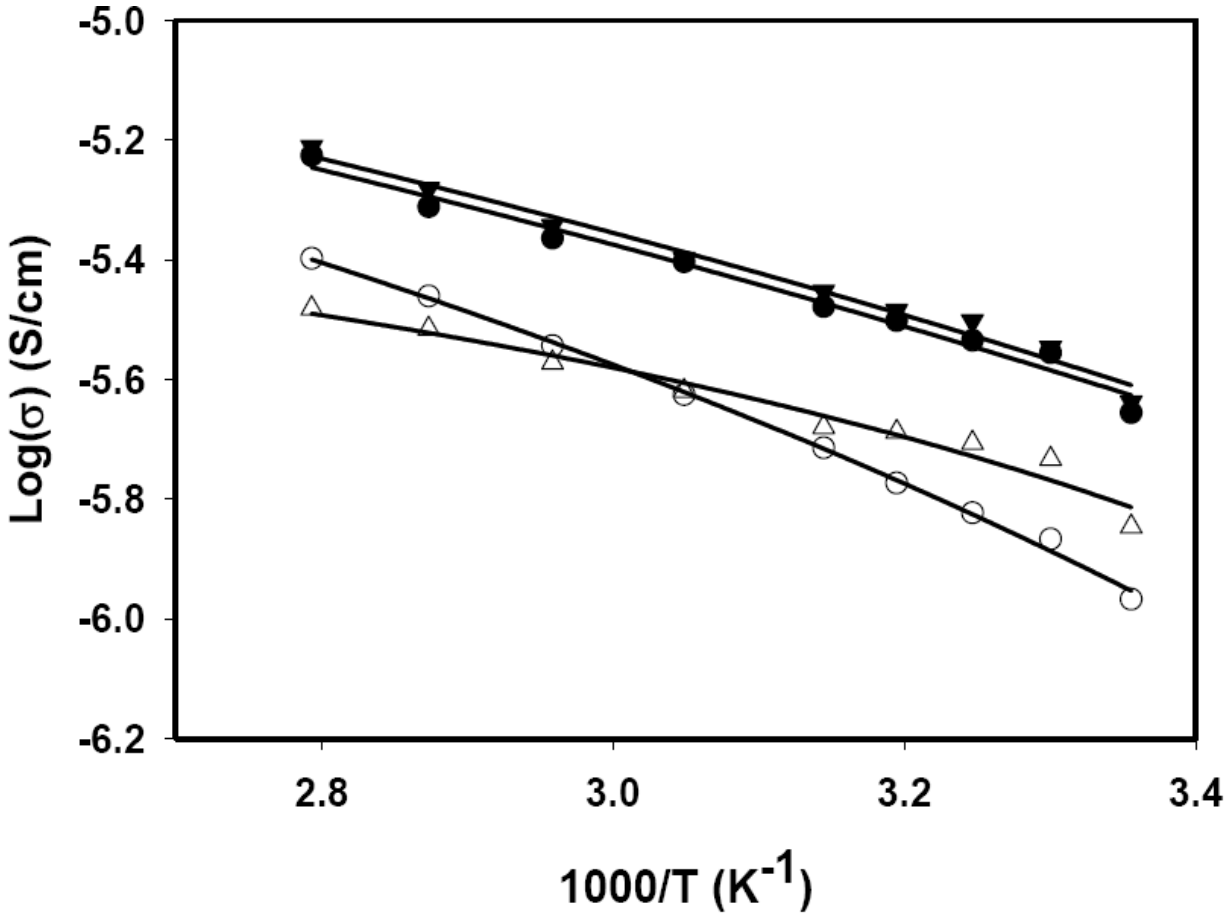

Figure 3.9: Activation Plot for Proton Conductivity: Activation Plot for proton conductivity for $MePEG_{16}$ copolymers and 0.26 M $MePEG_7SO_3H$ concentration with VTF best fit line shown: ● $MePEG_{16}$ polymer (**4d**); ○ $MePEG_{16}/Ph_2Si$ (**5d**);▼ $MePEG_{16}$/TFPSi (**6d**); Δ $MePEG_{16}$/iBuSi (**7d**).

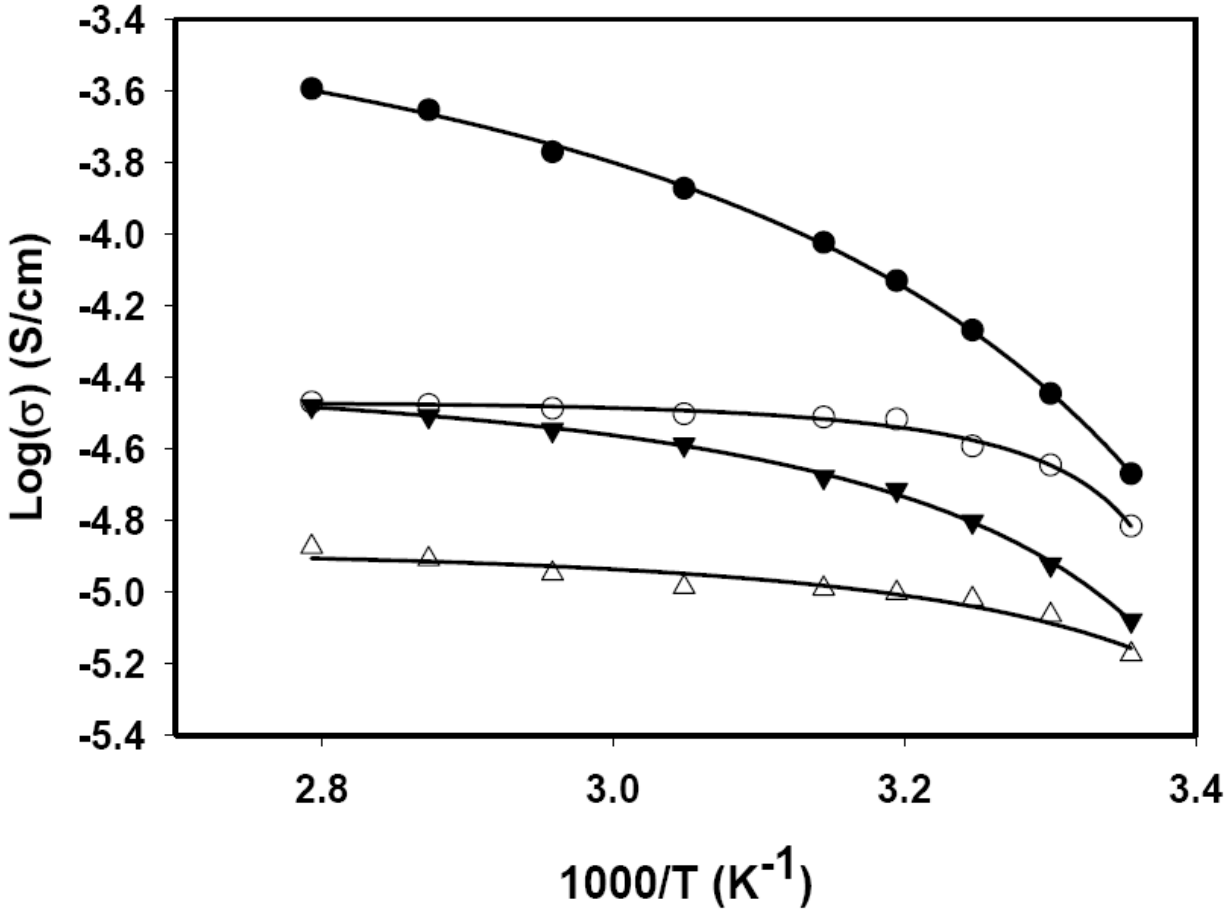

Figure 3.10: Activation Plot for Proton Conductivity: Activation Plot for proton conductivity for $MePEG_3$ copolymers and 1.32 M $MePEG_7SO_3H$ concentration with VTF best fit line shown: ● $MePEG_3$ polymer (**4a**); ○ $MePEG_3/Ph_2Si$ (**5a**); ▼ $MePEG_3$/TFPSi (**6a**); Δ $MePEG_3$/iBuSi (**7a**).

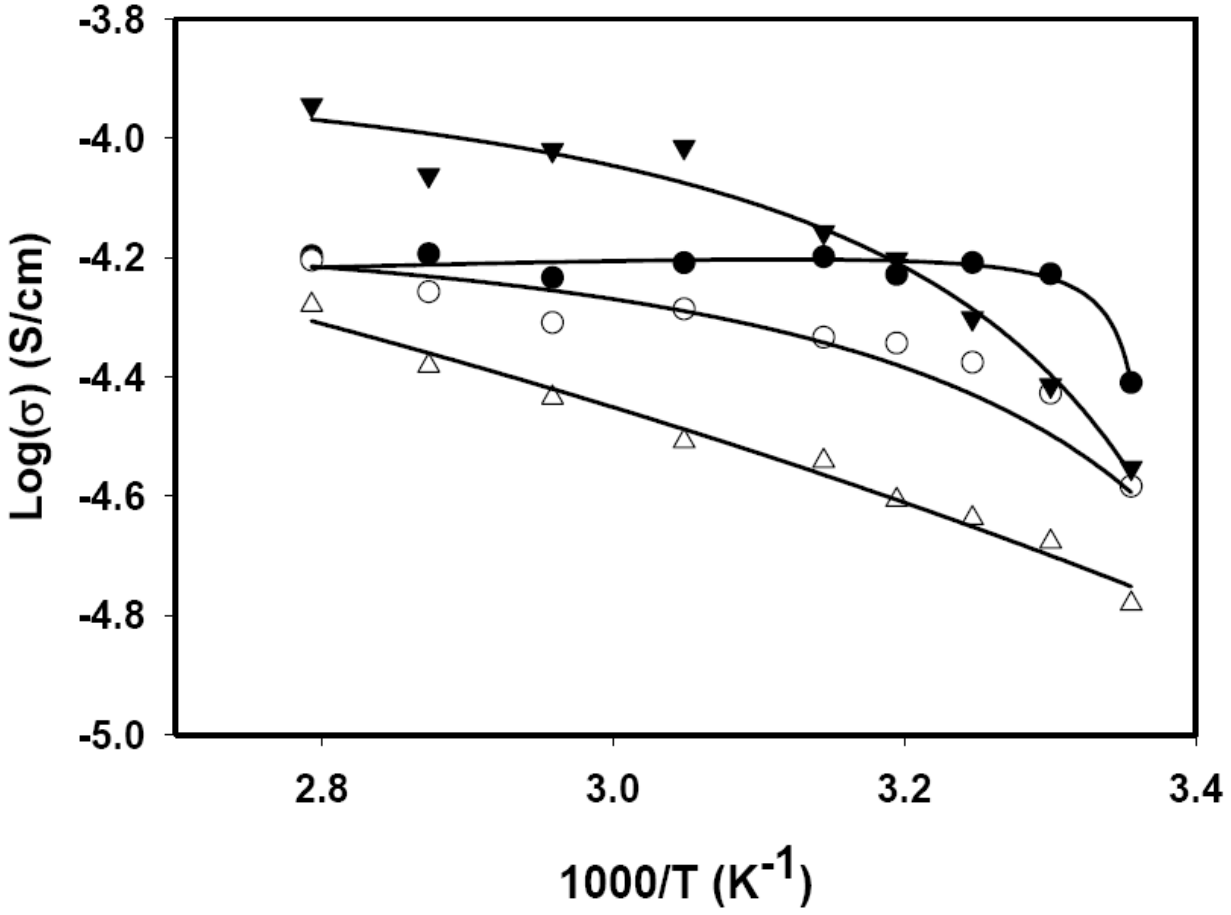

Figure 3.11: Activation Plot for Proton Conductivity: Activation Plot for proton conductivity for $MePEG_7$ copolymers and 1.32 M $MePEG_7SO_3H$ concentration with VTF best fit line shown: ● $MePEG_7$ polymer (**4b**); ○ $MePEG_7/Ph_2Si$ (**5b**); ▼ $MePEG_7$/TFPSi (**6b**); Δ $MePEG_7$/iBuSi (**7b**).

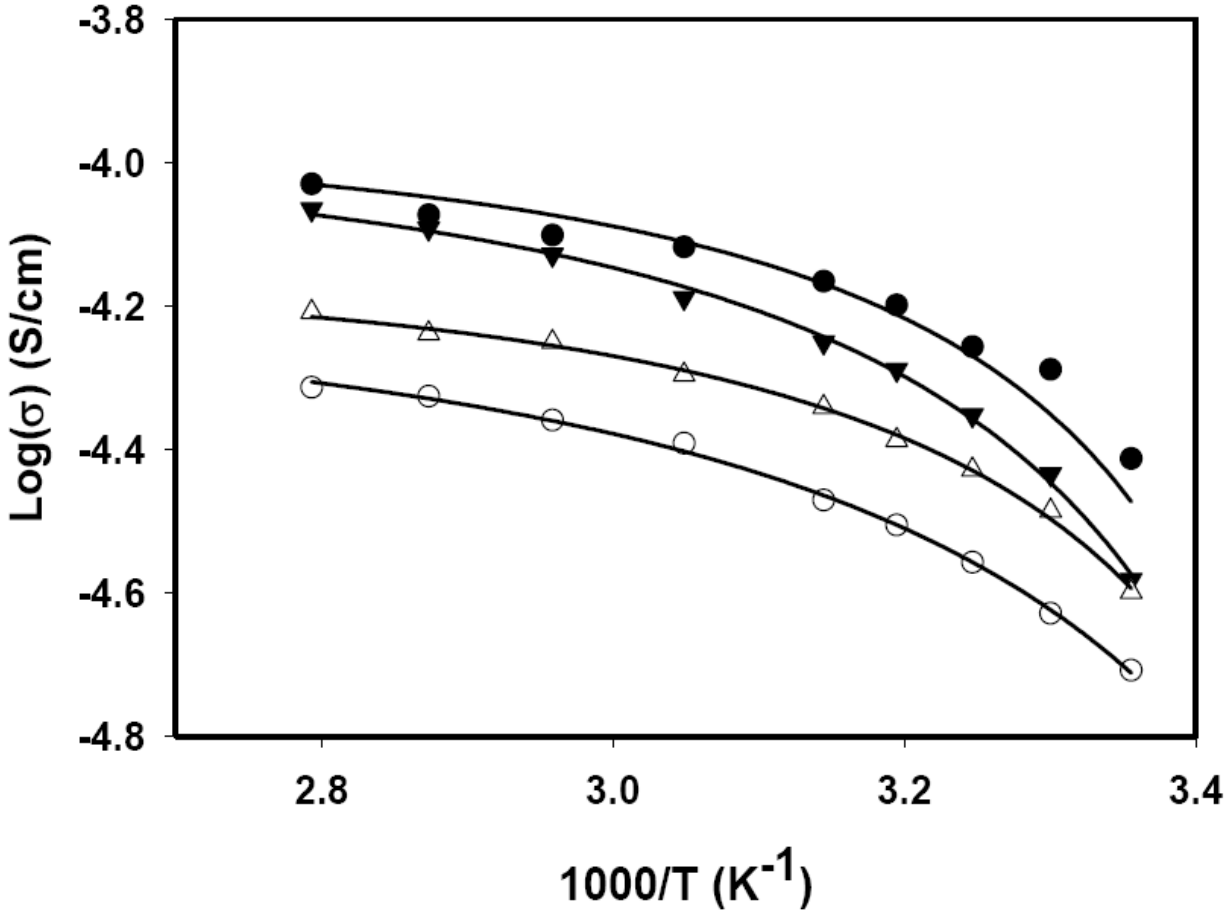

Figure 3.12: Activation Plot for Proton Conductivity: Activation Plot for proton conductivity for $MePEG_{12}$ copolymers and 1.32 M $MePEG_7SO_3H$ concentration with VTF best fit line shown: ● $MePEG_{12}$ polymer (**4c**); ○ $MePEG_{12}/Ph_2Si$ (**5c**); ▼ $MePEG_{12}$/TFPSi (**6c**); Δ $MePEG_{12}$/iBuSi (**7c**).

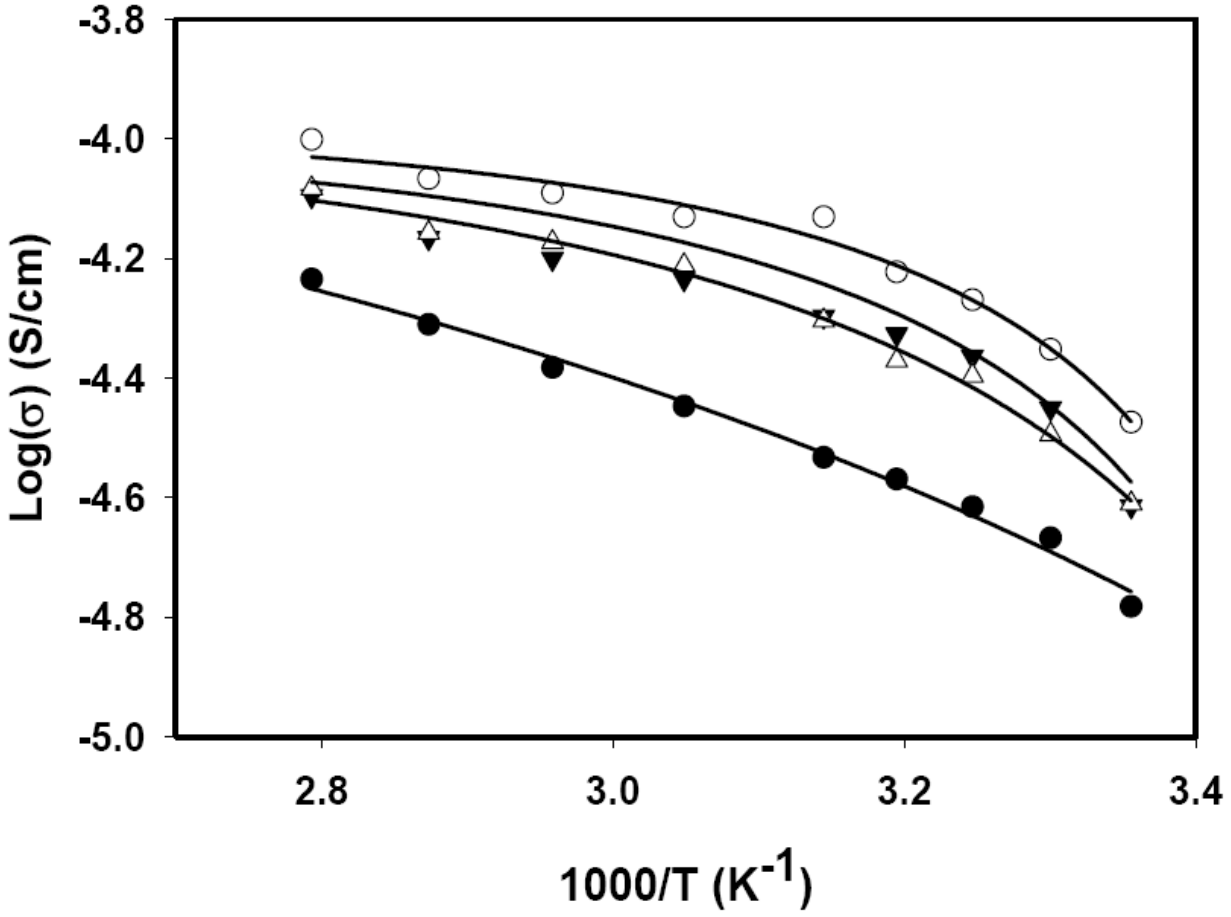

Figure 3.13: Activation Plot for Proton Conductivity: Activation Plot for proton conductivity for $MePEG_{16}$ copolymers and 1.32 M $MePEG_7SO_3H$ concentration with VTF best fit line shown: ● $MePEG_{16}$ polymer (**4d**); ○ $MePEG_{16}/Ph_2Si$ (**5d**); ▼ $MePEG_{16}$/TFPSi (**6d**); Δ $MePEG_{16}$/iBuSi (**7d**).

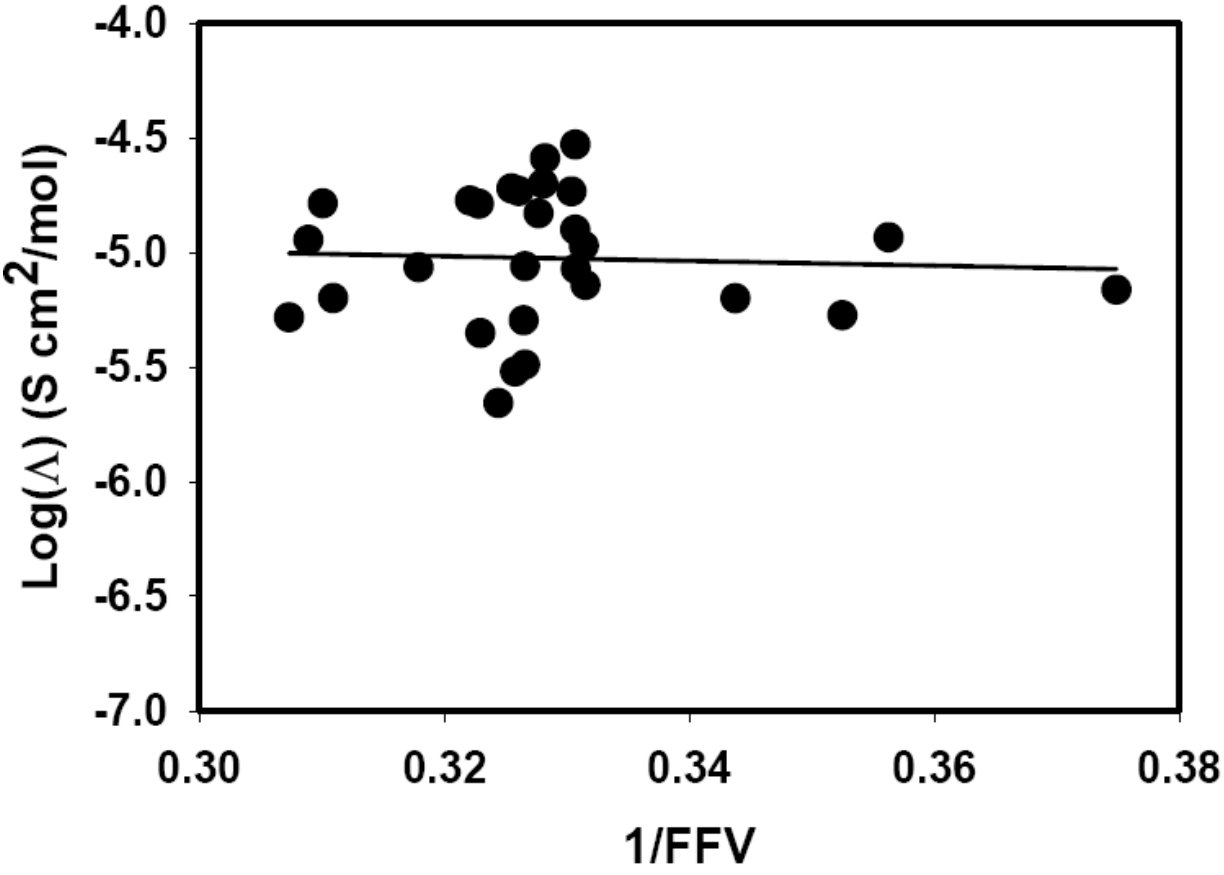

Figure 3.14: Forsythe Plot with FFV: Forsythe plot with fractional free volume for all $MePEG_n$ copolymers with best fit linear line shown. y = -1.027x - 4.6881, R^2 = 0.0025, p-value = 0.800523

on the volume fraction of PEG is due to the Grotthus mechanism being the predominate mode for proton conduction in the MePEG system.[27]

Figure 3.15 shows a Forsythe plot with molar equivalent conductivity correlated with $V_{f,PEG}$ for all of the $MePEG_n$ copolymers at 25 °C. While the linear fit has a low R^2 value (0.095), the p-value (0.11) indicates that there is a likelihood that there is no correlation (11 % probability that the relation is random). This poor correlation likely points towards the addition of the bulky groups actually impeding the flow of protons along succeeding PEG units to some degree in this system. These results show a deviation from the Forsythe relationship due to forces impeding the movements of protons. These forces effectively alter the diffusion coefficient by adding an additional barrier that is not included in the Stokes-Einstein equation. Stokes' law was formulated on the basis of the fluid being continuous. The addition of these bulky groups induces these polymers to no longer be continuous. It is expected that the addition of bulky comonomers to the polymer that do not interrupt the continuity of the fluid would be ideal in that they will follow the Forsythe relationship.

3.6 – Walden Plot

Figures 3.16 and 3.17 are Walden plots for the 0.26 M and 1.32 M copolymer electrolytes respectively. The diagonal line is the ideal Walden relationship with $\alpha = 1$. The data was fit to a linear best fit based on equation 9b where α is equal to the slope. For the 0.26 M copolymer electrolytes, the α values range from 0.15 to 0.66. For all MePEG chain lengths, the copolymers follow the trend in α where isobutyl < 3,3,3-trifluoropropyl < polymer < diphenyl. This trend appears to follow the polarity of the copolymers indicating that the acid dissociation constant (K_a) is a factor. The more polar the group, the better the acid will dissociate. The less

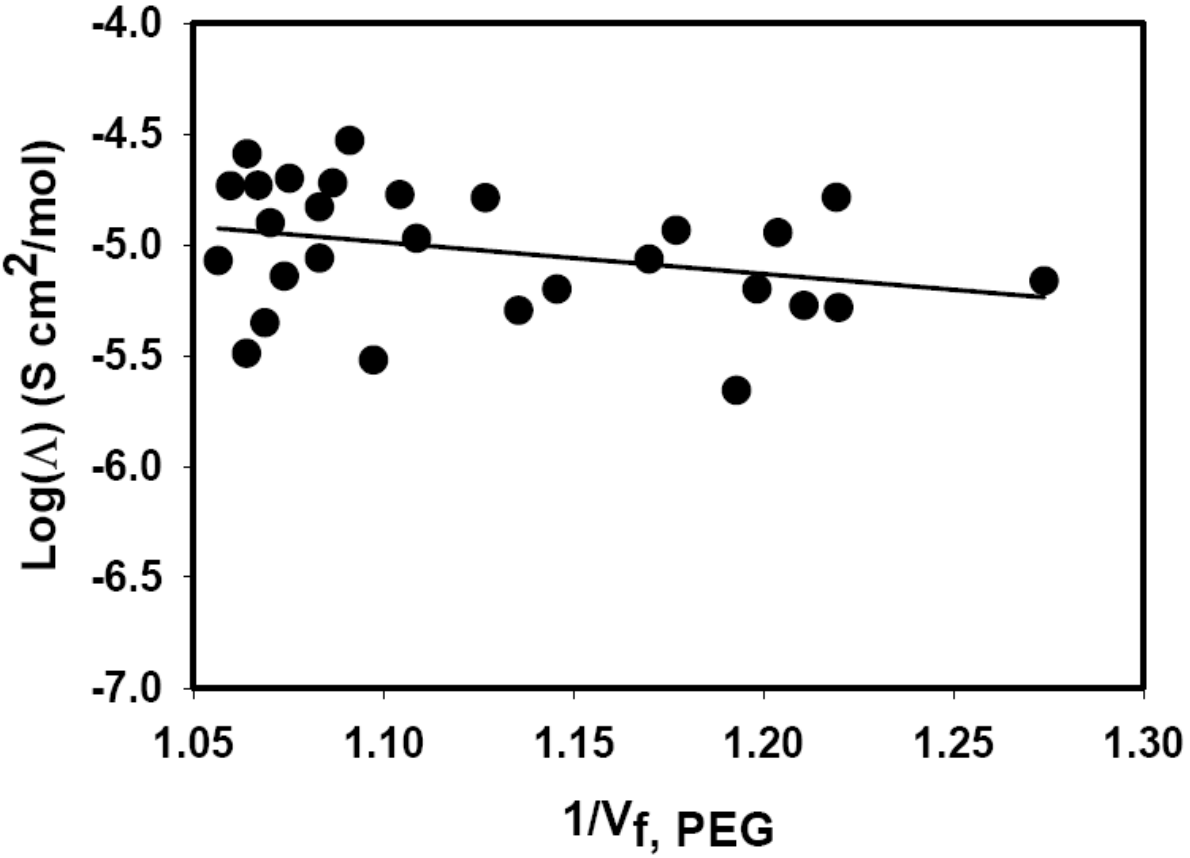

Figure 3.15: Forsythe Plot for $V_{f,PEG}$: Forsythe plot with volume fraction of PEG for all $MePEG_n$ copolymers with best fit linear line shown. y = -1.4292x - 3.4162, R^2 = 0.0946, p-value = 0.112043

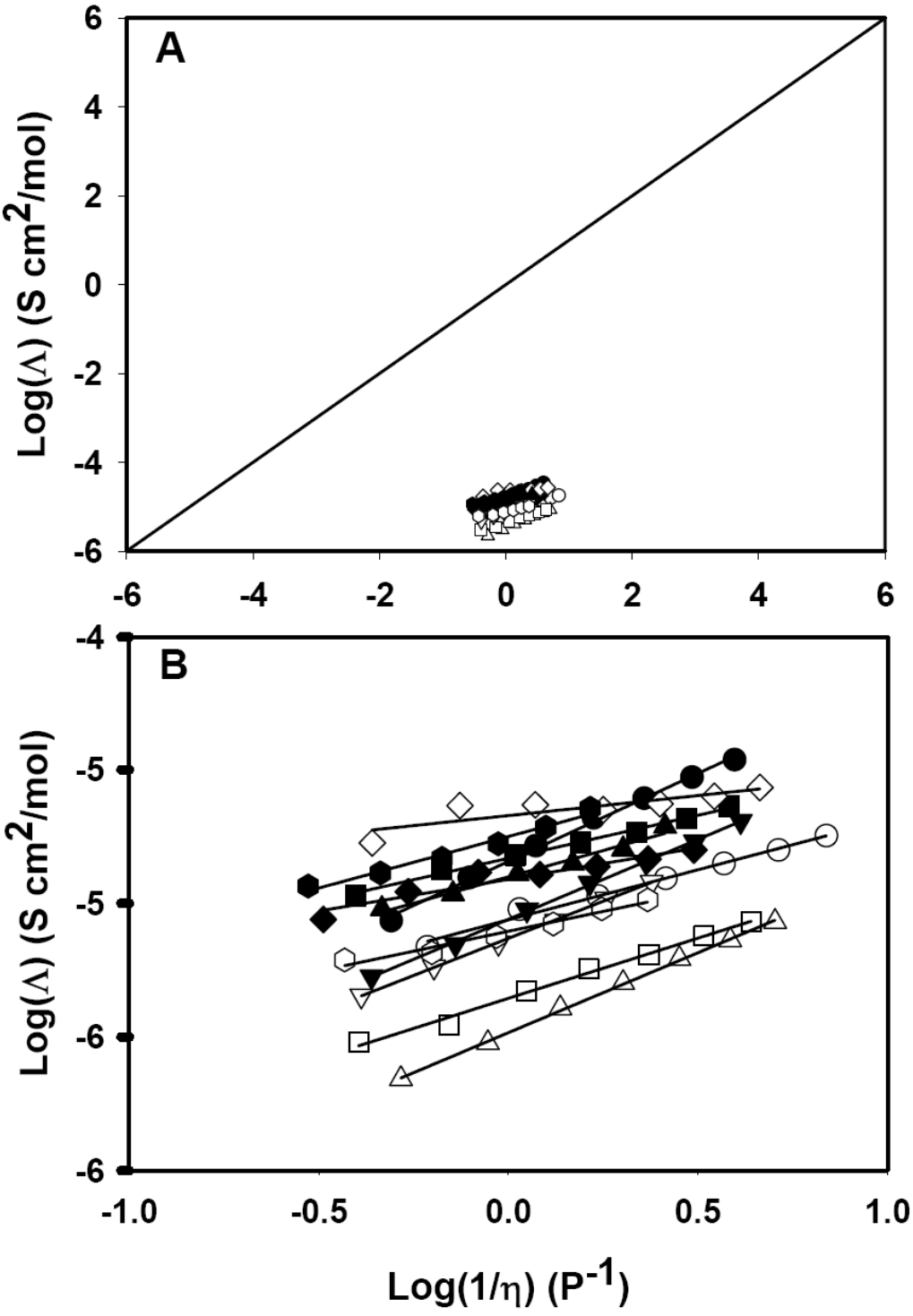

Figure 3.16: (**A)**: Walden Plot for 0.26M copolymer electrolytes with linear best fit line shown. (**B)**: is an expanded region of (**A)** ● $MePEG_7$ polymer (4b) ○ $MePEG_7/Ph_2Si$ (5b) ▼ $MePEG_7$/TFPSi (6b) Δ $MePEG_7$/iBuSi (7b) ■ $MePEG_{12}$ polymer (4c) □ $MePEG_{12}/Ph_2Si$ (5c) ♦ $MePEG_{12}$/TFPSi (6c) ◊ $MePEG_{12}$/iBuSi (7c) ▲ $MePEG_{16}$ polymer (4d) ∇ $MePEG_{16}/Ph_2Si$ (5d) ● $MePEG_{16}$/TFPSi (6d) ○ $MePEG_{16}$/iBuSi (7d)

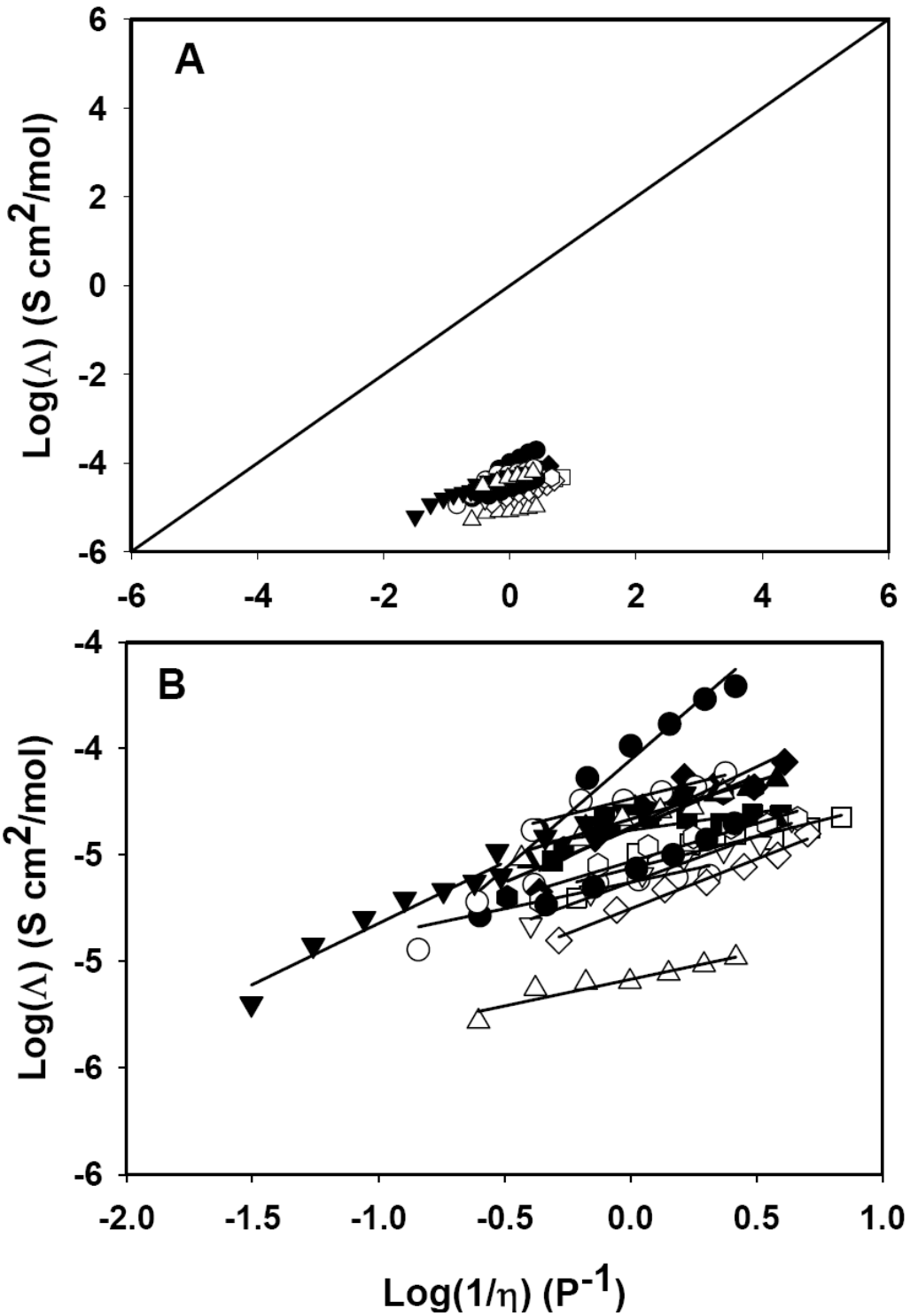

Figure 3.17: (**A**): Walden Plot for all 1.32 M copolymer electrolytes with linear best fit line shown. (**B**): is an expanded region of (**A**) ● $MePEG_3$ polymer (4a) ○ $MePEG_3/Ph_2Si$ (5a) ▼ $MePEG_3$/TFPSi (6a) Δ $MePEG_3$/iBuSi (7a)■ $MePEG_7$ polymer (4b) □ $MePEG_7$/ Ph_2Si (5b) ♦ $MePEG_7$/TFPSi (6b) ◊ $MePEG_7$/iBuSi (7b) ▲ $MePEG_{12}$ polymer (4c) ∇ $MePEG_{12}/Ph_2Si$ (5c) ● $MePEG_{12}$/TFPSi (6c) ○ $MePEG_{12}$/iBuSi (7c) ▼ $MePEG_{16}$ polymer (4d) Δ $MePEG_{16}/Ph_2Si$ (5d) ■ $MePEG_{16}$/TFPSi (6d) □ $MePEG_{16}$/iBuSi (7d)

polar the bulky groups are, the less that they contribute to proton mobility. For the 1.32 M copolymer electrolytes, the α values range from 0.16 to 0.57.

For all the MePEG chain lengths, the copolymers follow the same trend as for the 0.26 M copolymers. These low α values indicate that the copolymer electrolytes have other forces (polymer rigidity or small acid dissociation constant) impeding ion mobility other than the viscosity. A small acid dissociation constant would not physically impede the ion mobility but rather decreases the number of mobile protons, the Walden equation assumes that all of the available charge carriers are mobile. It should also be noted that all of the copolymer electrolytes fall within the area of the Walden plot that defines poor electrolytes. This likely indicates that not all of the protons are mobile in the electrolyte. This can probably be attributed to the acid dissociation constant (K_a)

3.7 – Summary

The synthesis of these materials is a simple route to novel inorganic/organic hybrid polymer electrolytes. The sol-gel condensation reaction results in a small fraction of uncondensed Si-OH units for all of the copolymers. The polymers and copolymers produced by this method have low molecular weight peaks (from GPC analysis) that correspond to monomer and "dimers" and also have high molecular weight peaks that correspond to oligomers having between 5 and 20 monomer units. The addition of the bulky copolymers successfully increased the fractional free volume and decreased the density for the shorter chain length MePEG polymers, but for the longer chain length MePEG polymers, the FFV was decreased and the density increased. These results also correspond to an increase of fluidity for shorter chain length polymers and a decrease in fluidity for longer chain length polymers. The fluidity did, in fact,

obey the behavior predicted by the Doolittle equation. For conductivity, however, the increase of FFV did not correspond to an increase of conductivity. There is evidence that this occurred due to the fact that increasing the fluidity decreased the number of PEG units in the copolymers.

For most of the electrolytes, the bulky group copolymers had lower conductivity than the corresponding MePEG polymers. There is also evidence that suggests that there may be different transport mechanisms at work in the copolymer systems. From the Walden plot, it is clear that some force, besides viscosity, is impeding the ion mobility. Possible sources that could impede ion mobility are the rigidity of the polymer, and a small acid dissociation constant. Analysis of the Forsythe plots provided further evidence that fractional free volume is not the only mechanism that controls proton conductivity but there is a strong probability that the conductivity is related to the volume fraction of PEG, indicating the Grotthus mechanism may be controlling proton conductivity. The results show that, for this set of experiments, free volume is less of a contributor to proton conductivity than the volume fraction of PEG.

IV. RESULTS AND DISCUSSION OF PEG/PPG COPOLYMERS

In this chapter, I report the analysis of a series of sol-gel polymers ($MePEG_7O(CH_2)_3Si(OCH_2CH_3)_3$, and $MePPG_nO(CH_2)_3$-$Si(OCH_2CH_3)_3$, n = 2 and 3) and copolymers ($MePEG_7/MePPG_3$, $MePEG_7/MePPG_2$, $MePPG_3/MePPG_2$). These copolymers were then combined with $MePEG_7SO_3H$ acid to create proton-conducting electrolytes. These electrolytes are viscous liquids at room temperature. These copolymer electrolytes were investigated to determine the relationship between fractional free volume and transport properties as outlined in free volume theory.

4.1– Fractional free volume

We have previously described how to determine the V_w, and FFV of a copolymer (Section 3.1). [39-41] The FFV data is summarized in table 4.1. In general, there is little difference of FFV between the PEG-PPG copolymers (>7 % difference) and there is no trend observed between mole fraction and fractional free volume. We have previously described how to determine the volume fraction of ether ($V_{f,ether}$) of a copolymer (Section 3.1). [55, 56] (Note that we have previously called this term the volume fraction of PEG, but have switched our notation because we are also using polypropylene glycol in this paper [1, 27, 55]). The $V_{f,ether}$ data is also summarized in table 4.1.

The calculation of the volume fraction of ether in a mixture of $MePEG_nSO_3H$ acid and $MePEG_n$ and $MePPG_n$ copolymers ($V_{f,ether,mix}$) has been described previously (Section 3.1). [55, 56] Table 4.2 summarizes the calculated values of the FFV and the volume fractions of ether in

Polymers and Copolymers		MW g/mol[a]	D g/mL	Molar volume (V_m)[b]	van der Waals volume (V_w)[c]	FFV[d]	$V_{f,ether}$[e]
$MePEG_7$ polymer		443	1.169	379	262	0.308	0.789
$MePPG_3$ polymer		299	1.109	270	183	0.321	0.697
$MePPG_2$ polymer		241	1.141	211	147	0.304	0.622
$MePEG_7$ / $MePPG_3$ copolymer	75:25[f]	407	1.151	354	242	0.314	0.772
	50:50	371	1.137	326	222	0.317	0.751
	25:75	335	1.148	292	203	0.305	0.727
$MePEG_7$ / $MePPG_2$ copolymer	75:25	393	1.159	339	234	0.310	0.763
	50:50	342	1.156	296	205	0.308	0.729
	25:75	292	1.136	257	176	0.315	0.685
$MePPG_3$ / $MePPG_2$ copolymer	75:25	285	1.104	258	174	0.325	0.681
	50:50	270	1.116	242	165	0.318	0.663
	25:75	256	1.123	228	156	0.314	0.644
$MePEG_7SO_3H$		414	1.212	342	267	0.330	-

[a] effective MW for copolymers represents the MW of one "repeat unit" of the polymer. One repeat unit of $MePEG_7$ polymer is defined as $MePEG_7OCH_2CH_2CH_2SiO_{3/2}$

[b] V_m for polymers and copolymers represents the weighted V_m calculated using the effective MW

[c] V_w for polymers and copolymers represents the weighted V_w calculated by the Bondi group contribution method

[d] Fractional Free Volume (FFV) is calculated according to equation…

[e] Volume fraction of ether ($V_{f,ether}$) is calculated according to equation…

[f] the 75:25 ratio indicates that this copolymer is 75% mole fraction $MePEG_7$ polymer, and 25% mole fraction $MePPG_3$ polymer (table 1).

Table 4.1: FFV and $V_{f,ether}$ Data: Fractional free volumes for PEG-PPG copolymers and $MePEG_7SO_3H$ acid.

Polymer		[$MePEG_7SO_3H$] (mol/L)	$V_{f,ether,mix}$[a]	FFV_{mix}[b]
$MePEG_7$ polymer		0.26	0.452	0.309
		1.32	0.455	0.316
$MePPG_3$ polymer		0.26	0.446	0.322
		1.32	0.454	0.324
$MePPG_2$ polymer		0.26	0.441	0.306
		1.32	0.453	0.314
$MePEG_7$ / $MePPG_3$ copolymer	75:25	0.26	0.450	0.315
		1.32	0.454	0.320
	50:50	0.26	0.449	0.318
		1.32	0.454	0.322
	25:75	0.26	0.448	0.307
		1.32	0.454	0.315
$MePEG_7$ / $MePPG_2$ copolymer	75:25	0.26	0.450	0.312
		1.32	0.454	0.318
	50:50	0.26	0.448	0.310
		1.32	0.454	0.317
	25:75	0.26	0.445	0.316
		1.32	0.454	0.320
$MePPG_3$ / $MePPG_2$ copolymer	75:25	0.26	0.445	0.325
		1.32	0.454	0.326
	50:50	0.26	0.444	0.319
		1.32	0.454	0.322
	25:75	0.26	0.443	0.316
		1.32	0.454	0.320

[a] $V_{f\ ether\ mixture}$ for copolymer electrolytes is the weighted $V_{f\ ether\ mixture}$ of the monomeric units and the $MePEGSO_3H$ acid.

[b] $FFV_{mixture}$ for copolymer electrolytes is the weighted $FFV_{mixture}$ of the monomeric units and the $MePEGSO_3H$ acid.

Table 4.2: $V_{f,Ether}$ and FFV Data for Acid Mixtures: Ether volume fractions for PEG-PPG copolymer electrolyte mixtures with 0.26 M and 1.32 M $MePEG_7SO_3H$ acid.

the copolymer/acid. For the 1.32 M polymer electrolytes, the $V_{f,ether}$ was essentially the same (> 0.5% difference) for all samples; but for the 0.26 M polymer electrolytes, the $V_{f,ether}$ went from the longest chains value to the shortest chains value along each series.

There were no trends observed for the FFV.

4.2 – Gel Permeation Chromatography (GPC)

GPC analysis was performed to determine the effects of cross-linking in the polymerization of the $MePEG_n$ and $MePPG_n$ polymers and copolymers. Evidence of cross-linking and degree of polymerization can be determined from GPC analysis from the mass and polydispersity index (PDI). The GPC analysis results for the $MePEG_n$ and $MePPG_n$ polymers and copolymers are summarized in Table 4.3. Two peaks were observed in the GPC for many of the copolymers that correspond to the polymer and dimer peaks. There is only one peak observed for several of the copolymers because the monomer and "dimer" of these copolymers have a small M_w. The ELS detector (sensitivity $\propto MW^2$) has difficulty detecting these low M_w components as described previously (Section 3.2).

For the polymers that have two peaks, there is a low molecular weight peak that corresponds to a mixture of monomers and dimers. For both the high and low MW peaks, there is no trend between mole fraction, M_w, M_n or PDI. The number of monomer units ranges from approximately 8 to 15 for the high MW peaks. For both the $MePEG_7/MePPG_3$ and $MePEG_7/MePPG_2$ copolymers, the number of monomer units decreased as the mole fraction of PPG increase. For the $MePPG_3/MePPG_2$ copolymers, the number of monomer units increased.

Those results together indicate that the polymerization does not occur at the same rate for MePEG as for MePPG. The smaller MePPG comonomers have less steric hindrance, which,

Polymers and Copolymers		"High" MW peak[c]			"Low" MW peak[d]			% Si–OH[e]
		M_w (Da)	PDI[a]	# of mono-mers[b]	M_w (Da)	PDI[a]	# of mono-mers[b]	
$MePEG_7$ polymer		3813	1.37	8.61	546	1.31	1.23	1.00
$MePPG_3$ polymer		2652	2.43	8.86	-	-	-	2.30
$MePPG_2$ polymer		3163	8.01	13.1	-	-	-	1.78
$MePEG_7$ / $MePPG_3$ copolymer	75:25	5017	1.53	12.3	550	1.55	1.35	1.44
	50:50	4140	1.51	11.2	577	1.50	1.55	4.74
	25:75	2794	4.70	8.33	-	-	-	4.96
$MePEG_7$ / $MePPG_2$ copolymer	75:25	4165	1.46	10.6	527	1.60	1.34	1.19
	50:50	4166	1.61	12.2	539	1.26	1.58	1.19
	25:75	3332	1.52	11.4	450	1.52	1.54	5.07
$MePPG_3$ / $MePPG_2$ copolymer	75:25	2191	4.57	7.69	-	-	-	1.07
	50:50	2485	2.98	9.20	-	-	-	1.96
	25:75	3813	3.06	14.4	-	-	-	1.19

[a] PDI = M_w/M_n

[b] # of monomers is calculated by dividing M_w by the weighted monomer molecular weight

[c] "High" MW peak is the peak observed with the highest M_w when more than one peak is present

[d] "Low" MW peak is the peak observed with the lowest M_w when more than one peak is present

[e] % uncondensed Si-OH is equal to ^{1}H NMR –OTMS divided by 3 Si-OH per monomer times 9 protons per TMS

Table 4.3: GPC and End Group Analysis Data: GPC data for copolymers with weight average molecular weight (M_w), polydispersity index (PDI), and number of monomers with the percent uncondensed Si-OH.

likely allow the condensation reaction to proceed faster than for the larger $MePEG_7$ comonomer. It is also noteworthy that the $MePPG_2$ had the highest number of monomers in the high molecular weight peak indicating that its polymerization rate is the fastest. Molecular weight has previously been observed to affect the rate of polymerization for other trialkoxysilanes.[57] For the polymers with the highest fraction of $MePEG_7$, the PDI was between 1.3 and 1.6 indicating relatively small dispersity in the polymer molecular weight. The polymers with higher fractions of PPG, especially $MePPG_2$ had considerably higher PDI values ranging from 2.4 to 8.0 indicating a very random polymerization compared to those polymers with the higher $MePEG_7$ fractions.

4.3 – End Group Analysis

End group analysis was performed to determine if the copolymers were completely condensed, and if the presence of the copolymer altered the degree of polymerization. The end group analysis results are also included in table 3.4. The copolymers ranged from 1% to 5% uncondensed Si—OH. These relatively low numbers indicate that the condensation was nearly complete. The highest percentage of uncondensed silanols were in the copolymers with the highest fraction of PPG. These could be caused by size incompatibilities or differences in polymerization rates. Both occurrences would be expected to increase the amount of uncondensed silanols.

4.4 – Viscosity

The viscosities of the copolymers were measured to determine the relationship between fractional free volume and viscosity for these copolymers. Figure 4.1-4.4 shows the activation

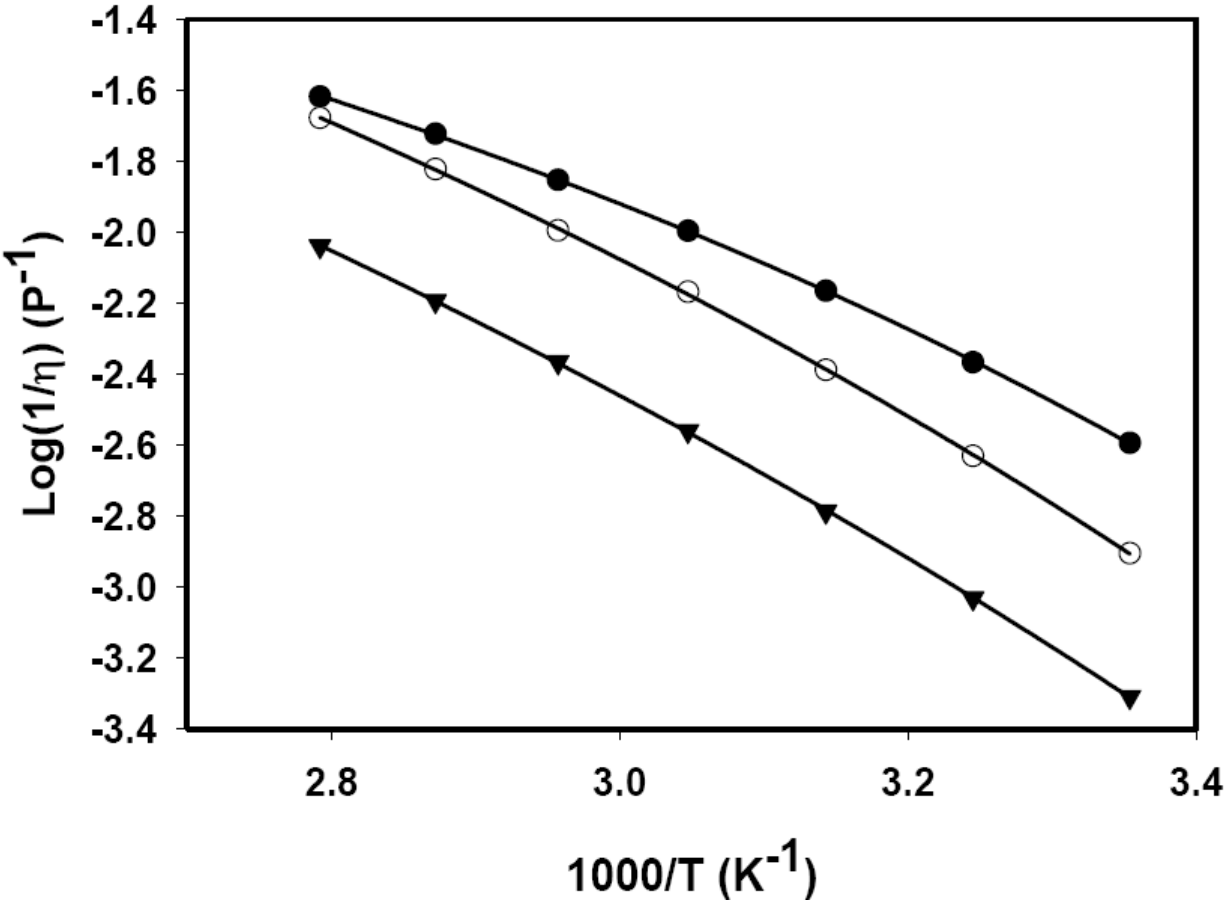

Figure 4.1: Fluidity Activation Plot: Fluidity activation plot for pure MePEG and MePPG copolymers with VTF best fit line shown: ● $MePEG_7$ polymer (**4a**); ○ $MePPG_3$ polymer (**4b**); ▼ $MePPG_2$ polymer (**4c**).

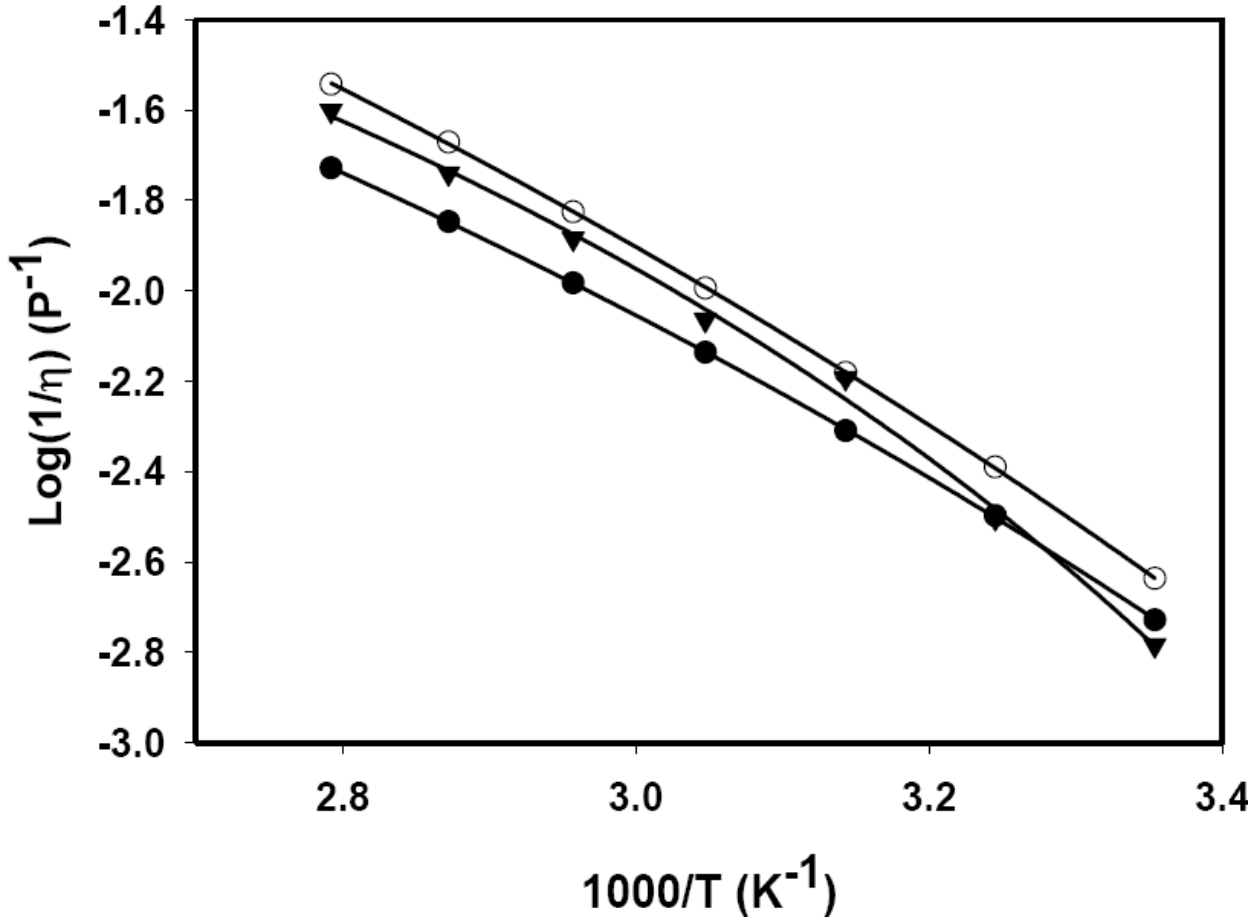

Figure 4.2: Fluidity Activation Plot: Fluidity activation plot for $MePEG_7/MePPG_3$ copolymers with VTF best fit line shown: ● 75% $MePEG_7$/25% $MePPG_3$ (**4d**); ○ 50% $MePEG_7$/50% $MePPG_3$ (**4e**); ▼ 25% $MePEG_7$/75% $MePPG_3$ (**4f**).

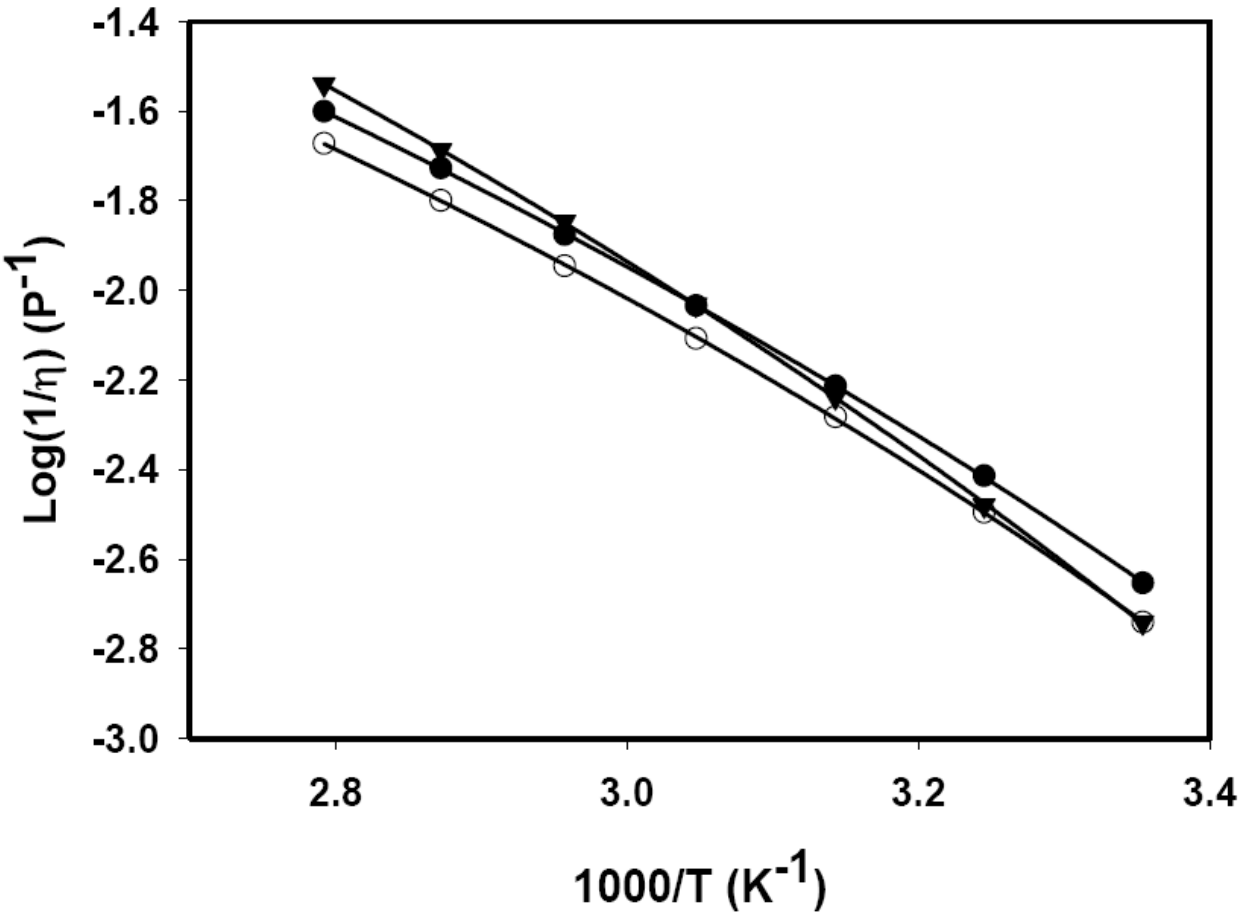

Figure 4.3: Fluidity Activation Plot: Fluidity activation plot for $MePEG_7/MePPG_2$ copolymers with VTF best fit line shown: ● 75% $MePEG_7$/25% $MePPG_2$ (**4g**); ○ 50% $MePEG_7$/50% $MePPG_2$ (**4h**); ▼ 25% $MePEG_7$/75% $MePPG_2$ (**4i**).

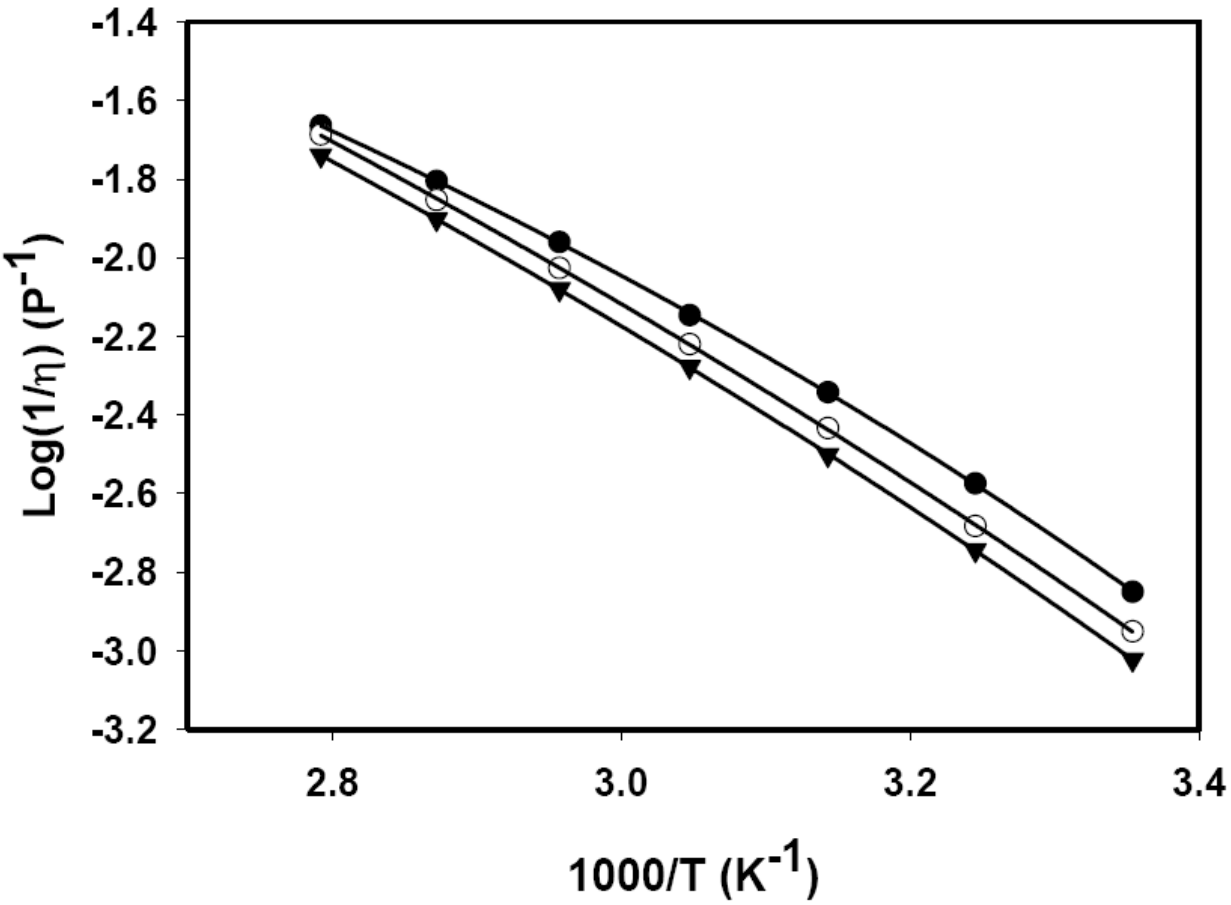

Figure 4.4: Fluidity Activation Plot: Fluidity activation plot for $MePPG_3/MePPG_2$ copolymers with VTF best fit line shown: ● 75% $MePPG_3$/25% $MePPG_2$ (**4j**); ○ 50% $MePPG_3$/50% $MePPG_2$ (**4k**); ▼ 25% $MePPG_3$/75% $MePPG_2$ (**4l**).

plot for viscosity for all of the copolymers. The fluidity of the pure polymers decrease in the order $MePEG_7$ > $MePPG_3$ > $MePPG_2$. We also see a similar decrease for the homopolymers $MePPG_3$/$MePPG_2$ copolymers in the order 75% $MePPG_3$ > 50% $MePPG_3$ > 25% $MePPG_3$. For the heteropolymers ($MePEG_7$/$MePPG_3$ and $MePEG_7$/$MePPG_2$) , the order of fluidity is 50% > 25% > 75%. This odd arrangement is counter intuitive and would be expected to follow the same trend as the homopolymers but this trend follows the FFV trend.

Figure 4.5 shows the Doolittle plot of all the copolymers at 25° C. The best fit line for all of the data points together had a poor R^2 value (0.0063) and a high p-value (0.8059) indicating that there is no relationship for this data. On further inspection, the linear fit of just the $MePPG_3$/$MePPG_2$ copolymers (in Figure 4.5) yielded a good R^2 value (0.9830) and a low p-value (0.0009) indicating that there is a strong relationship for these copolymers. Furthermore, the MePEG/MePPG copolymers (all copolymers except the $MePPG_3$/$MePPG_2$ copolymers, open circles in Figure 4.5) showed a poor R^2 value (0.0505) and a high p-value (0.6282). This indicates that the copolymers with heterogeneous monomers (i.e. MePEG versus MePPG) do not follow the Doolittle equation while those polymers with homogenous monomers do follow the Doolittle equation.

This result follows the results observed in Chapter 3, where the Doolittle fit for heterogeneous copolymers showed only a moderate R^2 value (0.5340), a low p-value (0.0020), and a shallow slope (-0.611). Those results indicated that the FFV and viscosity were correlated, but the moderate R^2 and shallow slope suggest the correlation is not strong, and the low p-value suggests a strong correlation. The low p-value may be an effect of the shallow slope, if this were the case then the p-value may not be indicative of a correlation and the FFV and viscosity may only be moderately correlated for that set of heterogeneous copolymers.

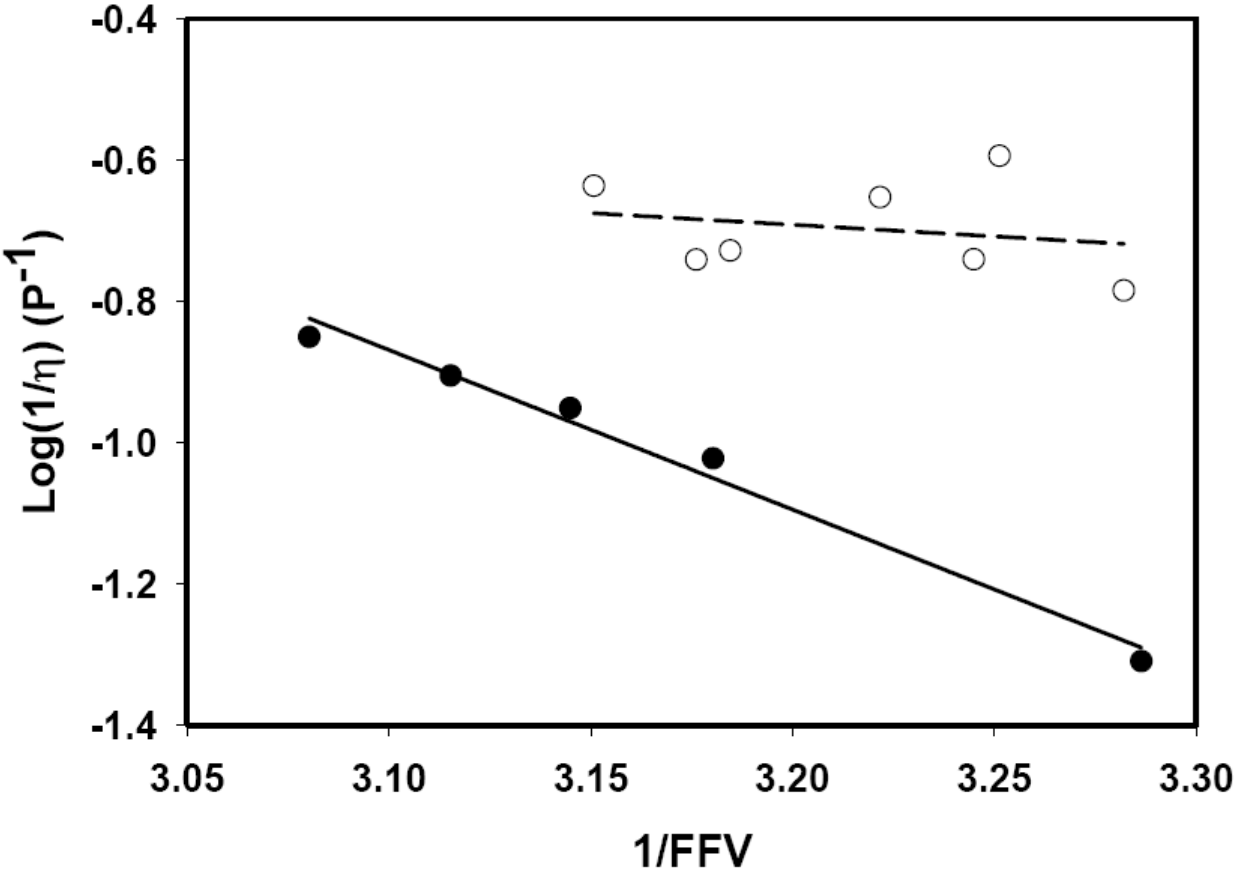

Figure 4.5: Doolittle Plot: Doolittle plot for all PEG-PPG copolymers with best fit linear line shown for the $MePPG_3$/$MePPG_2$ copolymers (———) and MePEG\/MePPG copolymers (– – –). ——— y = -2.2601x + 6.138, R^2 = 0.983, p-value = 0.0009; – – – y = -0.3294x + 0.3625, R^2 = 0.0505, p-value = 0.628817.

4.5 – Ionic Conductivity

The ionic conductivity of the copolymers was measured to determine the relationship between ionic conductivity and FFV for these copolymers. Figures 4.6-4.13 show Arrhenius activation plots for ionic conductivity for all copolymer electrolytes, made with both low and high $MePEG_7SO_3H$ acid concentrations. Comparing Figures 4.6-4.9 with 4.10-4.13, the low acid concentration electrolytes have a much lower conductivity than the high $MePEG_7SO_3H$ acid concentration electrolytes. This result was expected because the Forsythe equation (eq. 1.13) predicts that the increase in the concentration of charge carriers will have a higher ionic conductivity. For the pure polymers at 0.26 M acid concentration, the $MePPG_3$ and $MePPG_2$ had a conductivity lower than can be measured by our EIS instrumentation. At 1.32 M acid concentration, the $MePPG_3$ polymer had the highest conductivity followed by the $MePEG_7$. For the heteropolymers (MePEG/MePPG) at low acid concentration, the conductivity went in the order of fraction of MePEG (75% > 50% > 25%). At 1.32 M acid concentration, the trend follows the viscosity data observed previously. For the homopolymers, the trend for both low and high concentration is similar but with the high fraction of $MePPG_3$ having the highest conductivity at low concentration but the lowest conductivity at the high concentration. This data is not in agreement with the Stokes-Einstein (eq 1.8) and Nernst-Einstein equations (eq 1.9) for which a higher fluidity will result in a higher conductivity. Figure 4.14 shows a Forsythe plot correlating molar ionic conductivity with FFV for all copolymers at 25 °C. The linear best fit shown has a low R^2 value (0.0030) and a high p-value (0.7966) indicating a non significant result. These values together indicate that there is a great probability (≈ 80 %) that there is no correlation between molar equivalent conductivity and FFV for these copolymers. It has been previously observed for MePEG based polymers that there is a correlation between ionic

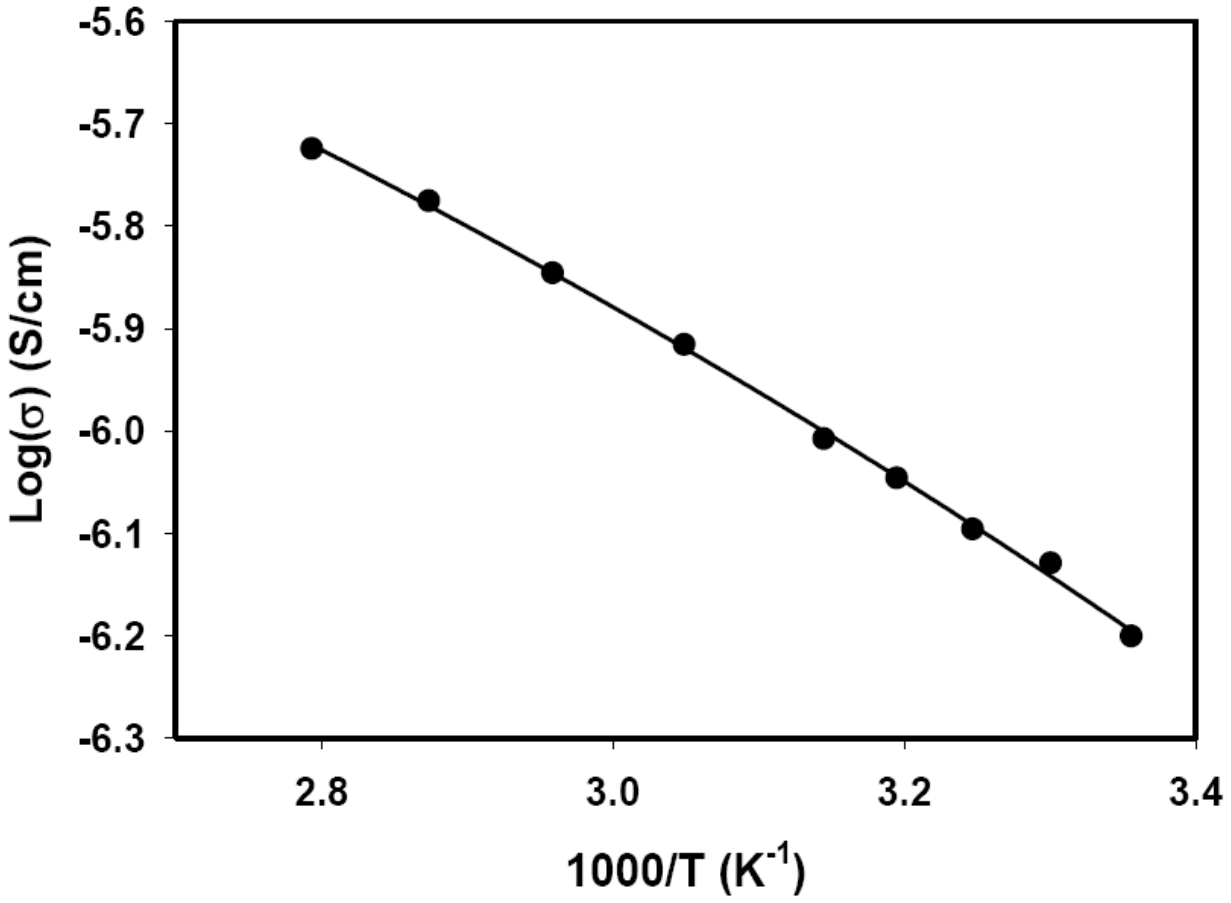

Figure 4.6: Activation Plot for Proton Conductivity: Activation Plot for proton conductivity for the pure $MePEG_7$ polymer and 0.26 M $MePEG_7SO_3H$ concentration with VTF best fit line shown: ● $MePEG_7$ (**4a**)

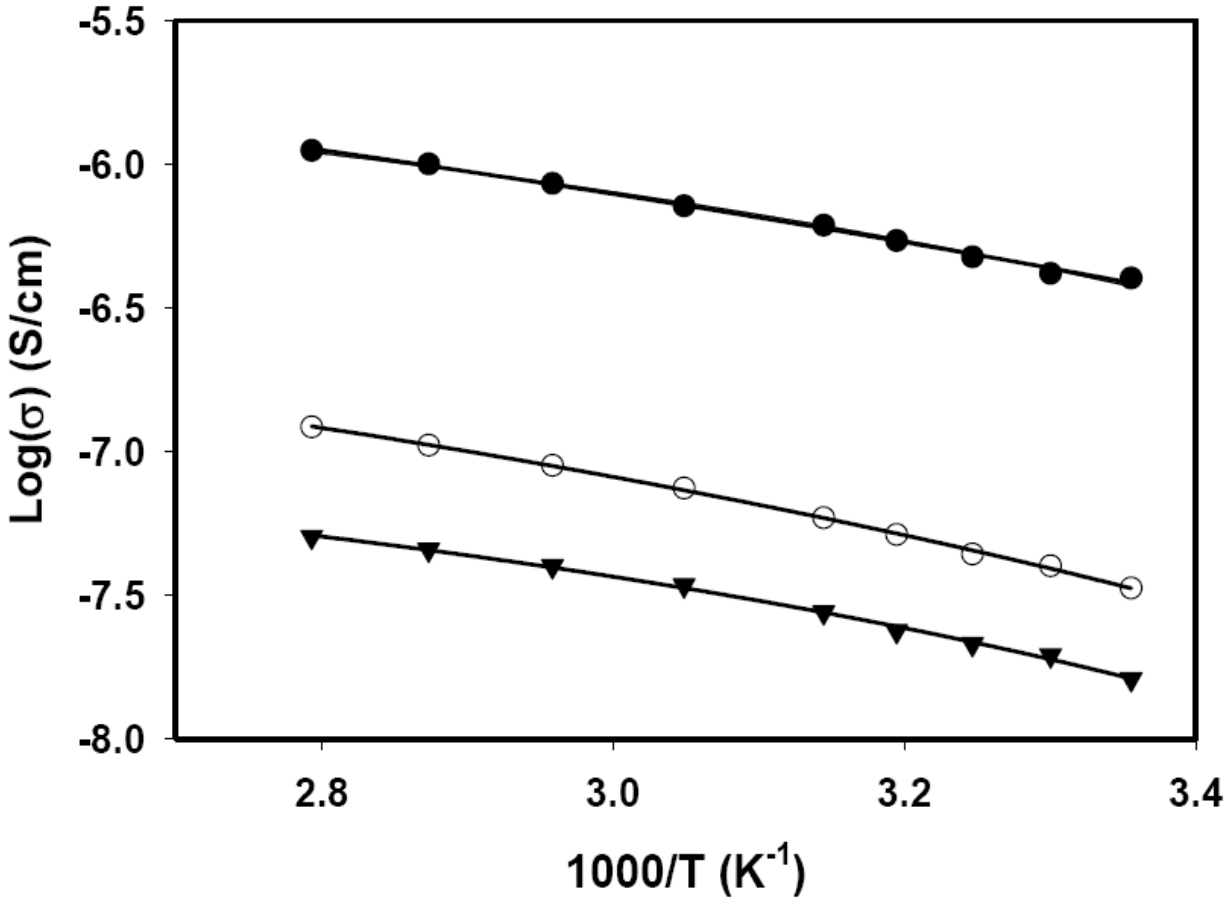

Figure 4.7: Activation Plot for Proton Conductivity: Activation Plot for proton conductivity for $MePEG_7$/$MePPG_3$ copolymers and 0.26 M $MePEG_7SO_3H$ concentration with VTF best fit line shown: ● 75% $MePEG_7$/25% $MePPG_3$ (**4d**); ○ 50% $MePEG_7$/50% $MePPG_3$ (**4e**); ▼ 25% $MePEG_7$/75% $MePPG_3$ (**4f**)

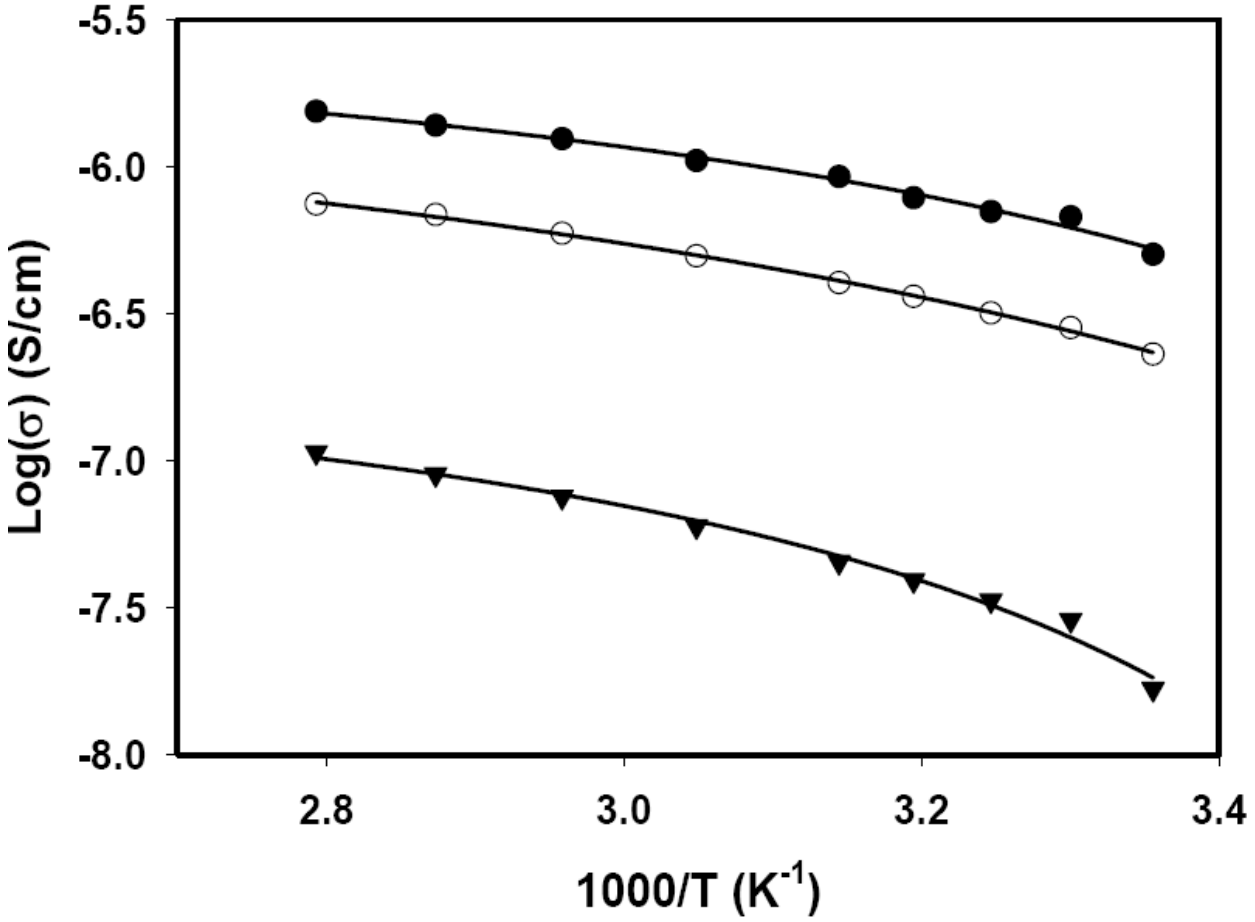

Figure 4.8: Activation Plot for Proton Conductivity: Activation Plot for proton conductivity for $MePEG_7/MePPG_2$ copolymers and 0.26 M $MePEG_7SO_3H$ concentration with VTF best fit line shown: ● 75% $MePEG_7$/25% $MePPG_2$ (**4g**); ○ 50% $MePEG_7$/50% $MePPG_2$ (**4h**); ▼ 25% $MePEG_7$/75% $MePPG_2$ (**4i**)

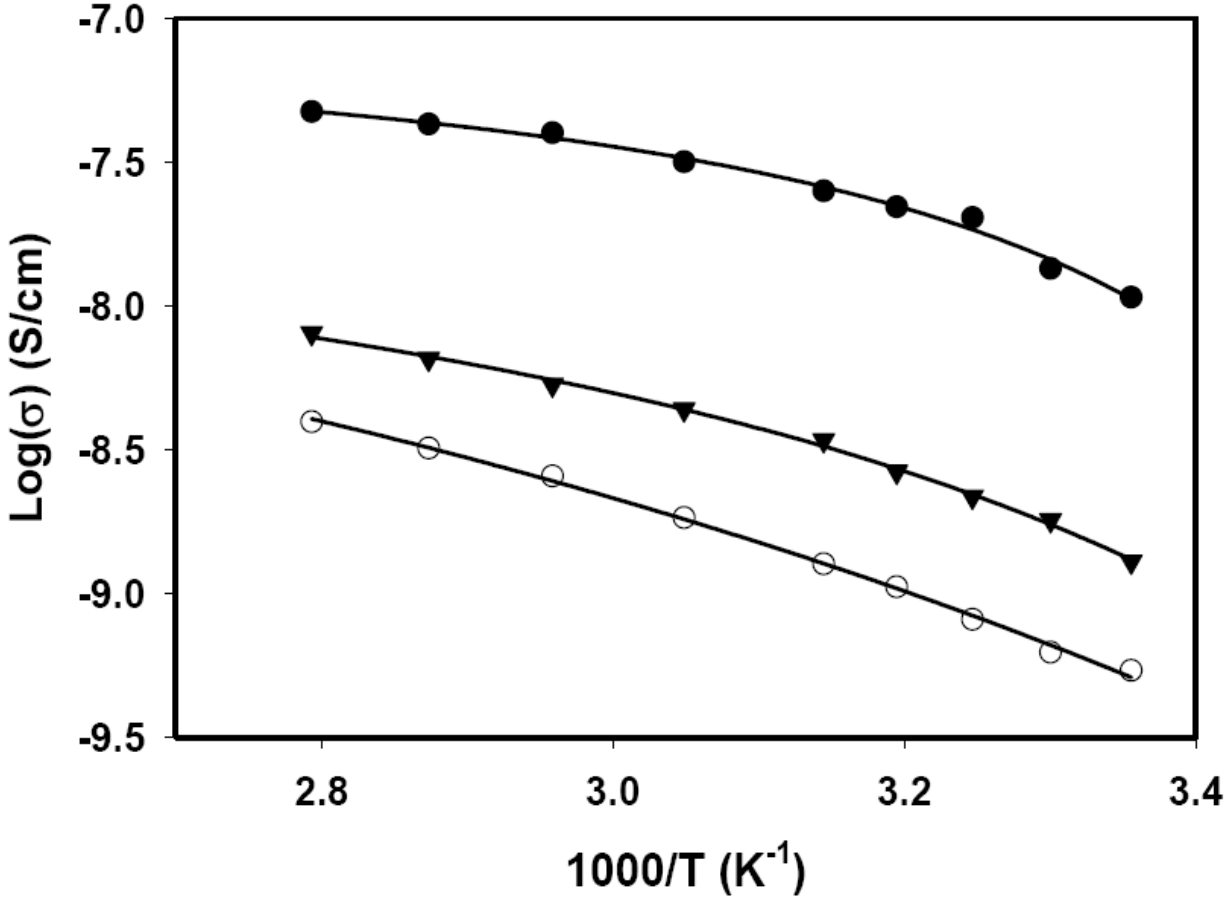

Figure 4.9: Activation Plot for Proton Conductivity: Activation Plot for proton conductivity for $MePPG_3/MePPG_2$ copolymers and 0.26 M $MePEG_7SO_3H$ concentration with VTF best fit line shown: ● 75% $MePPG_3$/25% $MePPG_2$ (**4j**); ○ 50% $MePPG_3$/50% $MePPG_2$ (**4k**); ▼ 25% $MePPG_3$/75% $MePPG_2$ (**4l**)

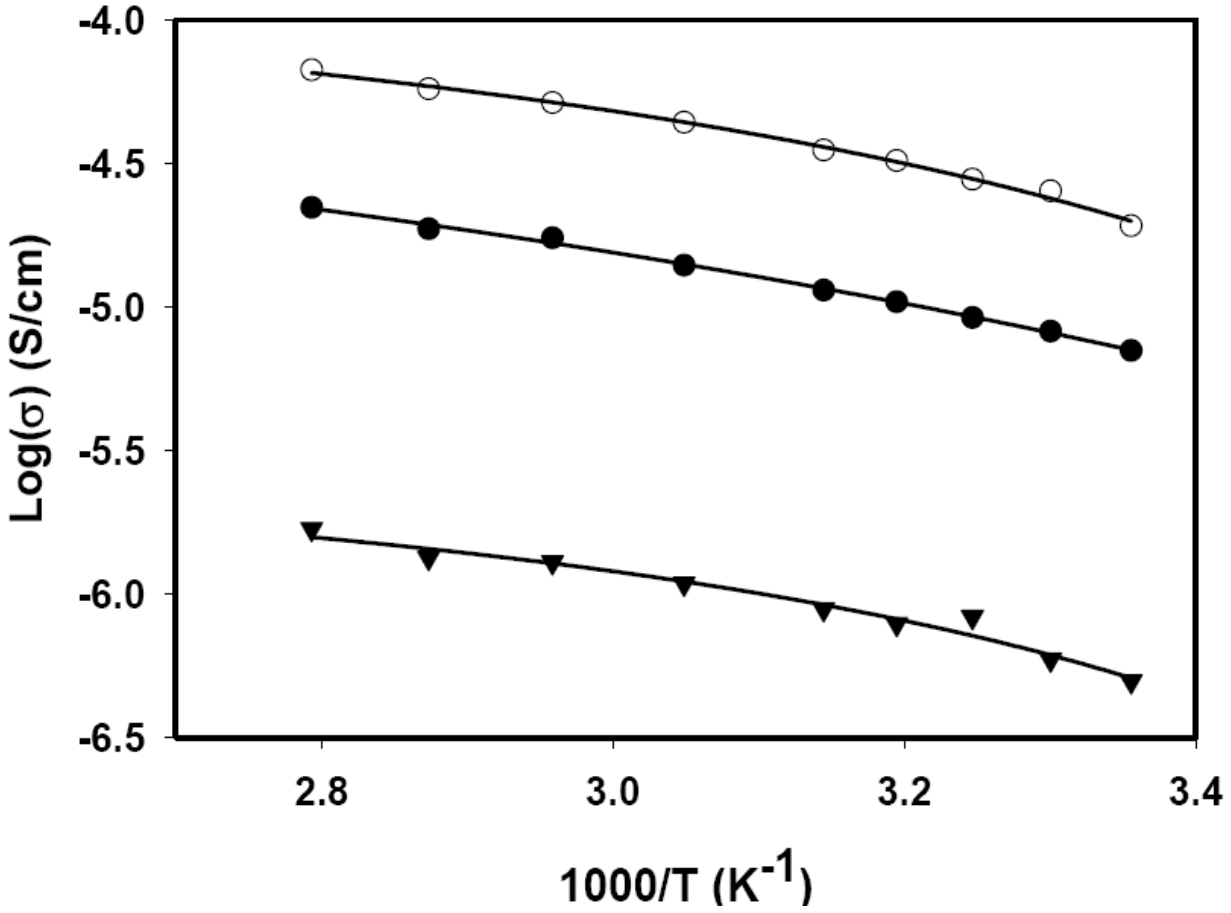

Figure 4.10: Activation Plot for Proton Conductivity: Activation Plot for proton conductivity for the pure MePEG and MePPG polymers and 1.32 M $MePEG_7SO_3H$ concentration with VTF best fit line shown: ● $MePEG_7$ (**4a**); ○ $MePPG_3$ (**4b**); ▼ $MePPG_2$ (**4c**)

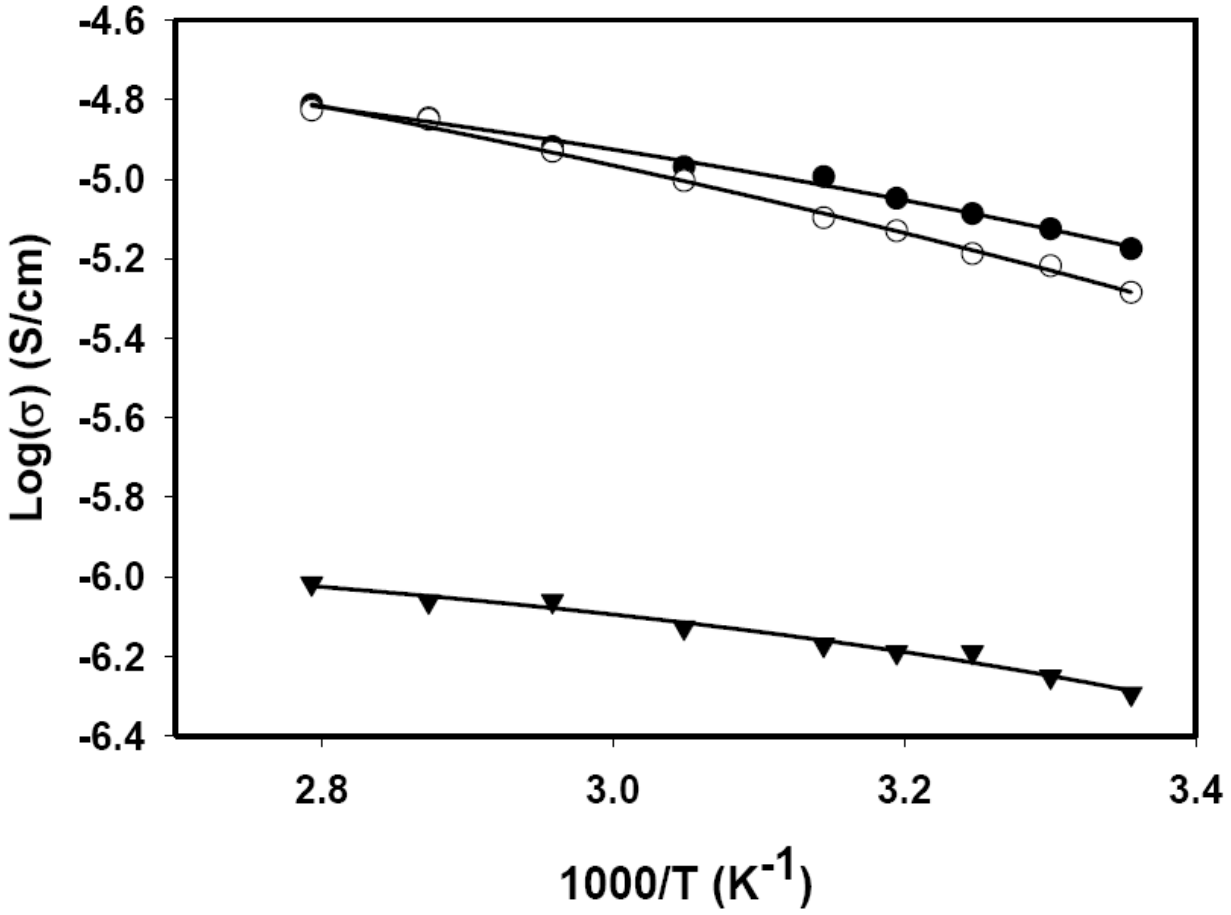

Figure 4.11: Activation Plot for Proton Conductivity: Activation Plot for proton conductivity for $MePEG_7$/$MePPG_3$ copolymers and 1.32 M $MePEG_7SO_3H$ concentration with VTF best fit line shown: ● 75% $MePEG_7$/25% $MePPG_3$ (**4d**); ○ 50% $MePEG_7$/50% $MePPG_3$ (**4e**); ▼ 25% $MePEG_7$/75% $MePPG_3$ (**4f**)

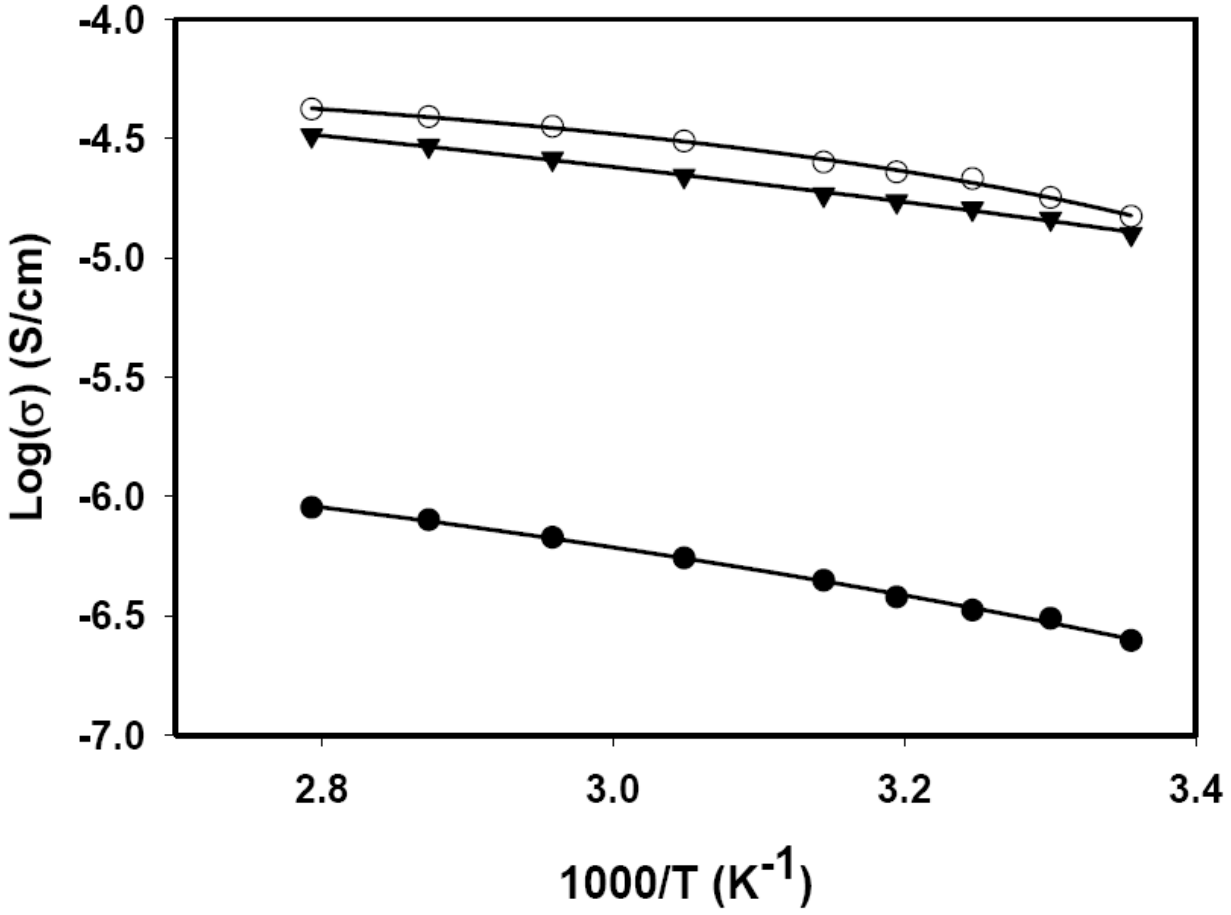

Figure 4.12: Activation Plot for Proton Conductivity: Activation Plot for proton conductivity for $MePEG_7/MePPG_2$ copolymers and 1.32 M $MePEG_7SO_3H$ concentration with VTF best fit line shown: ● 75% $MePEG_7$/25% $MePPG_2$ (**4g**); ○ 50% $MePEG_7$/50% $MePPG_2$ (**4h**); ▼ 25% $MePEG_7$/75% $MePPG_2$ (**4i**)

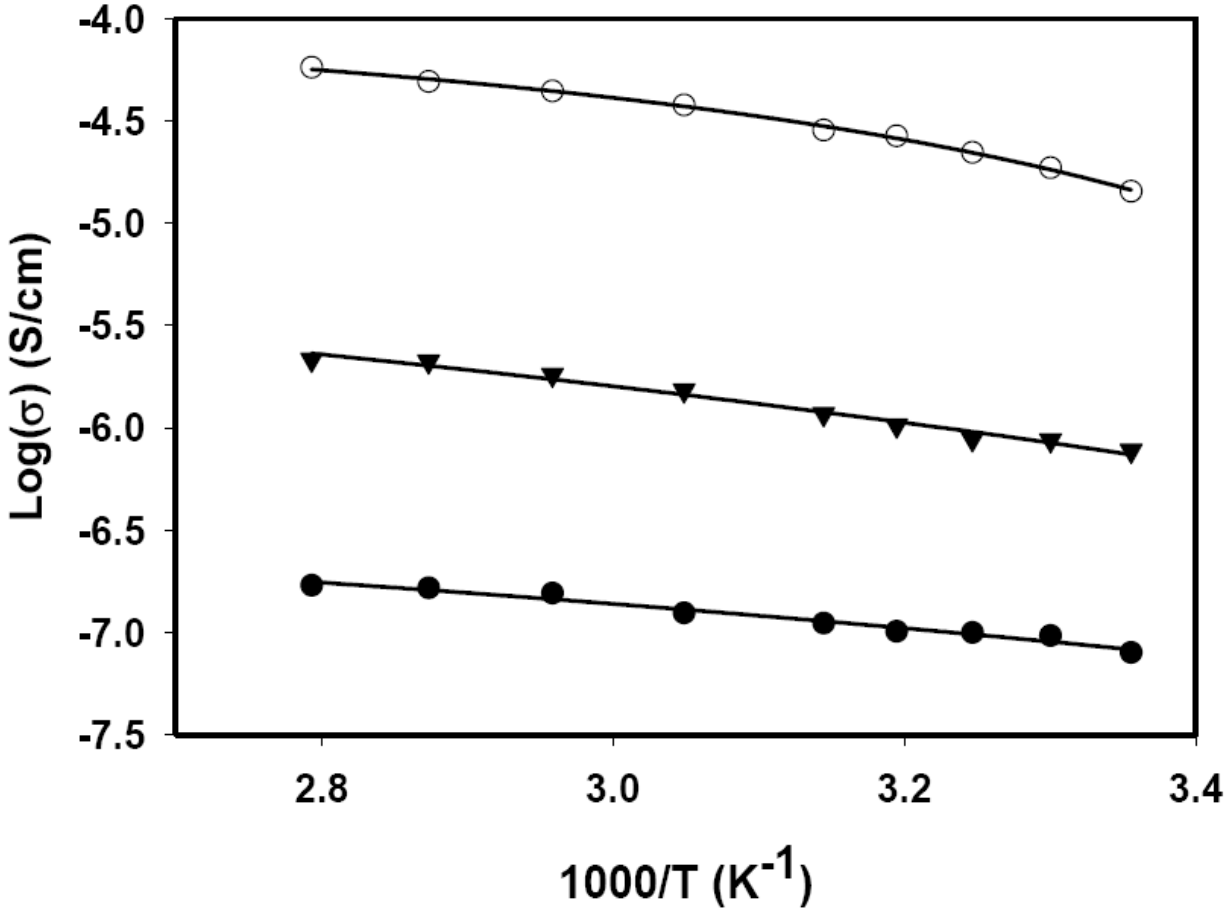

Figure 4.13: Activation Plot for Proton Conductivity: Activation Plot for proton conductivity for $MePPG_3/MePPG_2$ copolymers and 1.32 M $MePEG_7SO_3H$ concentration with VTF best fit line shown: ● 75% $MePPG_3$/25% $MePPG_2$ (**4j**); ○ 50% $MePPG_3$/50% $MePPG_2$ (**4k**); ▼ 25% $MePPG_3$/75% $MePPG_2$ (**4l**)

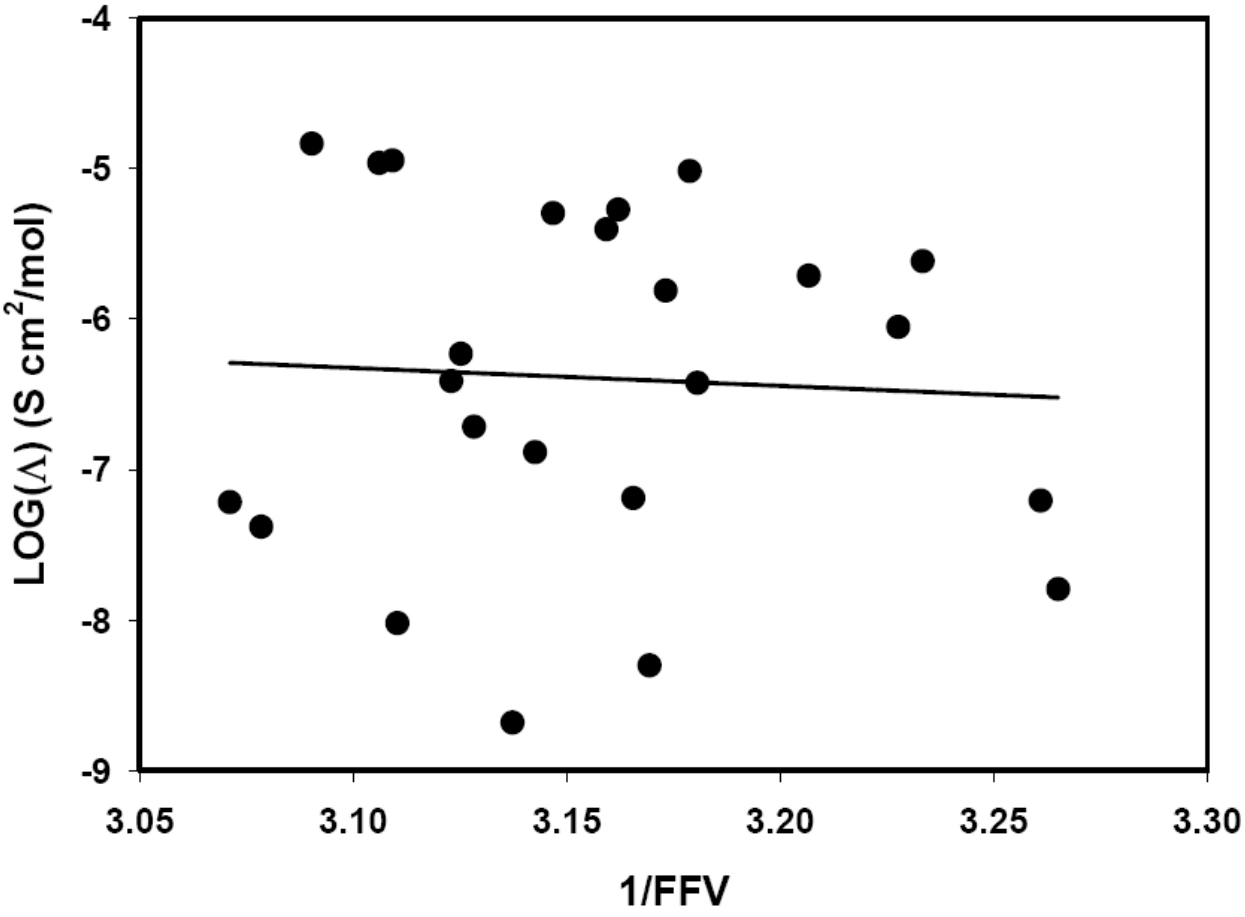

Figure 4.14: Forsythe Plot with FFV: Forsythe plot with fractional free volume for all PEG-PPG copolymers with best fit linear line shown. y = -1.1883x - 2.6406, R^2 = 0.0030, p-value = 0.7966

conductivity and $V_{f\,PEG}$. [27, 55] This polymer system contains PEG and PPG, both of which have repeating ether units. We believe that ionic conductivity results from the rearrangement of ether oxide units. Thus, the concentration of ether units is important to the overall ionic conductivity. For this work, the $V_{f\,PEG}$ concept has been extended to include the ethers of PPG making $V_{f\,ether}$.

Figure 4.15 shows a Forsythe plot with molar equivalent conductivity correlated with $V_{f,ether}$ for all copolymers at 25 °C. The linear best fit shown has a low R^2 value (0.6146) and a small p-value (< 0.0001) indicating a significant result. These values indicate that there is a strong probability that there is a correlation between $V_{f\,ether}$ and the ionic conductivity. This indicates that the MePPG copolymers change the ionic conductivity without reducing or blocking the ethers which transport the protons by the Grotthus mechanism.

4.6 – Walden Plot

Figures 4.16 and 4.17 are Walden plots for the 0.26M and 1.32 M polymer electrolytes respectively. The diagonal line shown in the top graph of the figure is the ideal Walden relationship with $\alpha = 1$. The data was fit to a linear best fit based on the fractional Walden rule (equation 1.10a) where α is the slope of the line for this relationship. For the 0.26 M copolymer electrolytes, the α values ranged from 0.4269 to 0.7738. For the 1.32 M copolymer electrolytes, the α values ranged from 0.2155 to 0.5611. No trend was observed for the α values for any of the copolymers series for both concentrations. These low α values indicate that other forces are impeding ion mobility other than viscosity (i.e. polymer rigidity, small dissociation constant, or ion pairing). The area of the Walden plot that these polymer electrolytes fall within also defines electrolytes that are not completely ionized. Electrolytes in this region demonstrate ionic

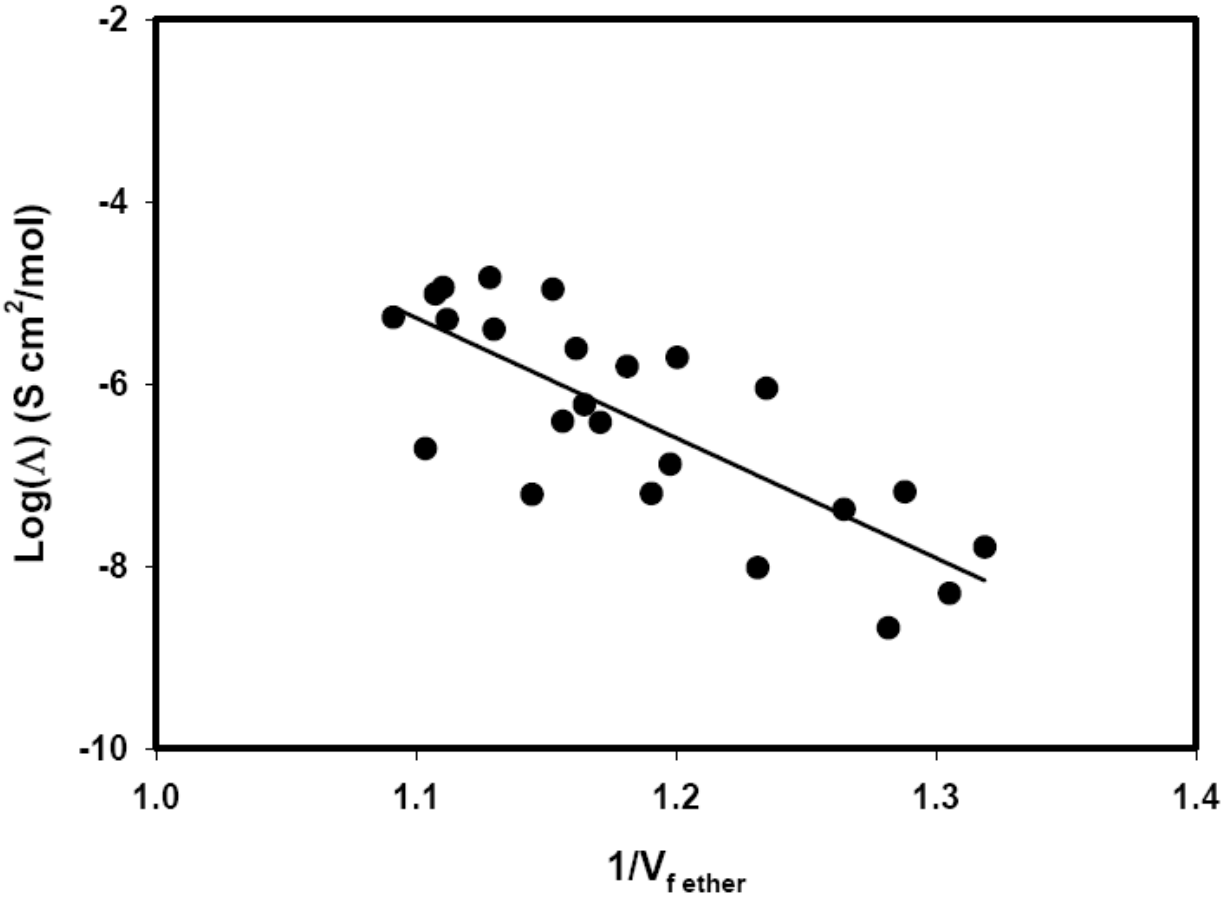

Figure 4.15: Forsythe Plot with $V_{f,ether}$: Forsythe plot with volume fraction of ether for all PEG-PPG copolymers with best fit linear line shown. y =-13.1827x – 9.2248, R^2 = 0.6146, p-value < 0.00001

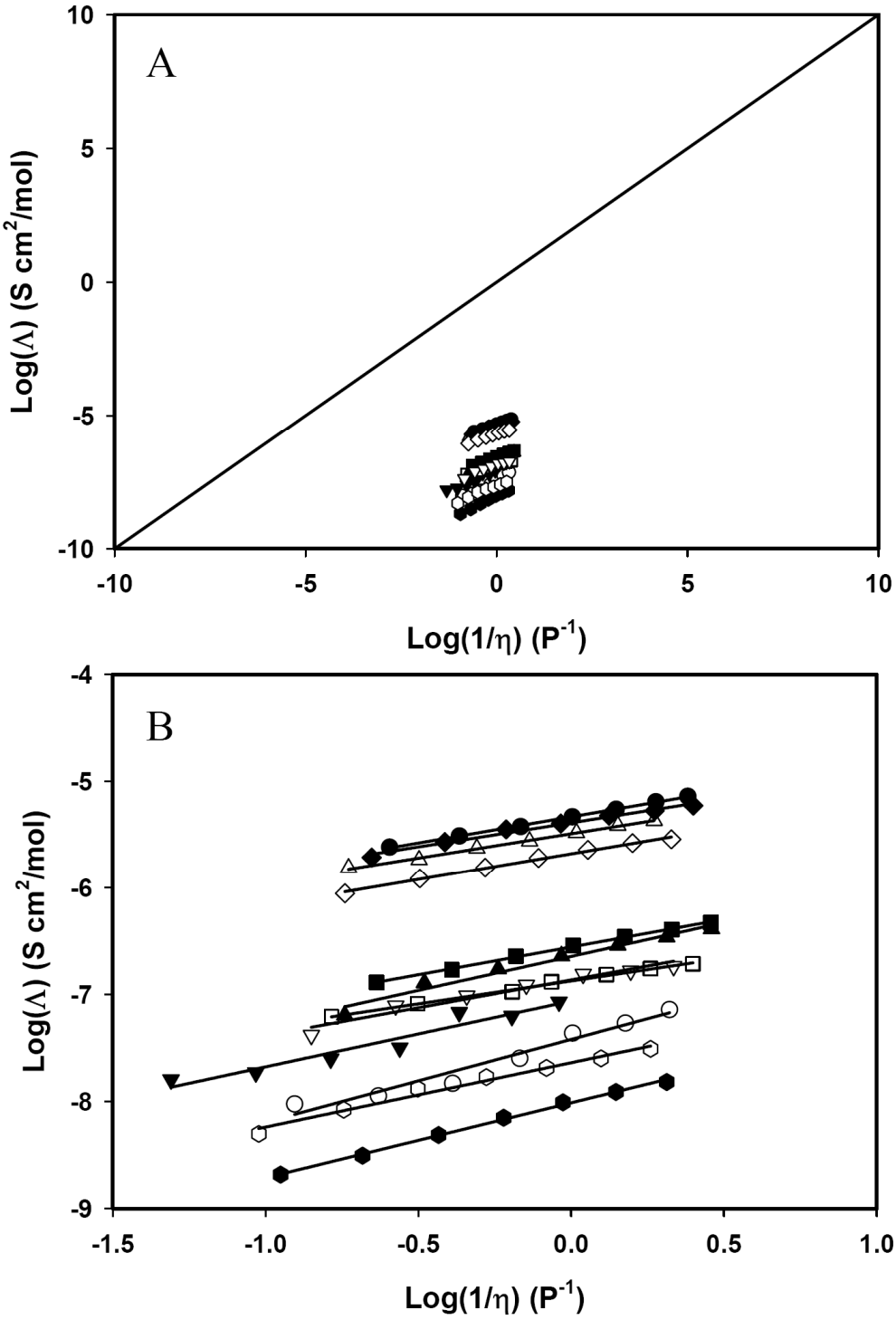

Figure 4.16: **A**: Walden Plot for all 0.26 M polymer electrolytes with linear best fit lines shown. **B**: is an expansion region of **A** ● 100 $MePEG_7$ (**4a**); ○ 100 $MePPG_3$ (**4b**); ▼100 $MePPG_2$ (**4c**); Δ 75 PEG_7/25 PPG_3 (**4d**); ■ 50 PEG_7/50 PPG_3 (**4e**); □ 25 PEG_7/75 PPG_3 (**4f**); ♦ 75 PEG_7/25 PPG_2 (**4g**); ◊ 50 PEG_7/50 PPG_2 (**4h**); ▲ 25 PEG_7/75 PPG_2 (**4i**); △ 75 PPG_3/25 PPG_2 (**4j**); ⬢ 50 PPG_3/50 PPG_2 (**4k**); **O** 25 PPG_3/75 PPG_2 (**4l)**

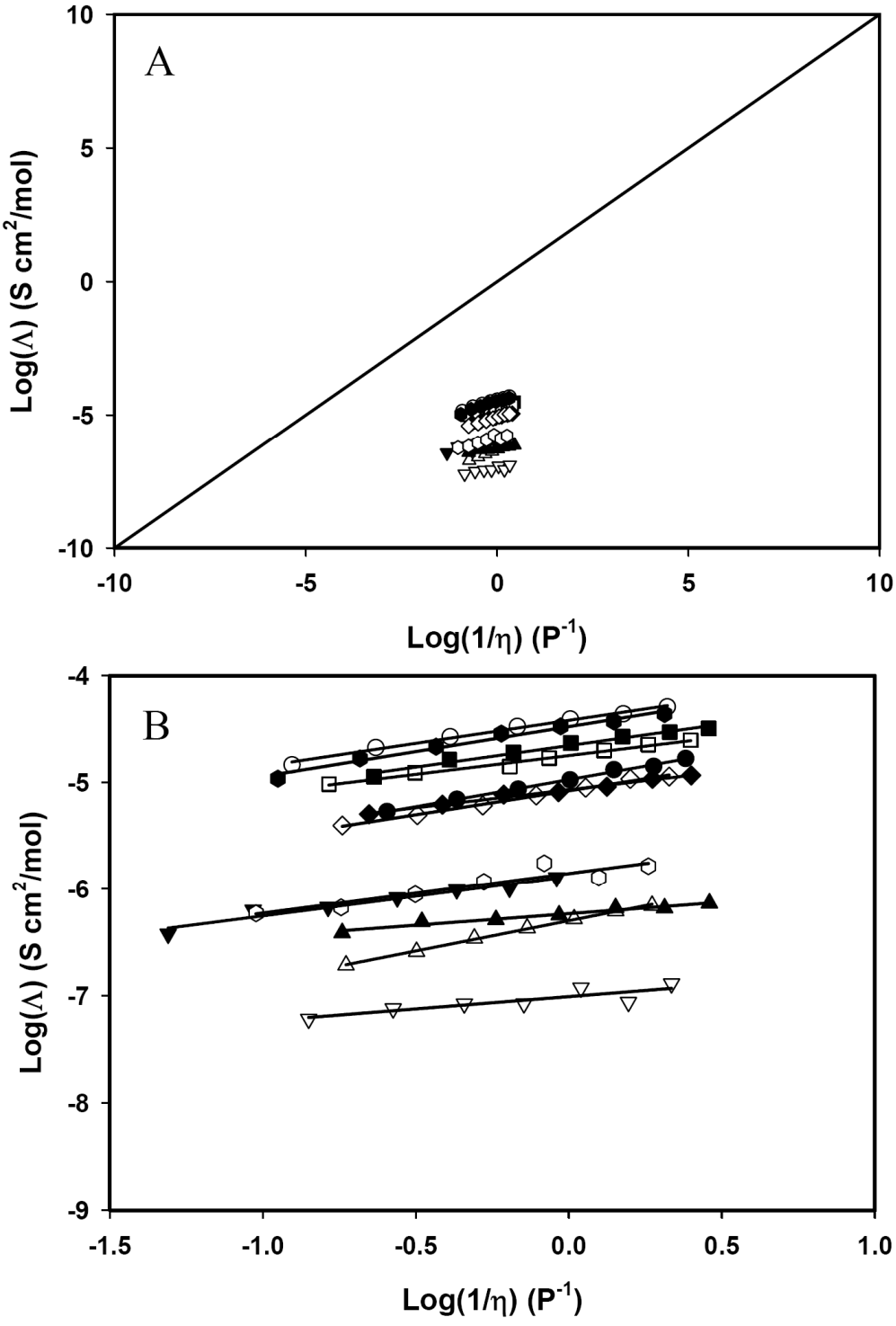

Figure 4.17: **A**: Walden Plot for all 1.32 M polymer electrolytes with linear best fit lines shown. **B**: is an expansion region of **A** ● 100 $MePEG_7$ (**4a**); ○ 100 $MePPG_3$ (**4b**); ▼100 $MePPG_2$ (**4c**); Δ 75 PEG_7/25 PPG_3 (**4d**); ■ 50 PEG_7/50 PPG_3 (**4e**); □ 25 PEG_7/75 PPG_3 (**4f**); ♦ 75 PEG_7/25 PPG_2 (**4g**); ◊ 50 PEG_7/50 PPG_2 (**4h**); ▲ 25 PEG_7/75 PPG_2 (**4i**); △ 75 PPG_3/25 PPG_2 (**4j**); ⬢ 50 PPG_3/50 PPG_2 (**4k**);**O** 25 PPG_3/75 PPG_2 (**4l)**

conductivity that is considerably smaller than an ideal electrolyte of the same viscosity. One possibility is that the low ionic conductivity results from ion pairing possibly indicating incomplete dissociation of our $MePEG_7SO_3H$ acid in these anhydrous copolymers.

4.7 – Summary

The materials explored in this work provide a simple route to novel inorganic/organic hybrid polymer electrolytes. The sol-gel condensation reaction results in a small fraction of uncondensed Si—OH groups for all of the copolymers. GPC analysis provided evidence that there is a large range of polymer sizes represented, from monomers and dimers observed in a small peak, to polymers with up to 15 monomer units. The copolymerization of the $MePPG_3$ with $MePPG_2$ allows for alteration of FFV to include values between the two pure polymers. This work, and the work by Ghosh et al., suggest that for the single component polymers, those with only PPG or PEG, the FFV can be systematically changed, while, for copolymers there seems to be no correlation between FFV and polymer composition. Only the PPG_2/PPG_3 copolymers followed the Doolittle equation, the other polymers were found to have no correlation to viscosity. There was no relationship found between FFV and ionic conductivity. However, a relationship between ionic conductivity and $V_{f\,ether}$ was observed for these polymers. These two observations together provide further evidence that proton conduction, in this polymer system, proceeds via the Grotthus mechanism in which protons are passed from an oxygen's coordination location to another's through segmental motions of the polymer. From the Walden plots, it is clear that there are forces greatly impeding ion mobility other than the viscosity. The results of this experiment show that, for heteropolymers, free volume is less of a contributor to ionic conductivity than the volume fraction of ether present.

V. RESULTS AND DISCUSSION OF THERMAL ANALYSIS

In this chapter, I report the thermal analysis of a series of sol-gel polymers ($MePEG_n$ polymer where n = 3, 7.24, 12.0, 16.3; and $MePPG_n$ polymer where n = 2 and 3) and co-polymers ($MePEG_n/Ph_2Si$, $MePEG_n$/TFPSi, $MePEG_n$/iBuSi; and $MePEG_7/MePPG_3$, $MePEG_7/MePPG_2$, $MePPG_3/MePPG_2$). These copolymers were then combined with $MePEG_7SO_3H$ acid to create proton-conducting electrolytes. These electrolytes are viscous liquids at room temperature. These copolymer electrolytes were investigated to determine the relationship between transport properties and thermal properties, as laid out in free volume theory.

5.1 – DSC and Viscosity VTF

The viscosity VTF plots were discussed previously (Section 3.4 and 4.4) with regard to the relative viscosities of the copolymers. The data was fit with the VTF equation (eq. 1.7a) using the infinitely slow glass transition temperature (T_0) as determined from the DSC data. The glass transition temperature (T_g) is related to T_0 by equation 5.1 and as previously described in Section 1.4. T_0 is the point where a decrease in temperature will no longer increase the viscosity or in another manner the point at which the viscosity of a sample is constant. ($\eta = 10^{13}$ P).

$$T_0 = T_g - 50°C \qquad (5.1)$$

Tables 5.1 and 5.2 summarize the DSC data and the A and B constants from the VTF equation (eq 1.7a) using equation 5.1 to calculate the T_0 to obtain the line fit. As stated previously, the B value is proportional to the activation energy. For the bulky copolymers

Polymer		T_g (K)	C_p [a] (J/g K)	VTF parameters	
				A	B
$MePEG_3$	**4a**	239	8.84	0.0056	-716
$MePEG_3/Ph_2Si$	**5a**	240	7.47	0.0036	-821
$MePEG_3$/TFPSi	**6a**	235	8.36	0.0429	-747
$MePEG_3$/iBuSi	**7a**	240	9.61	0.0049	-735
$MePEG_7$	**4b**	232	5.47	0.0046	-709
$MePEG_7/Ph_2Si$	**5b**	252	6.81	0.0031	-607
$MePEG_7$/TFPSi	**6b**	247	6.33	0.0058	-605
$MePEG_7$/iBuSi	**7b**	239	6.84	0.0033	-692
$MePEG_{12}$	**4c**	246	3.91	0.0055	-629
$MePEG_{12}/Ph_2Si$	**5c**	225	3.27	0.0018	-891
$MePEG_{12}$/TFPSi	**6c**	238	8.31	0.0054	-700
$MePEG_{12}$/iBuSi	**7c**	226	7.01	0.0018	-876
$MePEG_{16}$	**4d**	219	7.40	0.0031	-913
$MePEG_{16}/Ph_2Si$	**5d**	230	5.11	0.0046	-803
$MePEG_{16}$/TFPSi	**6d**	232	3.70	0.0082	-760
$MePEG_{16}$/iBuSi	**7d**	236	9.22	0.0050	-766

[a] C_p is determined at room temperature (25 °C or 298 K)

Table 5.1 – DSC and Viscosity Data: DSC and Viscosity VTF data for bulky copolymers

Polymer			T_g (K)	C_p (J/g K)	VTF parameters	
					A	B
$MePEG_7$	**4b**		221	4.07	0.3414	-892
$MePPG_3$	**4e**		234	7.73	0.2169	-943
$MePPG_2$	**4f**		230	3.92	0.3485	-1026
$MePEG_7/MePPG_3$	**8a**	75:25	249	6.81	1.2136	-608
$MePEG_7/MePPG_3$	**8b**	50:50	232	6.58	0.2704	-857
$MePEG_7/MePPG_3$	**8c**	25:75	251	2.91	0.4968	-692
$MePEG_7/MePPG_2$	**9a**	75:25	225	3.23	0.2825	-908
$MePEG_7/MePPG_2$	**9b**	50:50	232	3.93	0.4142	-834
$MePEG_7/MePPG_2$	**9c**	25:75	249	6.80	0.3698	-728
$MePPG_3/MePPG_2$	**10a**	75:25	225	4.00	0.1704	-1027
$MePPG_7/MePPG_2$	**10b**	50:50	230	5.36	0.1635	-1023
$MePPG_7/MePPG_2$	**10c**	25:75	231	4.58	0.1780	-1022

Table 5.2 – DSC and Viscosity Data: DSC and viscosity VTG data for MePEG/MePPG copolymers.

(Chapter 3) there is a correlation between B and T_g; as T_g increases activation energy decreases. This relationship is expected since the T_g was used to determine the B value from the VTF line fit. Also in free volume theory, viscosity results from the rearrangement of segments of a molecule. This relationship is not observed however for the $MePEG_3$ copolymers. The same relationship is observed for the MePEG/MePPG copolymers (Chapter 4) in table 5.2

For the bulky copolymers, the specific heat capacity shows no relationship to the viscosity activation energy. The MePEG/MePPG copolymers, also exhibited no correlation between viscosity activation energy and the specific heat capacity. Also, when all of the data is combined there still is no correlation. These results were not expected. Viscosity is essentially a rearrangement of free volume by the opening of voids caused by the motion of molecular segments, and free volume is a temperature dependent property. Specific heat capacity (C_p) is the amount of heat required to raise the temperature of one gram of material by 1 Kelvin, and C_P is a measure of how the bonds and intermolecular forces in a material respond to temperature either through rotations or vibrations. It stands to reason then that the C_p would be correlated to the activation energy for a molecular rearrangement only if intermolecular forces were involved. This simple view is complicated by many other factors such as differences in the way that different groups react to heat and unknown molecular motions. We see this more clearly with the pure MePEG polymers and $MePEG_n/Ph_2Si$ copolymers (**4a-d** and **5a-d** respectively) and the MePPG copolymers (**4e**, **4f**, and **10a-c)** which have moderate to good R^2 values (0.288, 0.344, and 0.893 respectively). While the R^2 values may not definitively indicate that there is a correlation, the MePPG copolymer's moderately high R^2 along with the Doolittle data observed in Section 4.4 indicate that the specific heat capacity may be a function of copolymer concentration in a binary copolymer system.

5.2 – DSC and Proton Conductivity Data

The proton (H^+) conductivity VTF plots were discussed previously (Sections 3.5 and 4.5) with regard to the relative H^+ conductivities of the copolymers. The data was fit with the VTF equation (eq. 1.7b) using the infinitely slow glass transition temperature (T_0) as determined from the DSC data.

Tables 5.3-5.6 summarize the DSC data and the A and B constants from the VTF equation (eq 1.7b) using equation 5.1 to calculate the T_0 to obtain the line fit. As stated previously, the B value is proportional to the activation energy, the more positive the value of B the lower the proton conductivity. For the bulky copolymers and MePEG/MePPG copolymers at both high and low concentrations, there is no correlation between B and T_g. This is expected since the T_g values used were for the copolymers, and not the copolymer electrolyte mixtures. Even though there is no correlation, the use of the T_g values allowed for superior fits to the VTF equation over fitting to A, B and T_0 simultaneously (i.e. two parameter fit as opposed to three parameter fit).

For the bulky copolymers at low acid concentration, the specific heat capacity shows no relationship to the H^+ conductivity activation energy. The MePEG/MePPG copolymers at low acid concentration also exhibited no correlation between activation energy of H^+ conductivity and the specific heat capacity. Also when all of the data is combined there still is no correlation. Also the MePEG/MePPG copolymers at high acid concentration exhibited no correlation between activation energy of H^+ conductivity andspecific heat capacity. These results correspond to the lack of a relationship between viscosity activation energy and specific heat capacity. However, when we analyze the relationship with the bulky copolymers at high concentration, we see a correlation.

Polymer		T_g (K)	C_p (J/g K)	VTF parameters	
				A	B
$MePEG_7$	**4b**	232	5.47	0.0028	446
$MePEG_7/Ph_2Si$	**5b**	252	6.81	0.0005	297
$MePEG_7$/TFPSi	**6b**	247	6.33	0.0015	445
$MePEG_7$/iBuSi	**7b**	239	6.84	0.0006	436
$MePEG_{12}$	**4c**	246	3.91	0.0005	247
$MePEG_{12}/Ph_2Si$	**5c**	225	3.27	0.0004	362
$MePEG_{12}$/TFPSi	**6c**	238	8.31	0.0003	187
$MePEG_{12}$/iBuSi	**7c**	226	7.01	0.0003	120
$MePEG_{16}$	**4d**	219	7.40	0.0006	297
$MePEG_{16}/Ph_2Si$	**5d**	230	5.11	0.0009	420
$MePEG_{16}$/TFPSi	**6d**	232	3.70	0.0006	299
$MePEG_{16}$/iBuSi	**7d**	236	9.22	0.0003	257

Table 5.3 –DSC and Proton Conductivity Data: A and B values from the conductivity VTF (eq. 1.7b) regression fit for the bulky copolymer electrolytes with 0.26 M $MePEG_7SO_3H$ acid concentration.

Polymer		T_g (K)	C_p (J/g K)	VTF parameters	
				A	B
$MePEG_3$	**4a**	239	8.84	0.0153	105
$MePEG_3/Ph_2Si$	**5a**	240	7.47	0.0010	32.5
$MePEG_3$/TFPSi	**6a**	235	8.36	0.0013	59.3
$MePEG_3$/iBuSi	**7a**	240	9.61	0.0003	27.1
$MePEG_7$	**4b**	232	5.47	0.0015	16.9
$MePEG_7/Ph_2Si$	**5b**	252	6.81	0.0016	32.7
$MePEG_7$/TFPSi	**6b**	247	6.33	0.0041	58.9
$MePEG_7$/iBuSi	**7b**	239	6.84	0.0014	45.8
$MePEG_{12}$	**4c**	246	3.91	0.0026	36.8
$MePEG_{12}/Ph_2Si$	**5c**	225	3.27	0.0017	46.3
$MePEG_{12}$/TFPSi	**6c**	238	8.31	0.0029	50.7
$MePEG_{12}$/iBuSi	**7c**	226	7.01	0.0018	39.2
$MePEG_{16}$	**4d**	219	7.40	0.0017	51.8
$MePEG_{16}/Ph_2Si$	**5d**	230	5.11	0.0030	44.9
$MePEG_{16}$/TFPSi	**6d**	232	3.70	0.0024	46.9
$MePEG_{16}$/iBuSi	**7d**	236	9.22	0.0026	51.3

Table 5.4 –DSC and Proton Conductivity Data: A and B values from the conductivity VTF (eq. 1.7b) regression fit for the bulky copolymer electrolytes with 1.32 M $MePEG_7SO_3H$ acid concentration.

Polymer			T_g (K)	C_p (J/g K)	VTF parameters	
					A	B
$MePEG_7$	**4b**		221	4.07	0.0004	467
$MePEG_7/MePPG_3$	**8a**	75:25	249	6.81	0.0001	307
$MePEG_7/MePPG_3$	**8b**	50:50	232	6.58	0.00003	471
$MePEG_7/MePPG_3$	**8c**	25:75	251	2.91	0.00001	317
$MePEG_7/MePPG_2$	**9a**	75:25	225	3.23	0.0003	430
$MePEG_7/MePPG_2$	**9b**	50:50	232	3.93	0.0002	428
$MePEG_7/MePPG_2$	**9c**	25:75	249	6.80	0.00003	467
$MePPG_3/MePPG_2$	**10a**	75:25	225	4.00	0.00002	580
$MePPG_7/MePPG_2$	**10b**	50:50	230	5.36	>0.00001	560
$MePPG_7/MePPG_2$	**10c**	25:75	231	4.58	0.00001	641

Table 5.5 –DSC and Proton Conductivity Data: A and B values from the conductivity VTF (eq. 1.7b) regression fit for MePEG/MePPG copolymer electrolytes with 0.26 M $MePEG_7SO_3H$ acid concentration.

Polymer			T_g (K)	C_p (J/g K)	VTF parameters	
					A	B
$MePEG_7$	**4b**		221	4.07	0.0056	484
$MePPG_3$	**4e**		234	7.73	0.0145	422
$MePPG_2$	**4f**		230	3.92	0.0003	422
$MePEG_7/MePPG_3$	**8a**	75:25	249	6.81	0.0002	363
$MePEG_7/MePPG_3$	**8b**	50:50	232	6.58	0.0072	377
$MePEG_7/MePPG_3$	**8c**	25:75	251	2.91	0.0032	264
$MePEG_7/MePPG_2$	**9a**	75:25	225	3.23	0.0019	340
$MePEG_7/MePPG_2$	**9b**	50:50	232	3.93	0.0028	400
$MePEG_7/MePPG_2$	**9c**	25:75	249	6.80	0.00006	182
$MePPG_3/MePPG_2$	**10a**	75:25	225	4.00	0.00002	321
$MePPG_7/MePPG_2$	**10b**	50:50	230	5.36	0.0118	371
$MePPG_7/MePPG_2$	**10c**	25:75	231	4.58	0.0005	425

Table 5.6 –DSC and Proton Conductivity Data: A and B values from the conductivity VTF (eq. 1.7b) regression fit for MePEG/MePPG copolymer electrolytes with 0.26 M $MePEG_7SO_3H$ acid concentration.

While the specific heat capacity data and H^+ conductivity activation data in table 5.4 has no correlation, if we analyze the individual copolymer series, we see a moderate correlation. We see a weak correlation with the $MePEG_n$/TFPSi copolymers ($R^2 = 0.319$), a moderate correlation with the $MePEG_n$ polymers and $MePEG_n$/iBuSi copolymers (0.665 and 0.647 respectively), and a strong correlation for the $MePEG_nPh_2Si$ copolymers (0.877). This result shows that the bulky groups impede H^+ conductivity. Simply put, more heat needs to be applied to the copolymers in order to induce sufficient motion in the bulky comonomers to allow H^+ conductivity, resulting in an increase in the observed activation energy.

In Chapter 3, I showed that the bulky comonomers disrupt the H^+ conductivity by decreasing the amount of PEG (for the Grotthus mechanism, proton conductivity occurs by passing protons from one oxygen to the next along the chain), thus impeding conductivity. The correlation between the specific heat capacity and activation energy for the copolymer groups helps support this conclusion. One possible reason that this is not observed in the MePEG/MePPG copolymers, is that the proton conductivity is controlled by the $V_{f,ether}$ whereas the bulky copolymers were controlled by the $V_{f,ether}$ to a lesser degree. All of these results support the previous conclusion that H^+ conductivity is controlled by the $V_{f,ether}$, but the bulky comonomers impede H^+ conductivity according to the Grotthus mechanism.

5.3 – Summary

The DSC data in this chapter has allowed us to obtain a superior fit to for the VTF data for both viscosity and H^+ conductivity. Even though there was no correlation observed between the specific heat capacity and the activation energy for viscosity for all data, the homopolymers

(MePPG), along with the pure MePEG polymers indicate that there may be a relationship for binary copolymers and pure polymers, but, further research is needed.

The correlation between the specific heat capacity and proton conductivity activation energy for the bulky copolymer series at high acid concentration supports the conclusion that the bulky comonomers impede H^+ conductivity. That together with the lack of correlation for the MePEG/MePPG copolymers further support the conclusion that the $V_{f,ether}$ controls the H^+ conductivity.

VI. RESULTS AND DISCUSSION OF ACID DISSOCIATION

In this chapter, I report the analysis of the acid properties of $MePEG_7SO_3H$ acid. This acid has previously been combined with $MePEG_n$ based polymers to create proton-conducting electrolytes. For this system, forces impeding H^+ conductivity besides viscosity have been observed. In these materials, a small acid dissociation constant would act like ion-ion pairing in the Walden plot. This chapter is focused on measuring the acid dissociation constant (K_a) of the $MePEG_7SO_3H$ acid, especially in MePEG media, and determining its role in H^+ conductivity.

6.1 – Viscosity

Figure 6.1 shows the Arrhenius plot of viscosity fit to the VTF equation (eq. 1.7a). The viscosity of the $MePEG_7SO_3H$ acid fits very well to the VTF equation ($R^2 = 0.9996$). This is to be expected since it is a pure liquid that is non-Newtonian. Viscoelastic materials, like these polymers, are non-Newtonian and are compressible and the viscosity is not constant across the fluid. The viscosity is also much lower than previously reported $MePEG_n$ polymers but compares to the acid's synthetic starting material $MePEG_7OH$.

6.2 – Proton Conductivity

Figure 6.2 shows the Arrhenius plot of H^+ conductivity fit to the VTF equation (eq. 1.7b). The H^+ conductivity of the $MePEG_7SO_3H$ acid fits the VTF equation very well ($R^2 = 0.9968$). The acid shows relatively high proton conductivity compared to previously reported $MePEG_n$/$MePEG_7SO_3H$ acid mixtures. This is due to the acid concentration being much higher

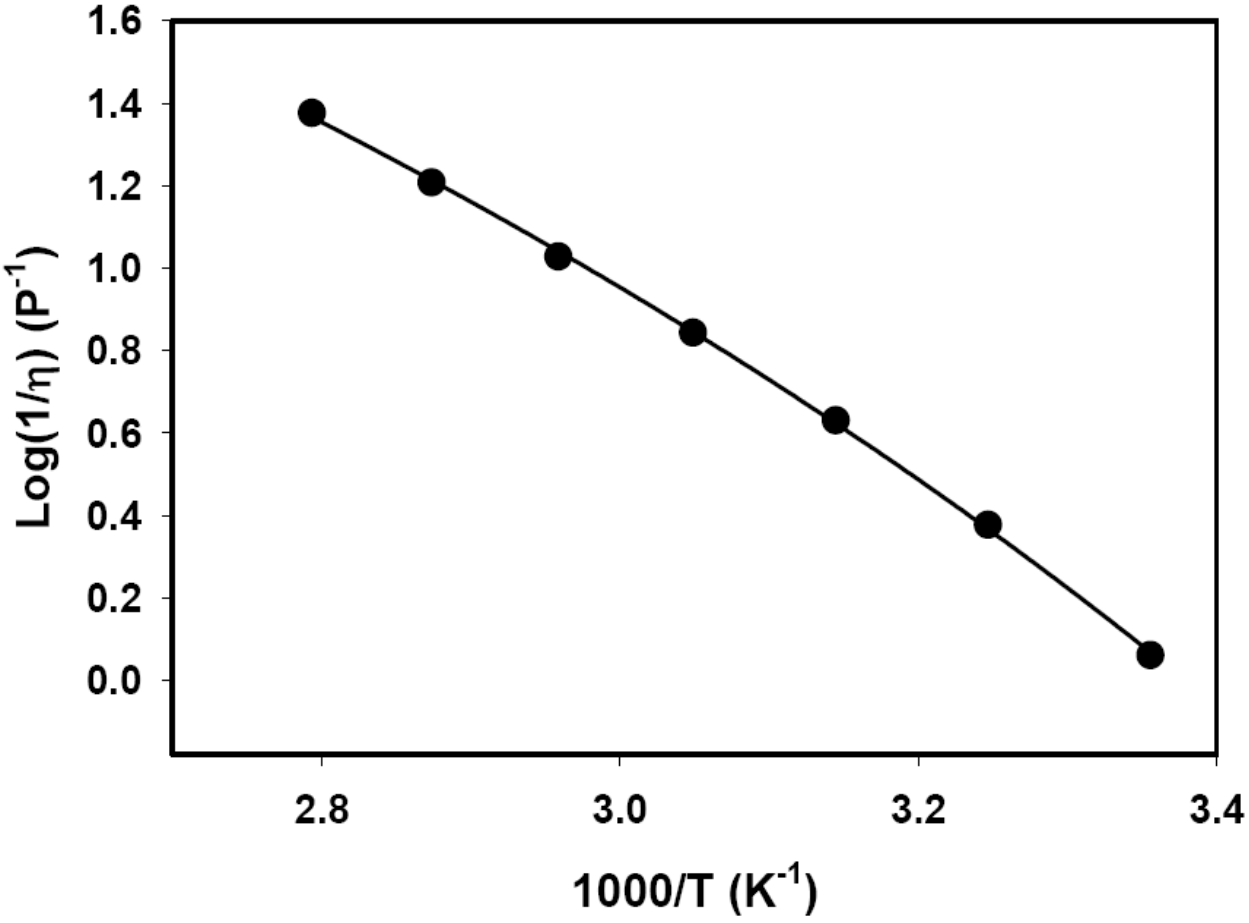

Figure 6.1 – Fluidity Activation Plot for $MePEG_7SO_3H$: Activation plot for neat $MePEG_7SO_3H$. Line shown is a VTF (eq. 1. 7a) fit, $R^2 = 0.9996$. VTF values from fit: $A = 0.0001$, $B = -1088$, $T_0 = 177.2$.

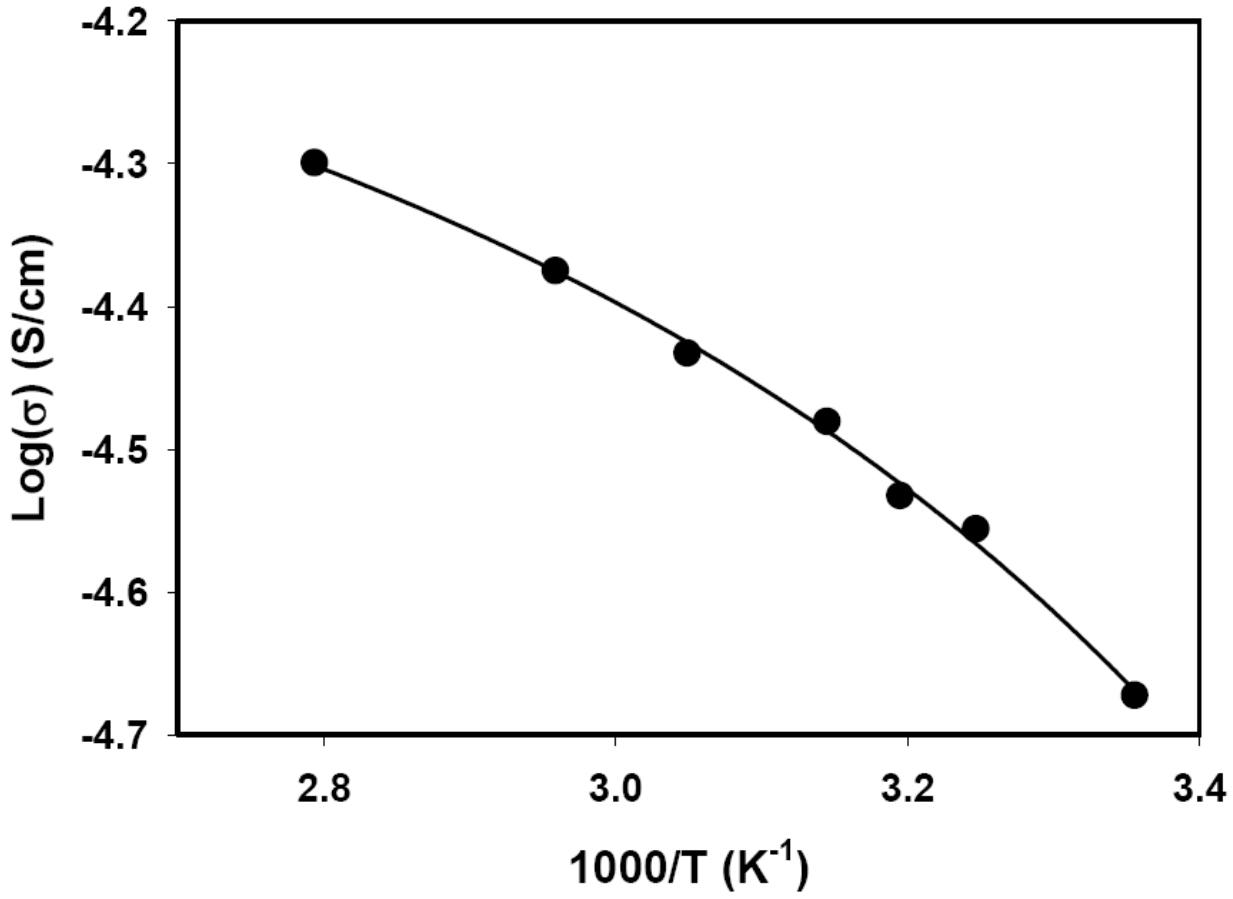

Figure 6.2 – H^+ Conductivity Activation Plot for $MePEG_7SO_3H$: Activation plot for $MePEG_7SO_3H$. Line shown is a VTF (eq. 1. 7b) fit, $R^2 = 0.9968$. VTF values from fit: A = 0.0028, B = 143.1, $T_0 = 227.8$.

than in polymer/acid mixtures. The molar equivalent conductivity (Λ) is similar to the polymer/acid mixtures. This seems reasonable, as molar equivalent H^+ conductivity is normalized to the molarity of the conducting species present. There is also a difference in the T_0 value determined for the VTF fit for both the viscosity and conductivity. These VTF fits were determined by a three parameter fit instead of a two fit parameter.

6.3 – Walden Plot

Figure 6.3 shows the Walden plot (eq. 1.10b) for the $MePEG_7SO_3H$ acid with a linear best fit. The data is located in the region of a Walden plot that indicates weak electrolytes. The α value for $MePEG_7SO_3H$ is 0.269 which indicates that there are other forces besides viscosity impeding the H^+ conductivity. This result is similar to other results in this dissertation. One of the possible forces impeding the conductivity may be ion-ion interactions. Since the α value is much smaller for the $MePEG_7SO_3H$ acid than the copolymer electrolytes previously described in this dissertation, we can infer that the impeding forces are stronger in this sample. Also since this is a measurement on the pure acid, the ionic strength of the material is larger. I have previously suggested that a possible source of ion-ion interactions may be undissociated $MePEG_7SO_3H$ acid. Since the sample has a higher H^+ concentration, any effects from this type of ion-ion pairing would be more evident. The two proposed mechanisms of H^+ conduction (vehicle mechanism and Grotthus mechanism) have previously been shown to both occur in MePEG based polymers.[27] We have shown that the mechanism is predominately the Grotthus mechanism. The vehicle mechanism is dependent on ion-ion pairing for H^+ conductivity, so a low value would indicate that this mechanism may be partially responsible for the H^+ conductivity.

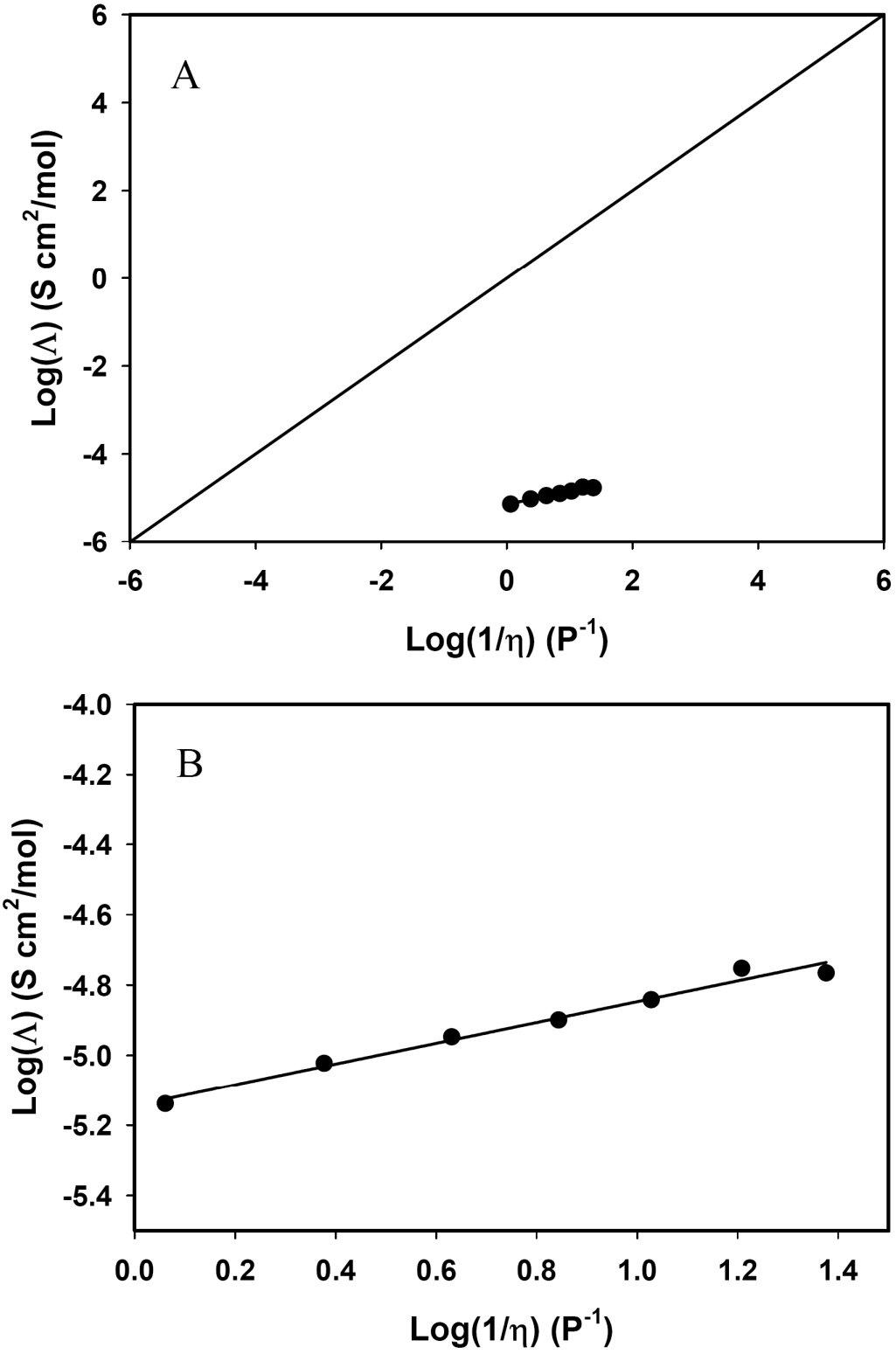

Figure 6.3 – $MePEG_7SO_3H$ Walden Plot: Walden plot for pure $MePEG_7SO_3H$ acid. **A**: H^+ Conductivity and viscosity measurements were taken over a range of temperatures. Best fit line shown. $y = 0.296x - 5.143$, $R^2 = 0.9794$. **B**: an expansion region of **A**

6.4 – pH Titrations

Figures 6.4 - 6.8 are the pH titration curves for the series of binary solutions consisting of deionized water and $MePEG_7OH$. $MePEG_7OH$ was selected as a model system because it is the starting material for the acid synthesis and it is one of the materials of which previous polymers were composed. The **x** symbol on each plot represents the V_e and $½V_e$ as determined from a Gran plot. Table 6.1 summarizes the experimentally determined values obtained from the pH titrations. The differences in the equivalence volumes were due to differing initial volumes and acid concentrations and base concentrations, a slight variation in either of these parameters will greatly affect the titration volume. It was assumed that the $MePEG_7SO_3H$ acid would be a strong acid as it is a sulfonic acid. The pH titration of the $MePEG_7SO_3H$ acid in pure deionized water confirmed this assumption as the pH at the equivalence point was 7, which is the case with the titration of other strong acids with strong bases. A pH titration in water is not an effective way to determine the pKa of a strong acid because the Henderson-Hasselbalch equation is only valid for weak acids titrated with strong bases.

The pK_a decreases as the mole fraction of $MePEG_7OH$ increases. Our hypothesis was that the acid becomes weaker in PEG based solvents. While the decrease in pK_a seems counterintuitive at first, consider that the pK_a of protonated alkyl ether is approximately -4.0 and the pK_a of protonated water is -1.7. Therefore, as the amount of $MePEG_7OH$ increases, the pK_a of the protonated solvent decreases. In water, a weak acid has a pK_a that is higher than the pK_a of protonated water, and the weaker the acid, the bigger difference between its pK_a and the pK_a of protonated water. This is also the case in non-aqueous systems. Even though the pK_a of the acid is decreasing, the pK_a of the protonated solvent is decreasing by a larger degree, making the acid weaker in each subsequent solution.

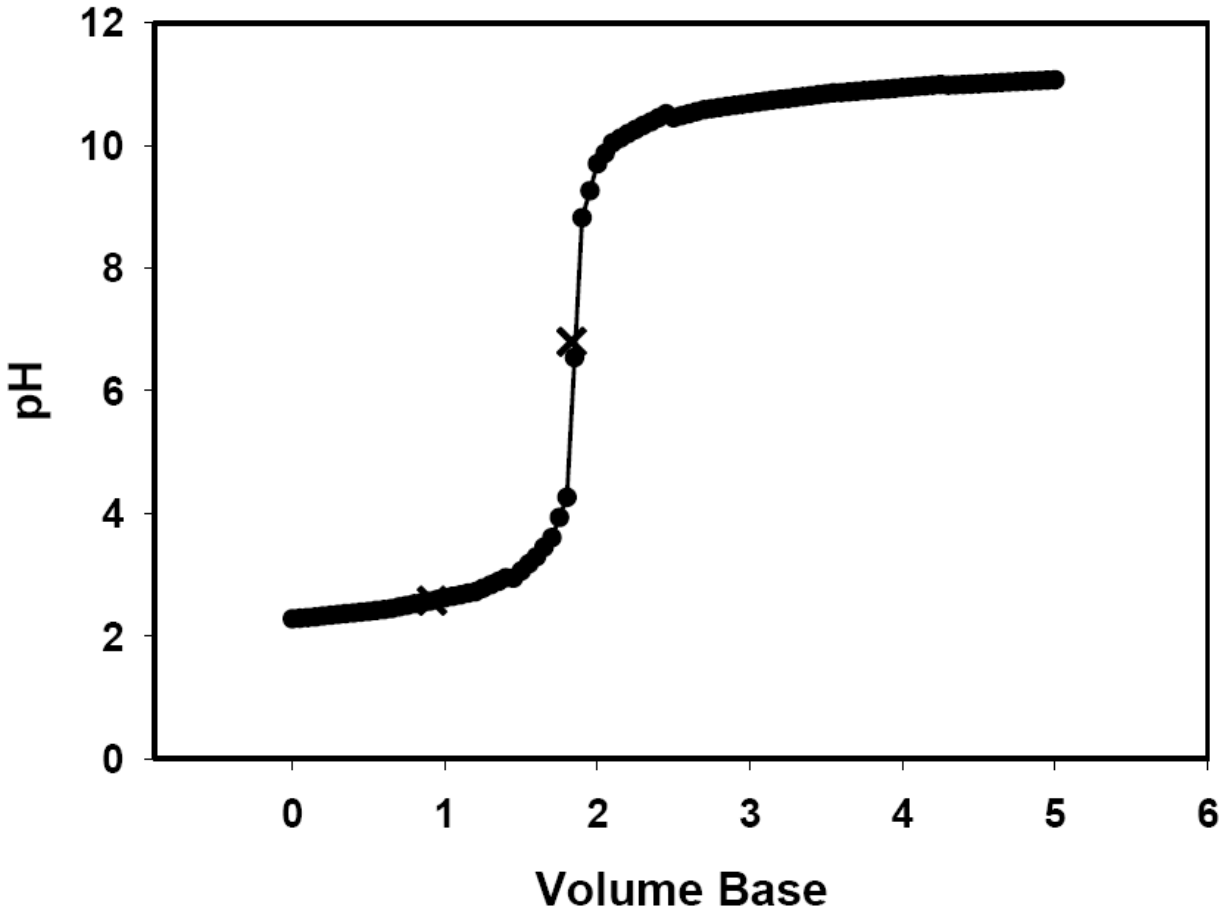

Figure 6.4: 0% MePEG$_7$OH/H$_2$O Titration: pH titration curve in deionized water, base concentration 0.10 M, and acid concentration 0.01 M. The symbol **x** represent V_e and $\frac{1}{2}V_e$ as determined from the Gran plot.

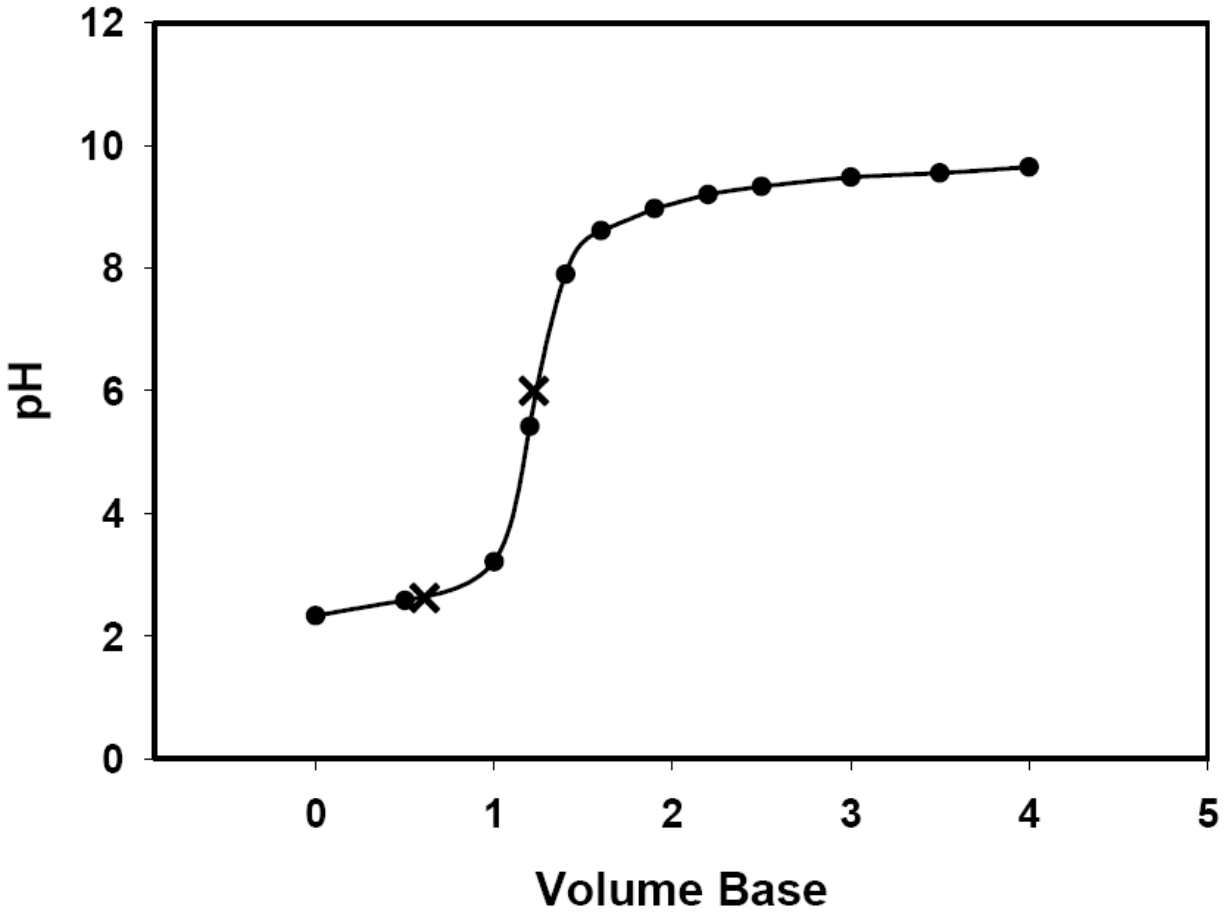

Figure 6.5: 20% $MePEG_7OH/H_2O$ Titration: pH titration curve with binary solution of $MePEG_7OH$ in deionized water with X = 0.2, base concentration 0.10 M, and acid concentration 0.01 M. The symbol **x** represent V_e and $½V_e$ as determined from the Gran plot.

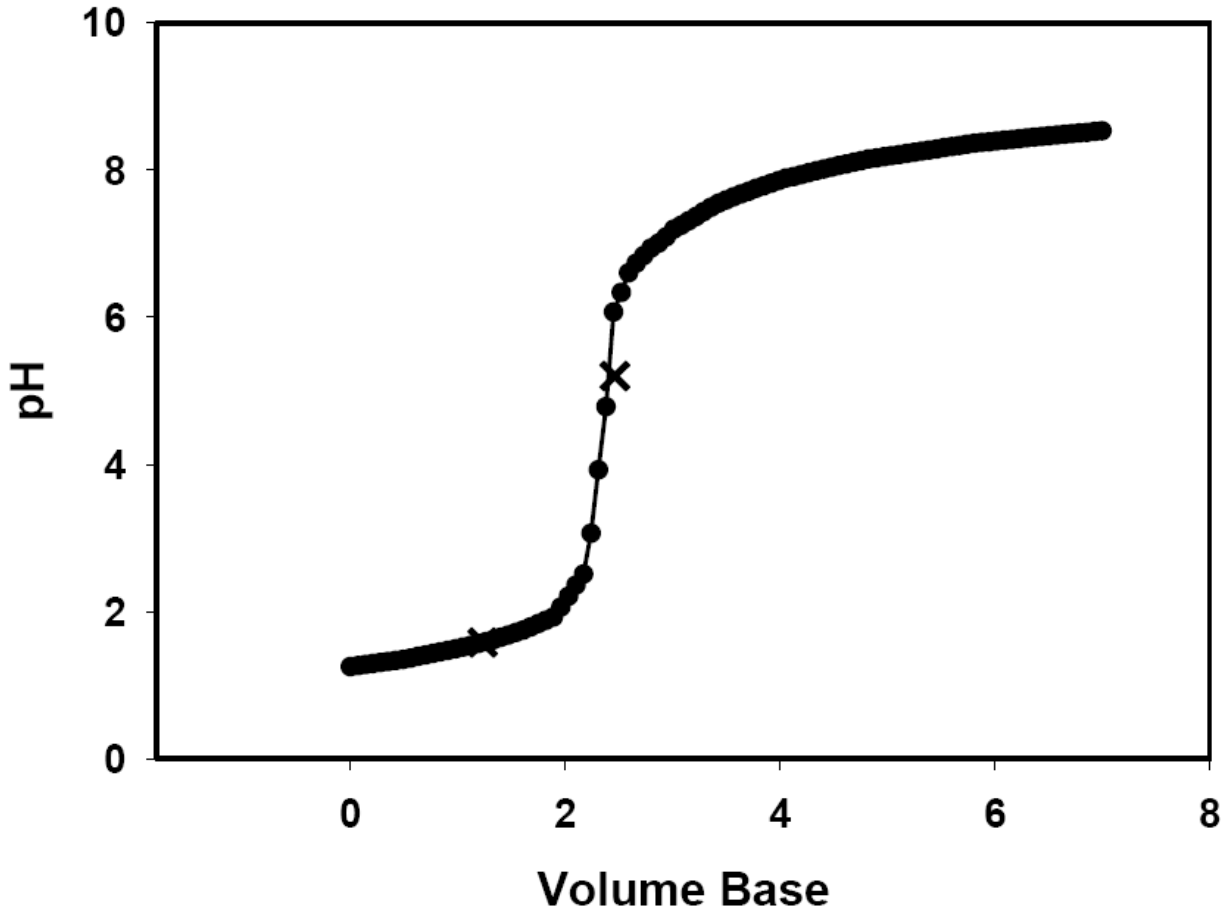

Figure 6.6: 40% MePEG$_7$OH/H$_2$O Titration: pH titration curve with binary solution of MePEG$_7$OH in deionized water with X = 0.4, base concentration 0.10 M, and acid concentration 0.01 M. The symbol **x** represent V_e and ½V_e as determined from the Gran plot.

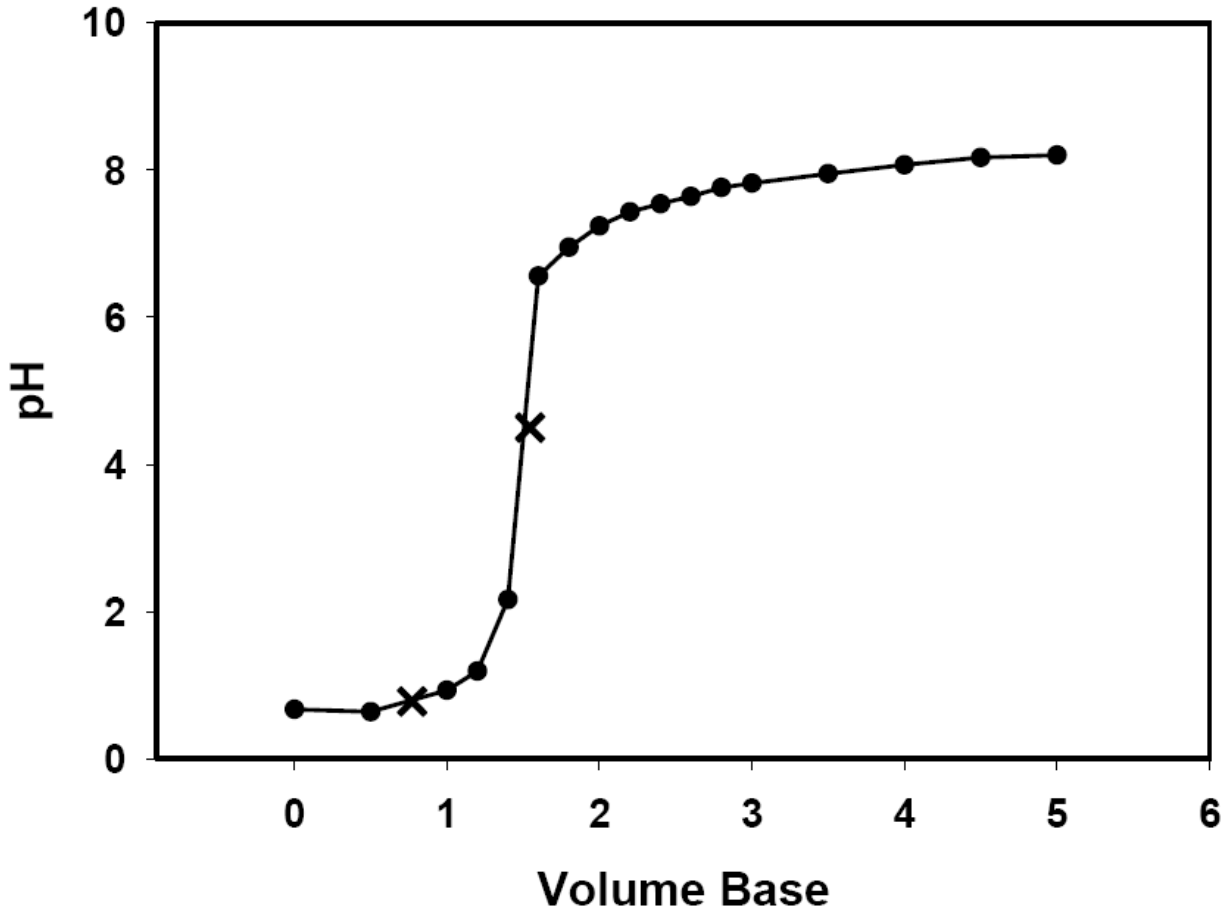

Figure 6.7: 60% $MePEG_7OH/H_2O$ Titration: pH titration curve with binary solution of $MePEG_7OH$ in deionized water with X = 0.6, base concentration 0.10 M, and acid concentration 0.01 M. The symbol **x** represent V_e and $½V_e$ as determined from the Gran plot.

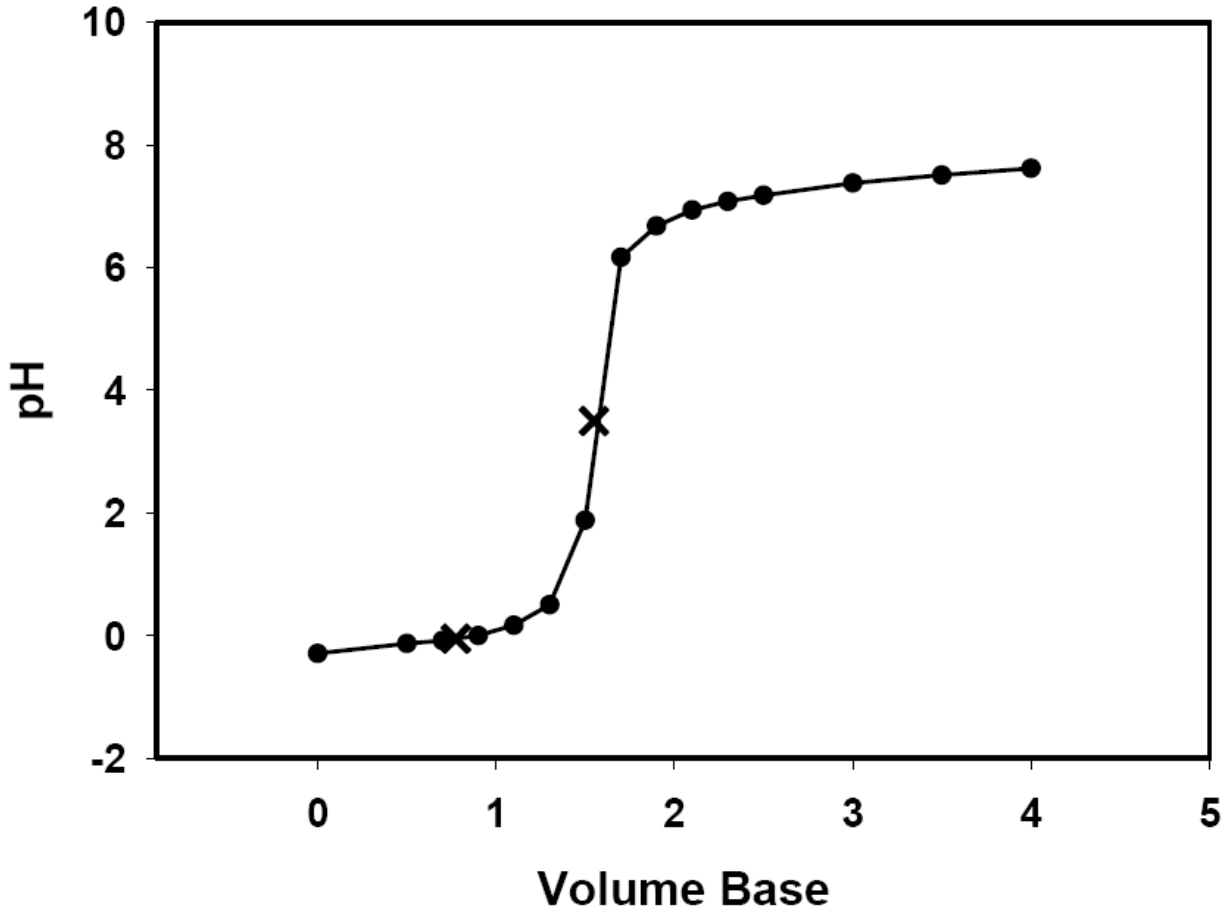

Figure 6.8: 80% MePEG$_7$OH/H$_2$O Titration: pH titration curve with binary solution of MePEG$_7$OH in deionized water with X = 0.8, base concentration 0.10 M, and acid concentration 0.01 M. The symbol **x** represent V_e and ½V_e as determined from the Gran plot.

Mole Fraction X	pK_a[a]	Acid Constant K_a	Equivalence Volume V_e[b]	Mean Activity Coefficient $\gamma\pm$[b]
0.2	2.777	1.67×10^{-3}	1.313	0.957
0.4	1.578	2.64×10^{-2}	2.462	1.310
0.6	0.799	1.59×10^{-1}	1.544	1.322
0.8	-0.050	1.12	1.549	1.325
1.0	-1.039	10.94	-	-

[a] pK_a @ ½V_e was determined from the equivalence volume using the Henderson-Hasselbalch equation
[b] V_e and $\gamma\pm$ were determined from a Gran plot and used to determine pK_a

Table 6.1: pH Titration Data: Experimental values obtained by pH titration.

Also worth noting is the mean activity coefficients ($\gamma \pm$), which are calculated from the Gran plot data. These values are all very similar with a general trend of decreasing with increasing mole fraction of $MePEG_7OH$. The activity should decrease as the polarity of the solvent decreases. This corresponds well with the idea that the acid strength is decreasing; a less active acid is a weaker acid. All of the above stated suppositions point to an increase in ion-ion pairing for the $MePEG_7SO_3H$ acid.

Figure 5.9 shows the pK_a of $MePEG_7SO_3H$ acid as a function of mole fraction $MePEG_7OH$. The pKa of the $MePEG_7SO_3H$ acid in the unary solvent $MePEG_7OH$ was determined to be -1.04. This value is in accordance with the acid becoming weaker in MePEG based solvents. This is a much weaker acid than the protonated ether so there will be a large fraction of H^+ that remains associated. This also corresponds to the Walden plot data that suggest that there are forces impeding ion conduction other than the viscosity such as ion-ion interactions. The undissociated H^+ would remain either in place or be conducted via the vehicle mechanism. In free volume theory, molecular transport occurs by the movement of a particle into a void space. H^+ cations have a small van der Waals radius (3.44 mL/mol) compared to $MePEG_7SO_3H$ (267.36 mL/mol). Therefore, there are likely many more voids that will accommodate a dissociated proton than would accommodate an H^+ associated to $MePEG_7SO_3^-$. The vast size difference of the H^+ versus the $MePEG_7SO_3H$ acid would allow for the Grotthus mechanism to predominate, even though the acid is weak and a large fraction of associated H^+ exists that can participate in the vehicle mechanism.

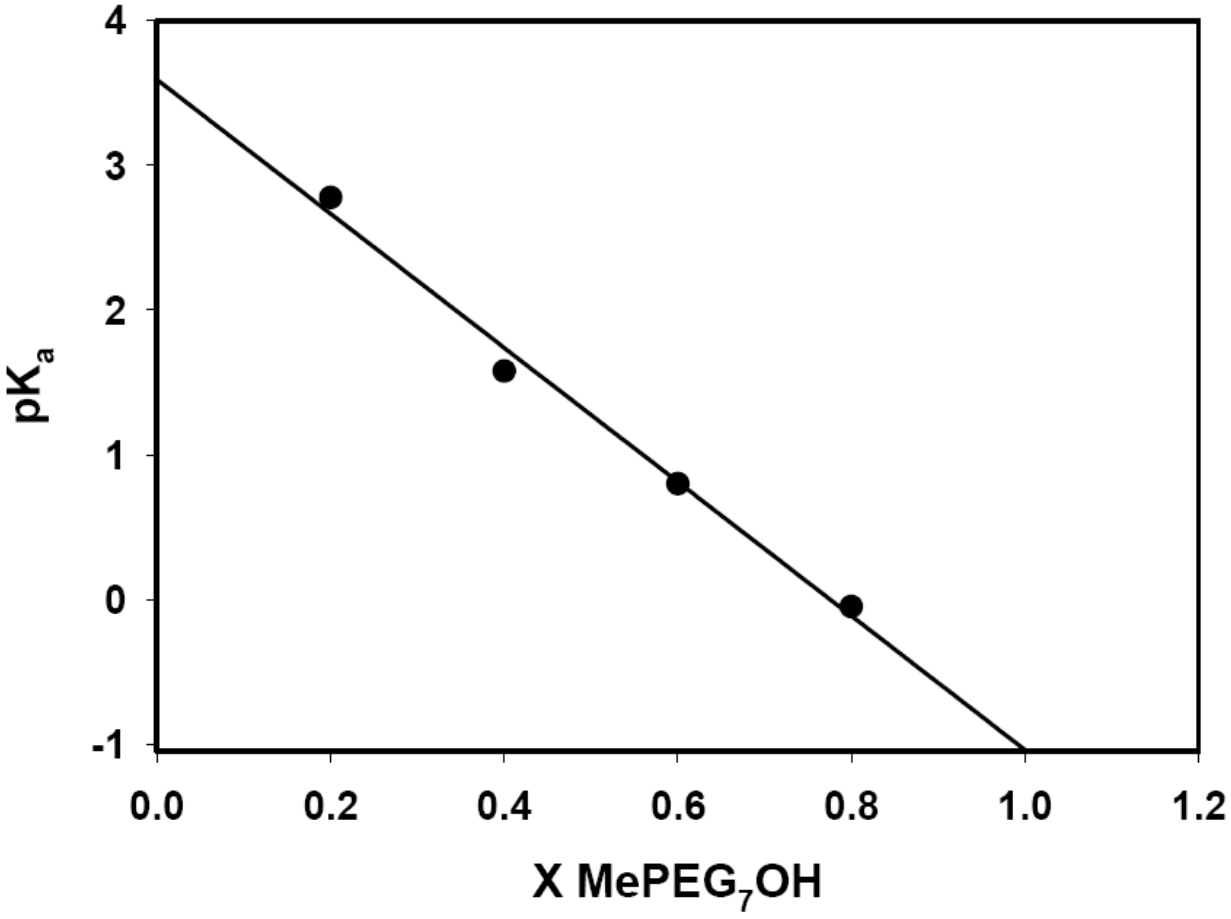

Figure 6.9: pK_a vs X $MePEG_7OH$: pK_a as a function of mole fraction of $MePEG_7OH$. Line shown is best fit linear: $y = -4.125x + 3.275$, $R^2 = 0.9974$. pK_a at X = 1.0 is -1.04

6.5 – Summary

From the viscosity and H^+ conductivity data we can use the $MePEG_7SO_3H$ acid as a model system for the ion-ion pairing effects previously reported for $MePEG_n$ based polymers. The similarity of this Walden plot to those observed for MePEG based copolymers also indicates that the same interactions are occurring in the $MePEG_7SO_3H$ acid that were occurring the $MePEG_n$ based polymers. The non-ideality found in the Walden plot has previously been explained in terms of ion-ion pairing. The increased α value in the Walden plot for $MePEG_7SO_3H$ over the $MePEG_n$ based polymers can be attributed to a rise in acid concentration. If you increase the concentration of a weak acid then there will be a higher percentage of associated protons.

A series of pH titrations in binary solutions were used to determine the pK_a of $MePEG_7SO_3H$ in a model system of $MePEG_7OH$**.** These results show that the acid is a weak acid in $MePEG_7OH$, and that the activity is lower, indicating ion-ion pairing due to H^+ cations associated with $MePEG_7SO_3^-$. This explanation helps to clarify the mechanism of proton conductivity in MePEG based polymer electrolytes. There are both the vehicle and Grotthus mechanisms contributing to H^+ conductivity as evidenced by $MePEG_7SO_3H$ acting as a weak acid. But due to the large difference in van der Waals volumes of H^+ cations and $MePEG_7SO_3H$, it is a minor contributor to the overall proton conductivity and merely acts as an overall impediment to the flow of protons.

VII. CONCLUSION

The goal of this dissertation was to gain a primary understanding of the mechanism of proton conductivity and how proton conductivity is affected by viscosity, diffusion, free volume, glass transition and specific heat capacity of our sol-gel synthesized, anhydrous proton conducting electrolytes. This chapter is a summary of all of the results discussed in terms of polymer electrolytes, fuel cells and free volume theory.

7.1 – Materials

The materials in this dissertation are novel, easy to synthesize and provide an inexpensive and efficient method to produce polymer electrolytes for fuel cell applications. The sol-gel polymerization provides randomly cross-linked, incompletely condensed polysiloxanes. These materials have had comonomers added to systematically alter the fractional free volume from that of the pure polymers in an effort to analyze proton conductivity in terms of free volume theory.

Many of the copolymers exhibited two peaks as measured by GPC, a high MW and a low MW peak. The low MW peak represented a "dimer" peak but was not observed for copolymers based on small MePEG and MePPG. For these copolymers, the MW of the polymers was smaller than the detection limit for the ELS detector (sensitivity $\propto MW^2$). End group analysis showed that all of the copolymers studied have a small fraction of uncondensed Si-OH units. This result was expected due to the polymerization conditions. It was also shown that the incorporation of the comonomers had an effect on FFV and density. The effect did not follow a trend; for the

small MePEG polymers with bulky copolymers, there was an increase in FFV and a decrease in density, for the large MePEG polymers with bulky copolymers, there was a decrease in FFV and an increase in density, and for PEG/PPG copolymers, some had increased FFV while others had a decreased FFV in the same copolymer series.

7.2 – Viscosity

The results for fluidity of all copolymers corresponds to those for FFV. For the copolymers that had an increased FFV there was an increase in fluidity compared to the pure polymers and for the copolymers that had a decreased FFV there was a decrease in fluidity compared to the pure polymers. The results also followed the Doolittle equation (eq 1.11a) as shown in Figures 3.5 and 4.5. This indicates that the FFV is directly related to the fluidity in this system.

There was also a relationship observed between the fluidity activation energy and the T_g of the copolymers. The T_0 value used to fit the viscosity activation data was calculated from the T_g so this relationship follows. There was no trend observed between the specific heat capacity (C_p) of the copolymers and the activation energy for fluidity except for the $MePPG_3$/$MePPG_2$ copolymers. A relationship between activation energy for a process and C_p indicates that intermolecular forces are involved. The lack of trend for most of the copolymer series indicate that the copolymers follow free volume theory which in which viscosity is dependent on the rearrangement of molecules and should not involve the alteration of intermolecular forces. The PPG based copolymers on the other hand are relatively small and appear to have the intermolecular forces coupled to the viscosity of the system as observed in the relationship between C_p and the viscosity activation energy.

7.3 – Proton Conductivity

The proton conductivity data did not correspond to the FFV data or the viscosity data for any of the copolymer series. The H^+ conductivity data was plotted versus the FFV according to the Forsythe equation (1.12) for the bulky copolymers (Figure 3.14) and the PEG/PPG copolymers (Figure 4.14). The linear best fit lines of both plots had a poor R^2 value and a large p-value indicating that there was no correlation between FFV and H^+ conductivity. Previously our group developed the concept of volume fraction of PEG ($V_{f,PEG}$) to describe the fraction of a material that is composed of PEG units. The $V_{f,PEG}$ was developed to describe the Grotthus mechanism in terms or ethers available for H^+ conductivity. When $V_{f,PEG}$ was substituted in place of FFV in the Forsythe equation, the best linear fit for both plots (Figure 3.15 and 4.15) had a moderate R^2 value and a very low p-value (>0.0001) indicating that the $V_{f,ether}$ is correlated to the H^+conductivity.

There is no relationship observed between T_g and activation energy for H^+ conductivity. This was expected because the T_0 used for the two parameter fit for the VTF equation was calculated from the T_g of the copolymers and not the copolymer electrolyte mixtures. There was no trend observed between H^+ conductivity activation energy and C_p for the high and low $MePEG_7SO_3H$ acid concentration copolymer electrolytes for the MePEG/MePPG copolymers. There was also no trend observed for the low acid concentration copolymer electrolytes for the bulky copolymers. The fact that there are no relationships observed between C_p and H^+ conductivity activation energy for these copolymers indicates that the intermolecular forces are not controlling the H^+ conductivity. It provides further evidence for the conclusion that $V_{f,ether}$ is a controlling factor in H^+ conductivity. For the high acid concentration bulky copolymers, trends were observed for each bulky copolymer series. The correlation increased in order of polarity for

MePEG/TFPSi, MePEG/iBuSi, and the $MePEG_n$ polymers but the MePEG/Ph_2Si copolymers had the highest correlation. It would be expected that these copolymers would belong in the middle of the trend because of its low polarity but this ignores steric effects of the large planar benzene groups. These large groups are capable of blocking H^+ channels which will make these intermolecular forces much more important to H^+ conductivity than in the linear and branched alkanes. These correlations indicate that the bulky groups block H^+ channels along the ether backbone thus decreasing the H^+ conductivity.

7.4 – Walden Plots

The relationship between the viscosity and molar equivalent conductivity of a material is described by the Walden rule (eq. 1.10a). The fractional Walden rule (eq. 1.10b) is an extension of the rule that is used for electrolyte systems that deviate from the ideal situation described by the Walden rule. All of the copolymer electrolyte systems (bulky copolymers and MePEG/MePPG copolymers) deviated from the Walden rule as observed by the α values from the best linear fit. The α values ranged from 0.3 to 0.6. These α values indicate that there are other forces controlling ionic mobility besides the viscosity. The majority of the copolymers electrolytes were in the range between 0.42 and 0.47 with several outliers. The proximity of these values indicates that the same forces are controlling all of the copolymer electrolytes.

Some of the forces that can impede the ionic conductivity are the rigidity of the polymer, small dissociation constant, or the blocking of H^+ channels. The Grotthus mechanism is generally viewed as the predominant mechanism for H^+ conductivity for this system. In this mechanism, the H^+ ions are passed from one hydrogen bonding site to the next across the material. This mechanism depends on the rearrangement of the hydrogen bonding sites to shuttle

the H^+ ions but is also dependent on the properties of the acid and the hydrogen bonding sites. The other mechanism that is responsible for H^+ conductivity is the vehicle mechanism. In this mechanism, the H^+ ion is associated to an anion or and electronegative molecule, the associated H^+ is then moved across the material by the physical diffusion of the vehicle. The vehicle mechanism is generally governed by the viscosity of the system and can be subject to the dissociation constant of the vehicle and H^+ ion. The Grotthus mechanism, on the other hand, is greatly affected by forces such as polymer rigidity, the dissociation constant, and blocking of the H^+ channels.

7.5 – Acid Dissociation

As discussed previously, the dissociation constant of the H^+ from the anion is important to the overall conductivity of the systems being studied. The Walden plots provide evidence that there are other forces impeding ionic conductivity besides the viscosity of the material. The dissociation constant of the $MePEG_7SO_3H$ acid was determined from a series of titrations in binary $MePEG_7OH/H_2O$ solutions. For this series of titrations, the pK_a of the acid became smaller as the amount of $MePEG_7OH$ increased. The pK_a was extrapolated from the binary titrations and determined to be -1.04. This was not expected because we expected that the acid was a weak acid in PEG. The strongest acid in a solution is the protonated solvent. The pK_a of protonated alkyl ethers is much smaller than the pK_a of protonated H_2O (-4.0 compared to -1.7). The weakness of an acid is determined by the difference between the pK_a of the acid and the pK_a of the protonated solvent. Even though the pK_a of the $MePEG_7SO_3H$ decreased as the $MePEG_7OH$ increased, the acid's pK_a actually became farther away from the pK_a of the protonated solvent meaning that the acid became weaker in $MePEG_7OH$.

Also noted was the increase in the activity coefficient calculated from Gran plots. The mean activity coefficient increased as the fraction of $MePEG_7OH$ increased meaning that the H^+ was becoming more active even though the acid was becoming weaker. This is a consequence of the decreasing of the polarity of the solvent. As the solvent polarity decreases, the H^+ becomes less well solvated increasing its activity.

The vehicle mechanism is dependent on the H^+ being associated to an anion as a vehicle so a weak acid would be ideal for this mechanism, but the increased activity of the H^+ ion would be ideal for the Grotthus mechanism. In free volume theory, diffusion of occurs by reorganization of the material where voids open that are large enough to accommodate the diffusing species, in this case the vehicle. The probability of a void that can accommodate $MePEG_7SO_3H$ is very small. The large difference between the H^+ ion and the $MePEG_7SO_3^-$ indicates that the Grotthus mechanism is the predominant conductivity mechanism even though only a small fraction of H^+ ions are dissociated.

BIBLIOGRAPHY

1. Ritchie, J. E.; Crisp, J. A., "A Sol-Gel Synthesis of a Polyether Based Proton Conducting Electrolyte." *Anal. Chim. Acta* **2003,** *496*, 65-71.
2. Ratner, M. A., Shriver, D.F., "Ion Transport in Solvent-Free Polymers." *Chem. Rev.* **1988,** *88*, 109-124.
3. Kreuer, K. D., "Proton Conductivity: Materials and Applications." *Chem. Mater.* **1996,** *8*, 610-641.
4. Paddison, S. J., Paul, R., Zawodzinski, T. A., Jr., "Proton Friction and Diffusion Coefficients in Hydrated Polymer Electrolyte Membranes: Computations with Non-Equilibrium Statistical Mechanical Model." *J. Chem. Phys.* **2001,** *115*, 7753-7761.
5. Hickner, M. A., Ghassemi, H., Kim, Y. S., Einsla, B. R., and McGrath, J. E., Alternative Polymer Systems for Proton Exchange Membranes. Chem. Rev., 2004. 104, 4587-4612., "Alternative Polymer Systems for Proton Exchange Membranes." *Chem. Rev* **2004,** *104*, 4587-4612.
6. Lee, S. J., Mukerjee, S., Ticianelli, E.A., and McBreen, J., "Electrocatalysis of CO tolerance in hydrogen oxidation reaction in PEM fuel cells." *Electrochimica Acta* **1999,** *44*, 3283-3293.
7. Götz, M., and Wendt, H., "Binary and Ternary Anode Catalyst Formulations Including the Elements W, Sn and Mo for PEMFCs Operated on Methanol or Reformate Gas " *Electrochimica Acta* **1998,** *43*, 3637-3644.
8. Tawfika, H., Hunga, Y, and Mahajanb, D., "Metal Bipolar Plates for PEM Fuel Cell -A Review." *Journal of Power Sources* **2007,** *163*, 755-767.
9. Gosalawit, R., Chirachanchai, S., Manuspiya, H., Traversa, E., "Krytox-Silica-Nafion Composite Membrane: A Hybrid System for Maintaining Proton Conductivity in a Wide Range of Operating Temperatures,." *Catalysis Today* **2006,** *118*, 259-265.
10. Watanabe, M., Uchida, H., Emori, M., "Polymer Electrolyte Membranes Incorporated with Nanometer-Size Partices of Pt and/or Metal-Oxides: Experimental Analysis of the Self-Humidification and Suppression of Gas-Crossover in Fuel Cells." *J. Phys. Chem. B* **1998,** *102*, 3129-3137.
11. Mistry, M. K., Choudhury, N.R., Dutta, N.K., Knott, R., Shi, Z., and Holdcroft, S., "Novel Organic/Inorganic Hybrids with Increased Water Retention for Elevated Temperature Proton Exchange Membrane Application,." *Chem. Mater.* **2008,** *20*, 6857-6870.
12. Periera, M., Valle, K., Belleville, P., Morin, A., Lambert, S., Sanchez, C., "Advanced Mesostructured Hybrid Silica/Nafion Membranes for High-Performance PEM Fuel Cell." *Chem. Mater.* **2008,** *20*, 1710-1718.
13. Ritchie, J. E., Murray, R.W., "Electron Transfer Dynamics in Molten Salts of Mono- and Dinuclear Ruthenium Complexes." *J. Phys. Chem. B* **2001,** *105*, 11523–11528.
14. Ritchie, J. E., Murray, R.W., "Intermolecular Optical Electron Transfers in Polyether Hybrid Molten Salts of Mixed-Valent Ruthenium Complexes." *J. Am. Chem. Soc.* **2000,** *122*, 2964–2965.
15. Dickinson, E., Masui, H., Williams, M.E., Murray, R.W., "Effect of Position of Polyether Attachment on the Electron Self-Exchange Activation Barrier Energies of Redox Polyether Hybrid Molten Salts." *J. Phys. Chem. B* **1999,** *103*, 11028–11035.
16. Masui, H., Murray, R.W., "Room-Temperature Molten Salts of Ruthenium Tris(bipyridine)." *Inorg. Chem.* **1997,** *36*, 5118–5126.

17. Williams, M. E., Lyons, L.J., Long, J.W., Murray, R.W., "Transport and Electron Transfer Dynamics in a Polyether-Tailed Cobalt Bipyridine Molten Salt: Electrolyte Effects." *J. Phys. Chem. B* **1997,** *101*, 7584–7591.
18. Dahmouche, K., Sanilli, C.V., Pulcinelli, S.H., and Craievich, A.F., "Small-Angle X-ray Scattering Study of Sol-Gel-Derived Siloxane - PEG and Siloxane - PPG Hybrid Materials." *J. Phys. Chem. B* **1999,** *103*, 4937-4942.
19. Kao, H. M., Chao, S.W., Chang, P.C., "Multinuclear Solid-State NMR, Self-DIffusion Coefficients, Differential Scanning Calorimetry, and Ionic Conductivity of Solid Organic-Inorganic Hybrid Electrolytes based on PPG-PEG-PPG Diamine, Siloxane, and Lithium Perchlorate." *Macromolecules* **2006,** *39*, 1029-1040.
20. Markovic, E., Matisons, J., Hussain, M. Simon, G.P., "Poly(ethylene glycol) Octafunctionalized Polyhedral Oligomeric Silsesquioxane: WAXD and Rheological Studies." *Macromolecules* **2007,** *40*, 4530-4534.
21. Markovic, E., Ginic-Markovic, M., Clarke, S., Matisons, J., Hussain, M., Simon, G.P., "Poly(ethylene glycol)-Octafunctionalized Polyhedral Oligomeric Silsesquioxane: Synthesis and Thermal Analysis." *Macromolecules* **2007,** *40*, 2694-2701.
22. Jaffres, P. A., Morris, R.E., "Synthesis of Highly Functionalized Dendrimers Based on Polyhedral Silsequioxane Cores." *J. Chem. Soc., Dalton Trans.* **1998**, 2767–2770.
23. Duchateau, R., "Incompletely Condensed Silsesquioxanes: Versatile Tools in Developing Silica-Supported Olefin Polymerization Catalysts." *Chem. Rev.* **2002,** *102*, 3525-3542.
24. Neumann, D., Fisher, M., Tran, L., Matisons, J.G., "Synthesis and Characterization of Isocyanate Functionalizes Polyhedral Oligosilsesquioxane and the Subsequent Formation of an Organic-Inorganic Hybrid Polyurethane." *J. Am. Chem. Soc.* **2002,** *124*, 13998-13999.
25. Ito, K., Nishina, N., Ohno, H., "High Lithium Ionic Conductivity of Poly(ethyle oxide)s Having Sulfonate Groups on Their Chain Ends." *J. Mater. Chem.* **1997,** *7*, 1357–1362.
26. Ito, K., Ohno, H., "Design of Highly Ion Conductive Polyether/Salt Hybrids." *Electrochimica Acta.* **1998,** *43*, 1247-1252.
27. Ghosh, B. D., Lott, K.F., and Ritchie, J.E., "Conductivity Dependence of PEG Content in an Anhydrous Proton Conduction Sol-Gel Electrolyte." *Chem. Mater.* **2005,** *17*, 661-669.
28. Wu, P. W. H. S., Duong, A., Dunn, B., and Kaner, R., "A Sol-Gel Solid Electrolyte with High Lithium Ion Conductivity." *Chem. Mater.* **1997,** *8*, 1004-1011.
29. Loy, D. J. G., Baugher, B., Myers, S., Assink, R., and Shea, K., "Sol-Gel Synthesis of Hybrid Organic Inorganic Materials. Hexylene and Phenylene Bridged Siloxanes." *Chem. Mater.* **1996,** *8*, 656-663.
30. Hackley, V. A. a. F., C.F., Special Publication 956. In *National Institutes of Technology*, U.S. Department of Commerce: 2001.
31. Bard, A. J. a. F., L.R., *Electrochemical Methods: Fundamentals and Applications*. 2nd ed.; 2000.
32. MacDonald, R. J., "Theory of Space-Charge Polarization and Electrode Discharge Effects." *J. Chem. Phys.* **1973,** *58*, 4982-5001.
33. MacDonald, R. J., "Simplified Impedence/Frequency-Response Results for Intrinsically Conducting Solids and Liquids." *J. Chem. Phys.* **1974,** *61*, 3977-3996.
34. Wu, Y. C.; Berezansky, P. A., "Low Electrolytic Conductivity Standards." *J. Res. Natl. Inst. Stand. Technol.* **1995,** *100*, 521-527.

35. McLin, M. G., Angell, C.A., "Ion-Pairing Effects on Viscosity/Conductance Relations in Raman-Characterized Polymer Electrolytes: LiClo4 and NaCF3SO3 in PPG(4000)." *J. Phys. Chem.* **1991,** *95*, 9464-9469.
36. Doolittle, A. K., "Studies in Newtonian Flow. II. The Dependence of the Viscosity of Liquids on Free-Space." *J. Appl. Phys.* **1951,** *22*, 1031-1035.
37. Cohen, M. H., Turnbull, D. J., "Molecular Transport in Liquids and Gases " *Chem. Phys.* **1959,** *31*, 1164-1169.
38. Stern, S. A. a. F., H.L., "The Selective Permeation of Gases Through Polymers." *Annu. Rev. Mater. Sci.* **1981,** *11*, 523-550.
39. Bondi, A., "Van der Waals Volumes and Radii." *J. Phys. Chem.* **1964,** *68*, 441-451.
40. Van Krevelen, D. W., *Properties of Polymers*. 3rd Edition ed.; Elsevier Scientific Publishing Company: New York, 1990.
41. Van Krevelen, D. W. H., P.J., "Prediction of Polymer Densities." *J. Appl. Polym. Sci.* **1969,** *13*, 871-881.
42. Vogel, H., "The Temperature Dependence of Viscosity on Free-Space." *Phys. Z* **1921,** *22*, 645-656.
43. Tamman, G. a. H., G.Z., "The Temperature Dependence of VIscosity by Undercooled Liquids." *Anorg. Allg. Chem.* **1926,** *166*, 245-257.
44. Fulcher, G. S., "Analysis of Recent Measurements of the Viscosity of Glasses." *J. Am. Ceram. Soc.* **1925,** *8*, 339-355.
45. Bockris, J. O. M., Reddy, A. K. N., *Modern Electrochemistry*. 2nd ed.; Plenum Press: New York and London, 1998.
46. Xu, W., Cooper, E.I., and Angell, C.A., "Ionic Liquids: Ion Mobilities, Glass Temperatures, and Fragilities." *J. Phys. Chem. B* **2003,** *107*, 6170-6178.
47. Angell, C. A., Imrie C.T., and Ingram M.D., "From Simple Electrolyte Solutions Through Polymer Electrolytes to Superionic Rubbers: Some Fundamental Considerations." *Polymer International* **1998,** *47* (9-15).
48. Doolittle, A. K., "Studies in Newtonian Flow. III. The dependence of the Viscosity of Liquids on Molecular Weight and Free Space (in Homologous Series)." *J. Appl. Phys.* **1952,** *23*, 236-239.
49. Forsythe, M., Meakin, P., MacFarlane, D.R., and Hill, A.J. , "Free Volume and Conductivity of Polyether-Urethane Solid Polymer Electrolytes." *J. Phys. Condens. Matter.* **1995,** *7*, 7601-7617.
50. Angell, C. A., "Formation of Glasses from Liquids and Biopolymers." *Science* **1995,** *267*, 1924-1935.
51. Hohne, G., Hemminger, W.F., and Flammersheim, H.-J., *Differential Scanning Calorimetry*. 2nd ed.; 2010.
52. Rafols, C., Roses, M., Bosch, E., "Dissociation constants of several non-steroidal anti-inflammatory drugs in isopropyl alcohol/water mixtures." *Anal. Chim. Acta* **1997,** *350*, 249-255.
53. Safonova, L. P., Fadeeva, Y.A., Pryakhin, A.A., "Dissociation Constants of Phosphoric acid in Dimethylformamide – Water Mixtures at 298.15 K." *Rus. J. Phys. Chem. A* **2009,** *83*, 1747-1750.
54. Indhar, H. A. B., Khanzada, A.W.K., "Potentiometric Determination of Dissociation Constants and Gibb's Free Energies of 8-Hydroxyquinoline (oxine) and 2-

Methylquinoline Using Aqueous and Mixed Organic-Water Solvent Systems." *J. Chem. Soc. Pak.* **2001,** *24*, 3-9.
55. Ghosh, B. D., and Ritchie, J.E., "Effect of Polymer Structure on Ion Transport in an Anhydrous Proton Conducting Electrolyte." *Chem. Mater.* **2010,** *22*, 1483-1491.
56. Sun, C.; Ritchie, J. E., "Effects of Bulky Co-Polymers on Ion Transport in an Anhydrous Proton Conducting Electrolyte." *J. Electrochem. Soc.* **2010,** *157* (11), B1549-B1555.
57. Loy, D. A., Baugher, B.M., Baugher, C.R., Schneider, D.A., and Rahimian, K., "Substituent Effects on the Sol-Gel Chemistry of Organotrialkoxysilanes." *Chem. Mater.* **2000,** *12*, 3624-3632.

VITA

Benjamin Yancey was born in 1985 in Huntsville, Alabama. He was raised in nearby Somerville where his curiosity as to how the world worked was never stifled. Education was always encouraged for Mr. Yancey and allowed him to graduate 14th in the class of 2003 from A.P. Brewer High School in Somerville, Alabama. From there Mr. Yancey pursued a degree in chemistry, graduating from The University of Mississippi with a Bachelor of Science in Chemistry in 2007. Upon completion of his undergraduate studies, Mr. Yancey continued his education in the chemistry graduate program at the University of Mississippi. As a graduate student, Mr. Yancey became a member of Gamma Beta Phi honor fraternity. Mr. Yancey completed his Master of Science in Chemistry degree in December 2009. Mr.Yancey will complete his Doctor of Philosophy in Chemistry degree in May 2011.